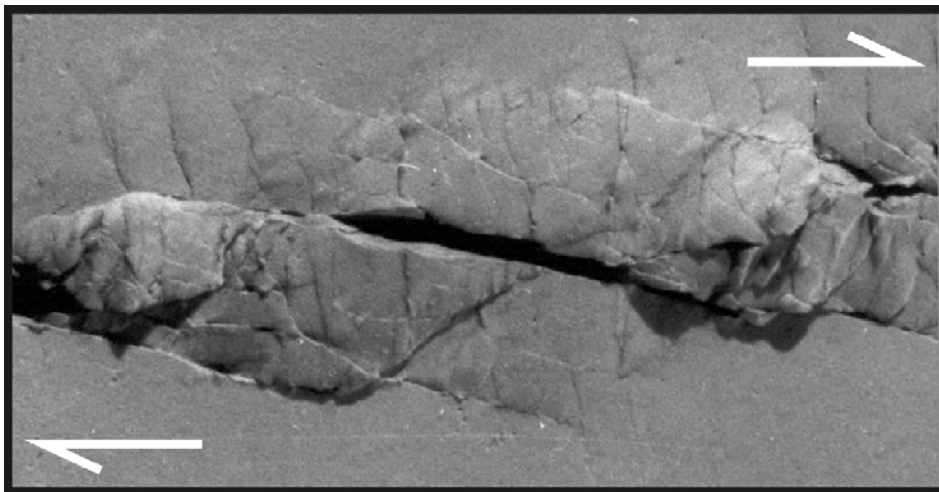


**DEVELOPMENT OF PULL-APART BASINS AND
ASSOCIATED STRUCTURES BY THE
RIEDEL SHEAR MECHANISM: INSIGHT FROM
SCALED CLAY ANALOGUE MODELS**



**Der Fakultät für Geowissenschaften
der Ruhr-Universität Bochum
zur Erlangung des Doktorgrades der
Naturwissenschaften**

**Vorgelegt von
Nassima Atmaoui
aus Algier**

**Bochum
2005**

TABLE OF CONTENTS

Table of contents	ii
List of figures	v
List of tables	ix
List of symbols	x
Abstract	xii
1. Introduction	
1.1. Statement of the problem and objectives	1
1.2. Organisation of the thesis	4
2. Previous analogue experiments on pull-apart basin	
2.1. Introduction	6
2.2. Analogue experiments of an echelon mechanism	6
2.3. Analogue experiments of distributed shear mechanism	6
2.4. Analogue experiments of Riedel shear mechanism	7
3. Dynamic scaling of tectonic models	
3.1. Historical use of tectonic models	9
3.2. Theory of scaling of tectonic models	9
3.3. Rock properties and behaviour to be simulated	10
3.4. Properties and behaviour of modelling material	13
3.4.1. Motivations for choosing clay as the modelling material	13
3.4.2. Previous tectonic clay models	14
4. Mechanical properties of soft clay used in analogue experiments	
4.1. Introduction	16
4.2. Physical state conditions in analogue modelling	
4.2.1. Consolidation state	17
4.2.2. Atterberg limits and degree of saturation	17
4.2.3. Drainage condition	18
4.3. Shear strength of modelling clay	
4.3.1. Introduction to critical state soil mechanics	19
4.3.2. Shear strength of modelling clay	19
4.3.3. Influence of clay mineralogy and fraction on material behaviour	21
4.4. Determination procedure of modelling clay properties	
4.4.1. Determination of the degree of saturation	23
4.4.2. Determination of the undrained shear strength	23
4.4.3. Determination of the critical angle of friction	24
4.5. Material properties of the clay slabs	

4.5.1. Mineralogical composition and grain size distribution	24
4.5.2. Index properties	26
4.5.3. Undrained shear strength, densities, void ratio, degree of saturation	26
4.5.4. Critical angle of shearing friction	29
4.6. Scaling of Kaolin-O properties	29
5. Experimental set-up	
5.1. The deformation table	31
5.2. The clay slab	32
5.3. Recording method	33
5.4. Measurement of heights	
5.4.1. Concept of shadow line casting	33
5.4.2. Determination of heights	34
5.5. Photo analysis and data evaluation	36
5.6. Overview of performed experiments	37
6. Analysis and results	
6.1. Standard experiment	38
6.1.1. Development of pull-apart structures	38
6.1.2. Development of push-up ridges	41
6.1.3. Structural features of the strike-slip zone	42
6.2. Influence of shear strength and thickness of the clay slab	42
6.2.1. Influence of the shear strength (series A)	45
6.2.2. Influence of the thickness of the clay slab (series B)	47
7. Comparison with other analogue modelling studies	
7.1. Introduction	50
7.2. Comparison with previous sand models	50
7.3. Comparison with previous clay models	51
8. Natural examples	
8.1. Riedel type pull-apart basins	53
8.1.1. Structure of the strait of Sicily Complex rift zone	53
8.1.2. The pull-apart basins and structures on Gozo Island	54
8.2. Simultaneous formation of pull-apart basins and push-up ridges	55
8.2.1. Structure of the Marmara Sea Basin	57
9. Interpretation and discussion	
9.1. Riedel type pull-apart basins	59
9.1.1. The strait of Sicily Complex rift zone	59
9.1.2. Models of pull-apart basin formation	60
9.2. Coeval formation of pull-apart and push-up structures	62

9.2.1. The complex Marmara Sea Basin	62
9.2.2. Models of complex strike-slip basin formation	64
9.3. Influence of the material properties	66
10. Conclusions	67
References	70
Appendices	77
Acknowledgements	
Curriculum vitae	

LIST OF FIGURES

- Fig. 1. Classical pull-apart basins at different length scale, and within various tectonic settings. A) The NE – SW trending dextral Bocono fault, Venezuela. Simplified from Beltran (1993). a) La Gonzales Basin, formed at a bend along the Bocono fault (modified from Schubert, 1982). b) Small scale pull-apart structures (called sag ponds and peats) formed along a discontinuous segment of Bocono fault at Morros de los Hoyos (from Audemard et al., 1999). B) The Death Valley pull-apart basin, California. The map shows the main fault traces, the saline pan (yellow) and the mudflat areas (green). The satellite image shows also the mountains surrounding the narrow valley (Landsat scale 1:100,000). C) The Dead Sea transform. (a) and (b) are Bouguer gravity anomaly maps from ten Brink et al. (1999). The maps reveal that the Dead Sea basin is further divided into several fault controlled sub-basins 20 to 30 km long.
- Fig. 2. Three mechanisms for the development of pull-apart basins. A) En echelon right-stepping dextral strike-slip faults. Pull-apart basins form at the overstep or bend (Mirror image for the left-stepping sinistral faults). B) Distributed shear. Pull-apart basins form during linking and coalescence of main faults. S_1 and S_1' are primary synthetic and antithetic strike-slip faults respectively. T and S_2 are tension and secondary synthetic strike-slip faults respectively (simplified from An and Sammis, 1996). C) Riedel shear. 1) Initiation and coalescence of first generation shears into Riedel faults. 2) Strike-slip displacement and rotation of Riedel shears. 3) Development of Y-faults, parallel to the principal displacement zone (PDZ). Pull-apart basins form at the passive Riedel faults (modified from Hagglaue-Ruppel, 1991).
- Fig. 3. Basement configuration of the three mechanisms in Figure 1 before and after deformation. Setup 1: two offset discontinuities for the en echelon mechanism. Setup 2: simple shear of a basal plate for the distributed shear mechanism. Set-up 3: one straight discontinuity for the Riedel shear mechanism.
- Fig. 4. Formation of a push-up ridge (grey field) between two adjoining Riedel shears (R). The dextral motion along the strike-slip discontinuity in the basement (PDZ) generates dextral left-stepping Riedel shear fractures in the overlying slab. The area between the neighbouring shears is under contraction.
- Fig. 5. Allegoric sketch illustrating the concept of the scaling of physical tectonic models for sedimentary rocks. The scaling parameters are: strength (τ), density (ρ), gravity (g) and length (λ).
- Fig. 6. A) Three-dimensional projection of the critical state line (CSL). B) The critical state strength in direct shear and triaxial tests (from Atkinson and Bransby, 1978).

- Fig. 7. A) Undrained (total) and critical (effective) strength envelopes for normally consolidated clays. B) Graph showing the location of the drained (D) and undrained (U) failure points on the CSL. q'_{fd} and p'_{fd} are the drained effective deviatoric and mean normal stresses at failure. q'_{fu} and p'_{fu} are the undrained effective deviatoric and mean normal stresses at failure (modified from Whitlow, 2001).
- Fig. 8. Particle size distribution curve for Kaolin-O. The material is a well graded silty clay. It has a wide distribution of particle sizes, from 1.5 μm to 55 μm . The clay size fraction CF of particles below 2 μm is about 45%.
- Fig. 9. Kaolin-O within the plasticity chart for classification of fine-grained soils. The A-line separates the clay and silty soils. Kaolin-O being on the A-line and having a W_L below 35%, it is classified as a silty clay soil of low plasticity.
- Fig. 10. Dry (ρ_d) and bulk (ρ_b) densities of Kaolin-O pastes at different water contents w .
- Fig. 11. Undrained shear strength S_u of Kaolin-O pastes at different water contents w from shear vane test results.
- Fig. 12. Empirical correlation between critical friction angle (ϕ_{cs}') and plasticity index (I_P) from triaxial compression tests on normally consolidated clays (simplified from Terzaghi et al., 1996).
- Fig. 13. Experimental set-up. A) The deformation table. PDZ: principal displacement zone, a discontinuity between two rigid boards. B) Installation of wooden frame for filling with clay and smoothing of surface. C) Removal of wooden frame, extension of strings above surface. D) Plane view of slab surface before deformation.
- Fig. 14. Control of clay smoothing direction on the type of Riedel shear formed in the slab. The anisotropy of direction, arrow on the half-circle, is induced by the repetitive smoothing of the clay surface at the same angle to the direction of the principal displacement zone. Synthesised from Erkan's clay Riedel experiments (1982).
- Fig. 15. The concept of shadow line casting.
- Fig. 16. Determination of the height h separating point P on the string from its shadow point M on the surface of the slab. A) Surface view of clay slab. B) Perspective view.
- Fig. 17. The geometrical features of the strike-slip deformation zone (in grey) formed in scaled clay experiments. A) Block diagram. B) View in profile. W : width; Z : thickness; D : basal displacement amount; PDZ: principal displacement zone.
- Fig. 18. Progressive development of pull-apart structures and secondary push-up ridges in standard experiment NA4 at normalised basal displacement magnitude (NBD). A) Initiation and development of Riedel shears. B) Initiation and development of the Y- and P-shears, incipient pull-apart structures. C) Fully formed pull-apart structures at the Riedel shears. D) Coalescence of neighbouring pull-apart structures.

- Fig. 19. Structural features of a part of the standard experiment NA4 after a NBD of 2 (basal displacement is twice the thickness of the slab). A) The raw image shows the strike-slip zone formed of alternating pull-apart structures with push-up ridges. B) Drawing of the image emphasizing the structural features. C) Topographic profile along the dashed line in (A), obtained with the shadow line casting method. The vertical scale has been twice exaggerated.
- Fig. 20. Plane view of strike-slip deformation zones in various models by comparison to the standard model. Series (A) Models of similar thickness (4 cm) and varying shear strengths. Series (B) Models of similar shear strength (1.5 kPa) and varying thickness value. The structures are shown for a normalised basal shear displacement to thickness ratio of about 0.82. Z and S are respectively the thickness and the shear strength of the clay slab.
- Fig. 21. The dependency of the width of the strike-slip zones on the thickness and the shear strength of the clay scaled models.
- Fig. 22. Evolution of the vertical displacements (uplift amount) at the push-up ridges with respect to the normalised basal shear displacement NBD for models NA7, NA4 and NA10 having different shear strengths.
- Fig. 23. Evolution of the vertical displacements at the push-up ridges with respect to the normalised basal shear displacement NBD for models NA9, NA4 and NA8 having different thicknesses.
- Fig. 24. The Strait of Sicily Complex rift zone. Modified after (Boccaletti et al., 1990 and Reuther, 1990).
- Fig. 25. Centimetre to several hundreds of metres long pull-aparts formed by Riedel shear mechanism on Gozo, Malta. A) after Kim et al., (2003); B) after Reuther (1990).
- Fig. 26. The Marmara Sea basin. A) Digital elevation model of northern Turkey showing the North Anatolian Fault Zone (NAFZ) in red, and its place within the North Anatolian Shear Zone (NASZ) (Image from US Geological Survey, tectonic data after Şengör et al., 2005). B) Colour shaded bathymetric map realised by Ifremer, Ecole Normale Supérieure, on board Le Suroit. The map shows the deformation zone, where three deep basins (in blue) are separated by two highs. C) Tectonic sketch of the complex Marmara Sea basin, NW Turkey. Modified after Aksu et al. (2000) and Imren et al. (2001).
- Fig. 27. A) Time-migrated seismic reflection profile along Seismic Line M13 showing the Central High. B) Structural interpretation according to Yaltirak (2002). The push-up ridge is an antiform bounded by two major thrust faults. The core is folded, and shallow normal faults develop on a detachment surface (simplified from Yaltirak, 2002).

- Fig. 28. Evolution of widths and lengths of pull-apart basins according to A) Aydin and Nur (1982), and B) the results of our clay analogue models.
- Fig. 29. The proposed tectonic models of the Marmara Sea after Yaltirak (2002, references therein). Bold lines represent the main active faults that form the Marmara Sea basin; thin lines show secondary faults. Dashed lines in (C) are the buried master fault in the basement.
- Fig. 30. Development of faults and related pull-apart basins in a strike-slip zone formed by the Riedel shear mechanism. A) Initiation of the Riedel and conjugate Riedel shears (R and R'), and of the tension fractures (T). B) Initiation of the Y- and P- shears. C) Strike-slip zone at a mature stage of development. (simplified from Sengör, 1995).
- Fig. 31. Coeval evolution of pull-apart basins and push-up ridges generated by Riedel mechanism. (A) Formation of the Riedel and conjugate Riedel shear fractures. (B) Clockwise rotation of the fractures, shear and dilatation of the Riedel shears. Small scale folding and reverse faulting at the push-up ridges. (C) Development of P- and Y-shear fractures. Formation of pull-apart structures at the Riedel shears. Further contraction at the push-up ridges till full linkage of the Y-shears within the strike-slip zone.

LIST OF TABLES

Table 1. Key properties of sediments and sedimentary rocks compiled from Attewell and Farmer (1976), Wohlenberg (1982), Rummel (1982), Schopper (1982), and Carmichael (1990). Some data from rock cores and in-situ rock mass were added (Japan Nuclear Cycle Institute, 2000).

Table 2. Boundary conditions and shear parameters of previous clay physical models.

Table 3. Mineralogical and chemical composition of Kaolin-O.

Table 4. Bulk density (ρ_b), undrained shear strength (S_u), void ratio (e), and degree of saturation (S_r) corresponding to the water content of the clay pastes (w %) used in this study. Note: water content is also termed moisture content or humidity in soil mechanics literature. It is the ratio of the weight of water contained in the pores to the weight of the solid dry material in a given mass of soil expressed as a percentage.

Table 5. Properties of the modelling material and of sedimentary rocks with the scaling ratios.

Table 6. Influence of the shear strength (S_u) and thickness (Z) of the clay slabs on the geometrical characteristics of the deformation zones formed in the models.

Table 7. Comparison of material properties between different clays. Sources: Tchalenko (1970), Morgenstern and Tchalenko (1967) and Lazarte and Bray (1996). P_L and W_L : Atterberg's plastic and liquid limits; PI: plasticity index or range; CF: clay fraction with size below 2 μm .

LIST OF SYMBOLS

α, β	Angle
c'	cohesion intercept of the τ_f - σ' envelope
CF	Clay fraction
CSL	Critical State Line
D	Distance
E	Young's modulus of elasticity
e	Void ratio
e_{cs}	Void ratio at critical state
ϕ_{cs}'	Angle of shear resistance at critical state
ϕ_u	Total angle of shear resistance obtained under undrained conditions
g	Acceleration due to gravity
G_s	Grain specific gravity of soil and sediment particles
H, h	Height
I_p (or PI)	Plasticity index
K_0	coefficient of earth pressure at rest, or lateral pressure coefficient
k	Hydraulic conductivity, or permeability
λ	Length scaling parameter
M	Slope of critical state line in p' - q' plane; image of point P
n	Porosity
n_e	Effective porosity
NBD	Normalised basal displacement
OCR	Overconsolidation ratio of clays
P	Pressure; point; synthetic shear fracture
PDZ	Principal displacement zone
p'	Mean normal stress (effective)
p'_{cs}	Mean normal stress at critical state
q'	Deviatoric stress (effective)
q'_{cs}	Deviatoric stress at critical state
R	Riedel shear fracture
R'	Conjugate Riedel shear fracture
ρ_d	Dry density of soil and sediment
ρ_b	Bulk density of soil and sediment
ρ_w	Density of water
S_r	Degree of saturation

S_u	Total shear stress measured under undrained conditions
σ	Total normal stress
σ'_1	Maximum principal effective stress
σ'_3	Minimum principal effective stress
σ' (or σ'_n)	Effective normal stress
σ'_{cs}	Effective normal stress at critical state
σ_t	Tensile strength
T	Temperature
t	Time
τ_f	Total shear stress at failure
τ'	Effective shear stress at failure
τ'_{cs}	Failure shear stress at critical state
u	Pore fluid pressure
UCS	Unconfined compressive strength
u_f	Fluid pressure at failure
v	Specific volume
V_{max}	Maximum vertical displacement
ν	Poisson's ratio
v_{cs}	Specific volume critical state
w	Water content
W_L (or LL)	Atterberg liquid limit
W_P (or PL)	Atterberg plastic limit
Y	Synthetic shear fracture
z, Z	Depth of sediments; thickness of slab

ABSTRACT

The physical and mechanical properties of clay materials required to scale the tectonic analogue experiments are analysed based on the modern soil mechanics concepts. A practical procedure for the determination of these properties is presented. Scaled clay experiments under Riedel shear mechanism produced a series of typical pull-apart structures. At the initial stages of the development of the deformation zone within the clay slab, the synthetic shear fractures (Riedel shears) display dilatational behaviour. With increasing basal displacement these dilated synthetic shears rotate and open further; long, narrow and deep troughs are formed. The shear displacements and the low angle of orientation to the direction of principal basal displacement definitely distinguish them from the tension fractures. Synthetic segments (Y-shears), which are parallel to the basal principal displacement fault, develop in a later stage and accommodate the continuing strike-slip deformation. They bound the troughs at the two tips of the initial Riedel shears and pull the sides further apart. Many rhomb shaped structures which characterise the pull-apart basins are then recognised. This development mechanism of pull-apart basins may explain why some en echelon segments of strike-slip faults display an extensional component in addition to the main shear displacement (transtension). The left-stepping arrangement of the Riedel shear fractures promotes the formation of push-up ridges at the overstepping areas separating them, of contractional features such as folds, reverse and thrust faults develop. The shear strength and the thickness of the clay slab control among other things the width of the deformation zone, the number and spacing of the Riedel shears, the presence or absence of the conjugate Riedel shears and the amount of basal shear displacement required for the shear fractures to appear at the surface. Pull-apart basins that may have formed by a mechanism corresponding to that observed in our experiment are found at different length scales on Gozo Island (Strait of Sicily rift zone), where major strike-slip systems were active from the Miocene to the Present. The coeval formation of push-up ridges can be followed in the complex strike-slip basin of the Marmara Sea.

CHAPTER 1: INTRODUCTION

1.1. STATEMENT OF THE PROBLEM AND OBJECTIVES

Pull-apart structures occur at different length scales (mm to plate boundary) in a wide range of tectonic settings (e.g. Woodcock, 1986, Fig. 1). Typical pull-apart basins form in the sedimentary cover above strike-slip faults in the basement. The formation and accumulation of hydrocarbons renders these basins economically important, and their structural evolution is of interest for oil, gas, and mineral exploration (e.g. Biddle and Christie-Blick, 1985; Sylvester, 1988; Nilsen and Sylvester, 1999). Therefore, pull-apart basins have been the subject of many geophysical, seismological, and geological investigations. Also, physical modelling has shed light on their progressive evolution.

Several mechanisms have been proposed for pull-apart basin formation. The most popular mechanism is local extension between two en echelon basement strike-slip fault segments (e.g. Aydin and Nur, 1982; Mann et al., 1983). These can be right-stepping with dextral shear or left-stepping with sinistral shear. The local extension is accommodated in the sedimentary cover by normal faults at the releasing oversteps and bends (Fig. 2A). As alternatives, two other mechanisms have been proposed for the formation of pull-apart basins: A distributed (simple) strike-slip shear mechanism and a Riedel shear mechanism.

Distributed shear is envisaged to occur in weak layers of evaporites or overpressured shales, and above a broad strike-slip zone in the basement. This causes distributed shear deformation in the overlying competent sedimentary layers. Pull-apart basins can develop at releasing steps during fault interaction, coalescence and linkage (An and Sammis, 1996; Fig. 2B).

The Riedel shear mechanism implies formation of pull-apart basins in the sedimentary cover along Riedel faults connected by segments of strike-slip faults, which are subparallel to a single principal displacement fault (PDZ) in the basement (Dewey, 1978; Soula, 1984; Hagglauer-Ruppel, 1991). The Riedel faults initiate first, while the strike-slip segments develop at a later stage and finally cause the formation of the pull-apart basins (Fig. 2C).

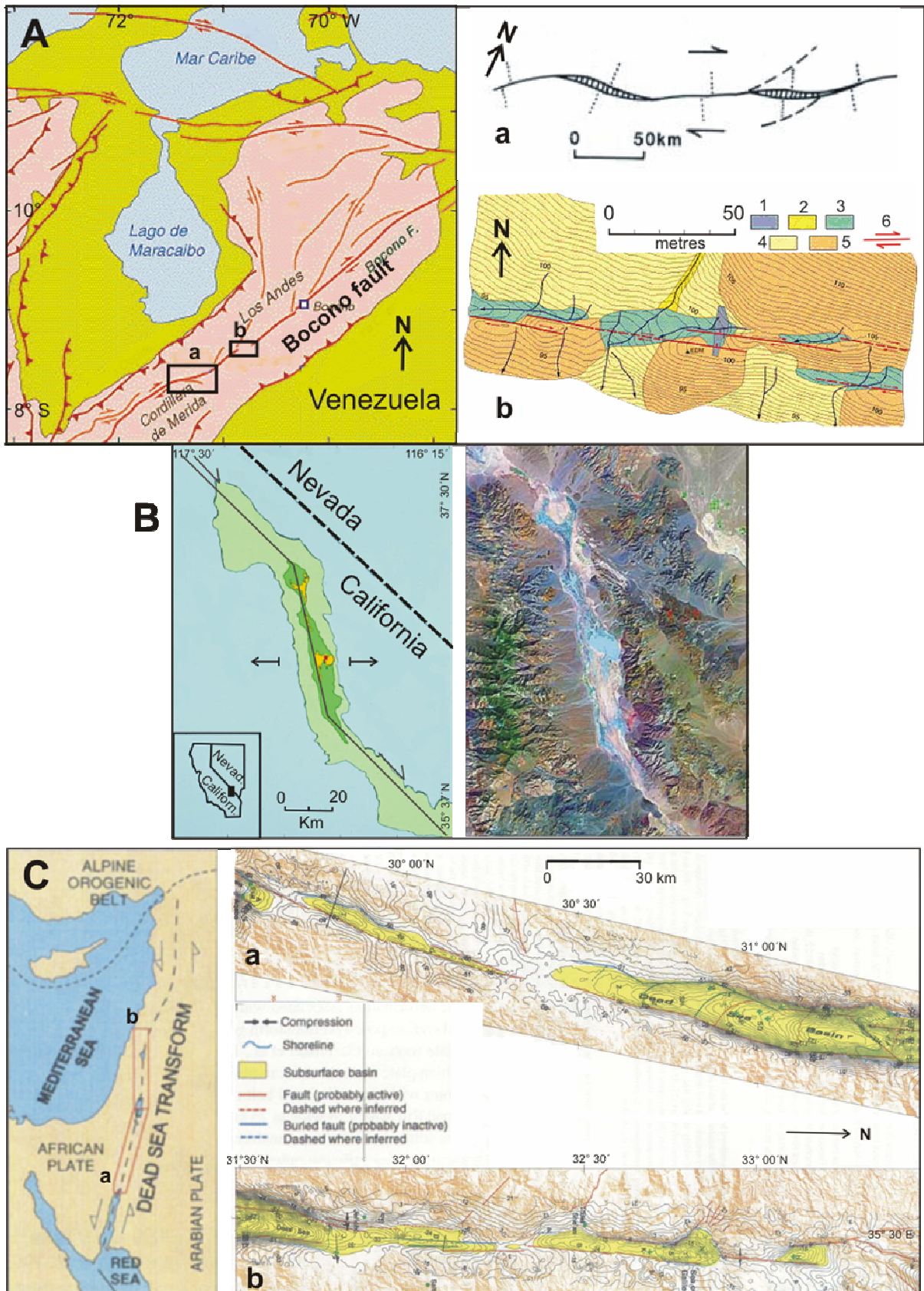


Fig. 1. Classical pull-apart basins at different length scale, and within various tectonic settings. A) The NE – SW trending dextral Bocono fault, Venezuela. Simplified from Beltran (1993). a) La Gonzales Basin, formed at a bend along the Bocono fault (modified from Schubert, 1982). b) Small scale pull-apart structures (called sag ponds and peats) formed along a discontinuous segment of Bocono fault at Morros de los Hoyos (from Audemard et al.,

1999). 1. Trench. 2. Active alluvial channel deposits. 3. Sag ponds. 4. Fan and older channel alluvium. 5. Bedrock. 6. Fault with slip direction. B) The Death Valley pull-apart basin, California. The map shows the main fault traces, the saline pan (yellow) and the mudflat areas (green). The satellite image shows also the mountains surrounding the narrow valley (Landsat scale 1:100,000). C) The Dead Sea transform. (a) and (b) are Bouguer gravity anomaly maps from ten Brink et al. (1999). The maps reveal that the Dead Sea basin is further divided into several fault controlled sub-basins 20 to 30 km long.

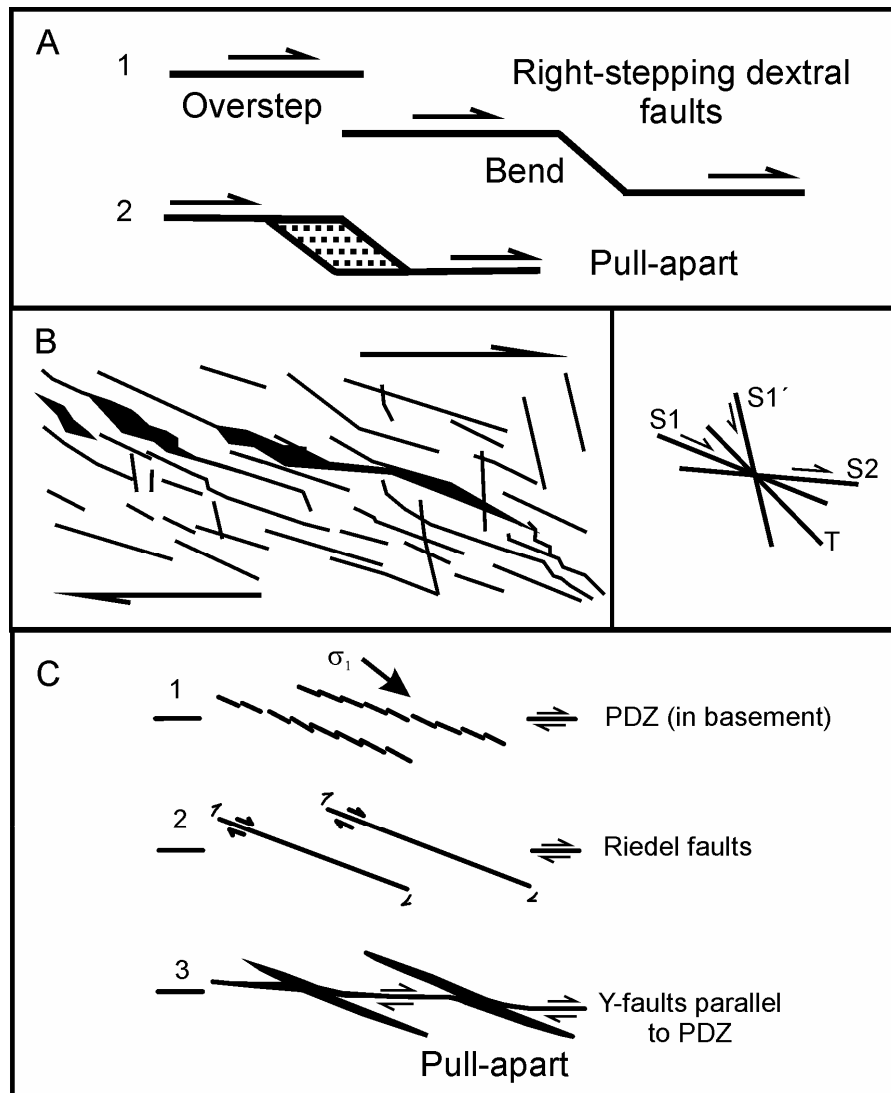


Fig. 2. Three mechanisms for the development of pull-apart basins. A) En echelon right-stepping dextral strike-slip faults. Pull-apart basins form at the overstep or bend (Mirror image for the left-stepping sinistral faults). B) Distributed shear. Pull-apart basins form during linking and coalescence of main faults. S_1 and S_1' are primary synthetic and antithetic strike-slip faults respectively. T and S_2 are tension and secondary synthetic strike-slip faults respectively (simplified from An and Sammis, 1996). C) Riedel shear. 1) Initiation and coalescence of first generation shears into Riedel faults. 2) Strike-slip displacement and rotation of Riedel shears. 3) Development of Y-faults, parallel to the principal displacement zone (PDZ). Pull-apart basins form at the passive Riedel faults (modified from Hagglauer-Ruppel, 1991).

Gamond (1983, 1987) described a similar mechanism, based on observations made in direct shear test experiments (unscaled) on overconsolidated varved clays. Although shear is involved, direct shear test does not simulate strike-slip tectonic conditions.

The development of pull-apart basins has been extensively investigated theoretically (e.g. Rodgers, 1980; Segall and Pollard, 1980), numerically (e.g. Gölke et al., 1994; Katzman et al., 1995), and experimentally for two en echelon strike-slip faults in the basement (e.g. Hempton and Neher, 1986; McClay and Dooley, 1995; Rahe et al., 1998). Their development by the Riedel shear mechanism is not yet sufficiently investigated. For such type of experiments, the boundary conditions and the material properties may control the development of the pull-apart structures during deformation.

In this study we performed clay analogue experiments to study the formation of pull-apart basins by the Riedel shear mechanism. The aim is (1) to gain insight into the structural and kinematic evolution of pull-apart basins and associated structures above a single strike slip fault in the basement, (2) to explore the boundary conditions and the properties of clays relevant for the scaling with respect to sediments and sedimentary rocks in geological models, and (3) to explore the influence of the shear strength of the clay and the thickness of the clay slab on the development of the structures, with the perspective of appropriate scaling.

1.2. ORGANISATION OF THE THESIS

The thesis is organised as follows: **chapter 2** summarizes the characteristics of pull-apart structures and secondary features formed in the experimental studies of previous workers on strike-slip zones. Next the parameters needed for the dynamic scaling of tectonic models are presented and discussed in **chapter 3**, with special regard to clay material. In **chapter 4** the physical and mechanical properties, as well as the different states and conditions of clay material is analysed for the first time. The relevant conditions and parameters for geological modelling are pinpointed, and a practical method for their determination is presented and applied on the clay used for the following experiments. **Chapter 5** describes the experimental

set-up and a simple method for the measurement of heights using normal two-dimensional photos. **Chapter 6** deals with the results of the clay analogue experiments. The initiation and evolution of the observed structures of interest are analysed, as well as the influence of the thickness and of the shear strength of the clay slab on their development. The experimental results are compared in **chapter 7** with previous sand and clay Riedel experiments from the literature. In the light of the new experimental results natural examples are presented in **chapter 8**, which are subsequently compared, discussed and interpreted in **chapter 9**. Finally **Chapter 10** summarizes the main results of this study, and makes some suggestions for further work.

CHAPTER 2: PREVIOUS ANALOGUE EXPERIMENTS ON PULL-APART BASIN FORMATION

2.1. INTRODUCTION

Here we give a short account of previous analogue experiments on the formation of pull-apart basins by the three principal mechanisms outlined in chapter 1.

2.2. ANALOGUE EXPERIMENTS OF EN ECHELON MECHANISM

In en echelon strike-slip basement fault experiments the set-up consists of two straight basement discontinuities laterally offset to form a stepover of pre-determined geometry (set-up 1 in Fig. 3). The location and geometry of the modelled pull-apart structures are primarily controlled by the prescribed geometry in the basement, such as varying separation and overlap distances (e.g. McClay and Dooley, 1995; Dooley, and McClay, 1997). In order to create a pull-apart structure, the basement faults are either right-stepping with dextral shear motion, or left-stepping with sinistral shear (set-up 1 in Fig. 3). When the stepping or the sense of motion is reversed, push-up ridges form instead in the modelling material. However, both pull-apart and push-up structures cannot develop simultaneously with this configuration. In order to do so, two right- and left-stepping basement discontinuities are necessary. In the en echelon mechanism the nature of the material used to simulate the sedimentary cover does not play a major role. Experiments performed with different sands and clays resulted always in the formation of pull-apart structures (e.g. Hempton and Neher, 1986; Dooley and McClay, 1997).

2.3. ANALOGUE EXPERIMENTS OF DISTRIBUTED SHEAR MECHANISM

The distributed strike-slip experiments are based on distributed flow in a weak layer (set-up 2 of Fig. 3). This can be simulated using a rubber or foam plastic sheet, or with sophisticated designs using multiple Plexiglas bars (Schreurs and Coletta, 1998; Schreurs, 2003) or multiple block units moving relative to each other in simple shear (Hoeppener et al., 1969).

The experiments of An and Sammis (1996) were based on gravity sliding of a clay slab on a tilting board. In such experiments, the materials used to model the sedimentary cover are mainly clays (Cloos, 1955; Hoepfner et al., 1969; An and Sammis, 1996). The pull-apart structures observed by Cloos (1955) and Hoepfner et al. (1969) mainly originated along primary shear fractures, while those developed in the experiments of An and Sammis (1996) were bound by primary (s_1 or s_1') and secondary shear fractures or tension joints (s_2 and T; Fig. 2B).

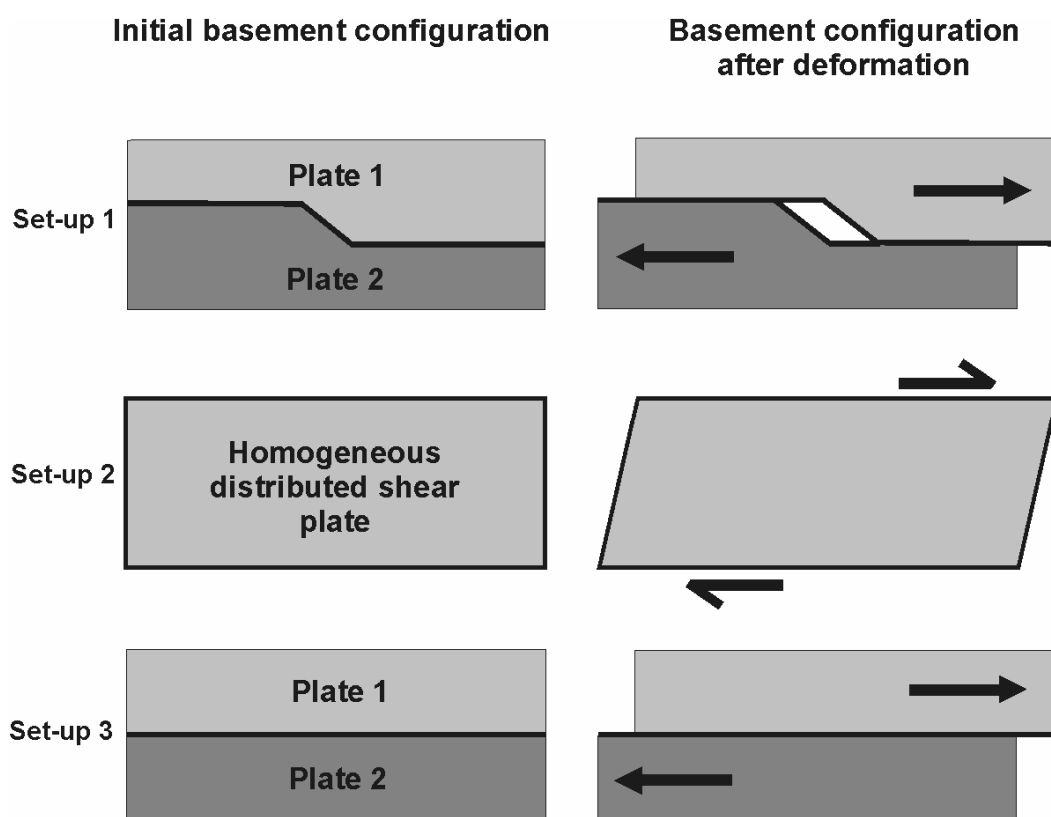


Fig. 3. Basement configuration of the three mechanisms in Figure 1 before and after deformation. Setup 1: two offset discontinuities for the en echelon mechanism. Here the dextral basement discontinuities are right-stepping. For pull-apart structures formed at left-stepping sinistral basement faults, see mirror image. Setup 2: simple shear of a basal plate for the distributed shear mechanism. The basal plate consists of a rubber or foam plastic sheet, multiple Plexiglas bars, or multiple block units moving relative to each other. Setup 3: one straight basal discontinuity for the Riedel shear mechanism.

2.4. ANALOGUE EXPERIMENTS OF RIEDEL SHEAR MECHANISM

The Riedel type experiments simulate the transfer of deformation from a reactivated single and straight strike-slip fault in the basement into an overlying initially undeformed

sedimentary cover. In the experiments, the single fault in the basement is simulated by two adjoining rigid plates, one of which can be moved parallel to the boundary in a dextral or sinistral manner (Cloos, 1928; Riedel, 1929, see set-up 3 of Fig. 3). In accordance with the stepping sense and the motion of the Riedel shear fractures, push-up ridges are mostly expected to form in the models (Fig. 4). Pull-apart structures bound by synthetic Riedel shears might have formed in the original clay experiments of Riedel, since he noted the opening of the synthetic shears at a later stage of deformation (Riedel, 1929, p. 363). For this type of experiments, the properties of the material used for the simulation of the sedimentary cover are suspected to play a crucial role. In the wet clay experiments of Hagglaue-Ruppel (1991), very small pull-apart structures formed occasionally at the earliest small shear fractures, similar to the distributed shear experiments described above, but also at Riedel shears (Fig. 1C). Additionally, push-up ridges formed between some neighbouring Riedel shears. Soula (1984) obtained similar results using sand and talc as analogue materials. The results of Soula (1984) and Hagglaue-Ruppel (1991) are significantly different from the Riedel type strike-slip experiments of earlier workers (e.g. Tchalenko, 1970; Wilcox et al., 1973; Mandl, 1988); possible reasons are discussed in a later section with respect to differences in material properties.

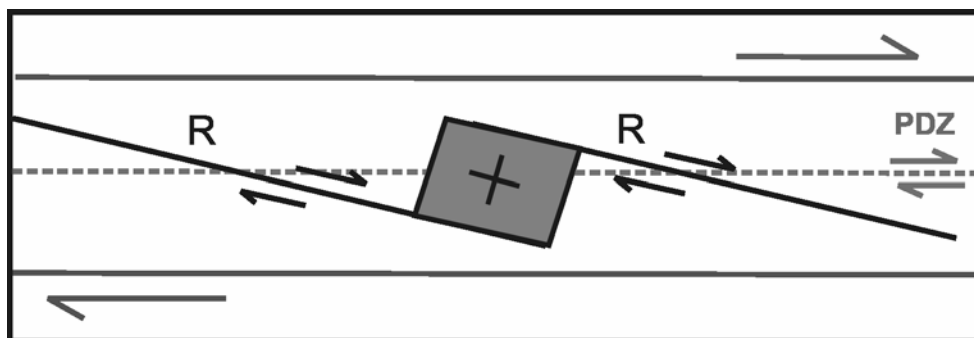


Fig. 4. Formation of a push-up ridge (grey field) between two adjoining Riedel shears (R). The dextral motion along the strike-slip discontinuity in the basement (PDZ) generates dextral left-stepping Riedel shear fractures in the overlying slab. The area between the neighbouring shears is under contraction.

CHAPTER 3: DYNAMIC SCALING OF TECTONIC MODELS

3.1. HISTORICAL USE OF TECTONIC MODELS

Tectonic physical models have been used since the 19th century to study and develop a better understanding of a wide range of geological structures and processes. Summers (1932) reviewed 80 references to the literature prior to 1930, mainly in the Anglo-Saxon countries. Belousov (1961) and Belousov and Gzovsky (1965) on the other hand focused mainly on the extensive work performed in the Soviet Union. The range of experimental set-ups as well as of analogue materials was extremely wide. The materials used in those early experiments included clay, paraffin, sand, and plaster of Paris, as well as bees-wax, jelly and cheese for their particular rheology. The series of clay experiments Cloos carried out in the 1920s, followed closely by Riedel (1929), had a large impact on later studies. They played a major role in the establishment of the concepts of experimental tectonics.

3. 2. THEORY OF SCALING OF TECTONIC MODELS

The application of scaled models is common and bears successful results in the engineering and geotechnical disciplines. Its spread into tectonics and structural geology, and its wide acceptance by the geological community is due to Hubbert (1937). In order to understand how a “rheologically weak” material, such as clay or sand, can simulate the deformation of much stronger rock materials, Hubbert developed a scale theory. This is based on the concept of similarity, where the geometrical, kinematic and geodynamic properties of the model and the modelled systems are related proportionally (Hubbert, 1937). At the upper parts of the crust formed of sediments and sedimentary rocks, the parameters that are scaled are the shear strength (τ), density (ρ), gravity (g) and length (λ) (Fig. 5). They are related in the form of the scaling law below:

$$\tau^* = \rho^* g^* \lambda^* \quad (1)$$

where the superscript (*) denotes the model to nature ratio.

Weijermars et al. (1993) provided a scaling approach specifically for the geological deformation of mainly clastic sedimentary covers. The predictive power of the analogue models depends strongly on the degree of dynamic similarity with the natural system. Thus, detailed knowledge of the rheology of these rocks is necessary in order to constrain the relevant parameters. After Weijermars et al. (1993), brittle or ductile behaviour of the clastic sedimentary rocks depends on the ambient conditions (P, T). Frictional sliding of these rocks at depths above 10 km is described by a Mohr-Coulomb yield criterion, where cohesion is zero MPa, and the friction coefficient “ $\tan \phi$ ” is between 0.25 and 0.52 for argillaceous rocks, and 0.85 for non argillaceous rocks. In this case, the model to nature ratio of shear strength is as follows:

$$\tau^* = \sigma^* \tan \phi^* = \rho^* g^* \lambda^* \tan \phi^* \quad (2)$$

Where σ and ϕ are the normal stress and the angle of shear resistance respectively.

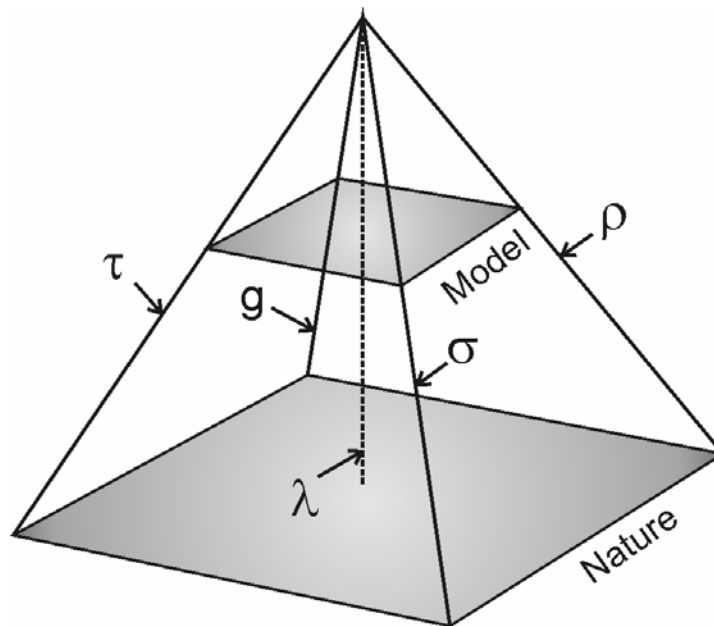


Fig. 5. Allegoric sketch illustrating the concept of the scaling of physical tectonic models for sedimentary rocks. The scaling parameters are: strength (τ), normal stress (σ), density (ρ), gravity (g) and length (λ).

3.3. ROCK PROPERTIES AND BEHAVIOUR TO BE SIMULATED

Sediments and sedimentary covers are nearly fully saturated with fluids below a particular level (water table, sea or water level). The physical, mechanical and hydraulic properties of

the sediments and sedimentary rocks cover a wide range of values related to the degree of lithification (consolidation, cementation) and age (Table 1).

Table 1. Key properties of sediments and sedimentary rocks compiled from Attewell and Farmer (1976), Rummel (1982), Wohlenberg (1982), Shopper (1982), and Carmichael (1990). Some data from rock cores and in-situ rock mass were added (Japan Nuclear Cycle Institute, 2000). The sediments are mainly Neogene soft rocks composed of argillaceous (mudstone) and arenaceous (sandstone) alternating layers.

		SEDIMENTS	SEDIMENTARY ROCKS
Physical properties	Bulk Density ρ [kgm^{-3}]	1.2 – 2.45	1.55 – 2.84
	Specific gravity G_s [-]	2.70	
	effective porosity n_e [%]	30	2
Mechanical properties	Unconfined compressive strength UCS [MPa]	5 – 25	22 - 175
	Youngs modulus E [MPa]	1 500 - 5 000	37 000
	Poisson's ratio ν [-]	0.30	0.25
	Cohesion c [MPa]	1 – 5	8 - 105
	Internal friction angle ϕ [°]	25 – 30	28 - 45
	Tensile strength σ_t [MPa]	2 – 10	15 - 25
	Lateral pressure coefficient K_0 [-]	$164/h + 0.74$ (h: depth or thickness [m])	
	Initial vertical stress σ_v [MPa]	$\rho h/100$ ($\equiv \rho g h/1000$) (g: gravitational acceleration [m s^{-2}])	
	Initial horizontal stress σ_h [MPa]	$K_0 \times \sigma_v$	
Hydraulic properties	Hydraulic conductivity k [ms^{-1}]	10^{-10} to 10^{-8} to 10^{-5} when fractured	

Of all these properties, the cohesion c needs careful handling. The values of c are mostly measured from small and intact samples (Rummel, 1982; Carmichael, 1990). These values are known to decrease when sample dimension increases, due to the presence of joints fissures and fractures (Pinto da Cunha, 1993). How much is the cohesion reduced for the bulk sedimentary rocks at a basin or regional scale is left to the decision of the geoscientist. Most of the geologists using analogue modelling approach prefer to ignore cohesion on the assumption that at such scales its value becomes negligible. In the geomechanics and

geotechnical and petroleum disciplines empirical methods are developed to estimate cohesion of rock masses taking into account the scaling effects. The characterisation of the rock masses is based on large scale in-situ tests. The results reveal the noticeable presence of cohesion in the sediments (up to 5 MPa in Table 1), and its significance in the Tertiary sedimentary rocks not affected yet by tectonism (up to 40 MPa, e.g. Japan Nuclear Cycle Institute, 2000). The impact of a non-negligible cohesion on the scaling and the results of tectonic models still needs to be discussed.

Although the upper part of the crust is brittle and strength is generally governed by friction, the sedimentary cover shows a distinct behaviour. Both brittle and ductile deformation is possible, especially at depths of less than 6 km. The presence of pore fluids strongly affects the physical, hydraulic, thermal and mechanical properties of these rocks. Furthermore, their deformation driven by tectonic stresses depends on porosity, rock composition and water content (e.g. Bjørlykke, 1997; Maltman, 1994). The coupling of these properties is already present in the example of a subsiding and partly overpressured basin that is not affected yet by tectonism (Bjørlykke, 1997). At depths less than 2.5-4 km, sandstones and shales are usually poorly cemented and ductile, whereas at higher depths limestones and carbonate-cemented shales become brittle and fluids flow in fractures. However, overpressure reduces the effective stress and favours brittle deformation of the shallow sediments. Also, diagenetic processes such as dissolution and precipitation may cause well-cemented sandstones and limestones to deform in a ductile way in response to long-term (geologic) stress. This behaviour is not shown by short-term laboratory tests. At great depth increased cementation causes the sedimentary rocks to be more brittle, although the increasing confining pressure and temperature prevent it and make the rocks more ductile. In the deeper parts of the basin clayey rocks dehydrate, their permeability becomes very small, and in overpressured areas much of the flow is controlled by hydro-fracturing. Tectonic forces may generate similar dual (ductile and brittle) behaviour in the sedimentary cover.

3.4. PROPERTIES AND BEHAVIOUR OF MODELLING MATERIAL

Fine grained particulate materials such as sand and clay are the most widely chosen materials in tectonic physical modelling. Dry sand became increasingly employed since the 1980's. It is considered as the ideal representative of a purely frictional material to simulate the brittle behaviour of the upper crust (e.g. Hubbert, 1951, 1988; Krantz, 1991; Schellart, 2000), although the elasto-plastic behaviour of sand has been experimentally proved (Bolton, 1986; Wood, 1990; Lohrmann et al., 2003). In contrast, the present study is based on the use of wet clay as analogue material for sedimentary rocks.

3.4.1. Motivations for choosing clay as the modelling material

One of the aims of this study is to explore the influence of the shear strength of the modelling material on the development of the deformational structures formed by the Riedel shear mechanism. Shear strength is easily varied in clays through variation of the water content. Also, the presence of water in this material simulates closely the wet condition of the represented sediments and sedimentary rocks described above. In wet state, other effects related to the nature of clays are worth to be considered. For example, it might be possible to scale the grain size, which is known to control the thickness of the shear fractures and zones (shear bands in soil mechanics). Another reason for choosing this material is that the development of pore pressure during deformation, and the influence of the primary anisotropy related to shape preferred orientation of the grains can be investigated.

However, a laboratory constituted clay is suitable for the purpose of analogue modelling, provided that its strength parameters (cohesion and friction angle) are scalable. The sediments and sedimentary rocks are dynamically scaled in clay models only if the cohesion of the used clay is negligible, and if the angle of internal friction corresponds to that of the sedimentary rocks (Weijermars et al., 1993).

3.4.2. Previous tectonic clay models

A review of previously published physical clay models reveals the scarcity of data related to the physical properties and appropriate mechanical properties of the materials (Table 2), with the exception of studies by Tchalenko (1970) and Sims (1993). The clays described by Tchalenko (1970) were overconsolidated clays of high shear strength (about 200 kPa). The cohesion intercept and the angle of internal friction were about 10 kPa and 23° respectively. These parameters were determined for an effective stress level considered to be characteristic for geotechnical purposes (i.e. between 200 and 400 kPa), but exceedingly high for physical modelling of tectonic processes. For comparison, the stresses generated by tectonic experiments with clays are typically below 3 kPa (Oertel, 1965; Reches, 1988). It is well known that large errors can result from using shear parameters extrapolated from tests at higher pressures, due to curved failure envelopes for most soils (Maksimovic, 1996). Thus the Riedel shear experiments of Tchalenko (1970) were not scaled for cohesion or shear strength, and the shear parameters were not determined at the stress levels pertinent to the experiments. Nevertheless, the study has brilliantly demonstrated the similarities of shear zones at different scales.

Table 2. Boundary conditions and shear parameters of previous physical clay models. (-): means no information is given. (*): references from the geotechnical disciplines.

Clay	Type of test	Stress range	Cohesion intercept	Friction angle	Reference
Kaolin Hydrite R	direct shear	200-1600 Pa	140 Pa	28°	El-Gharbawy 1998*
Kaolin Hydrite R	thin specimen direct shear	1-2400 Pa	50 Pa	55°-9 log (σ'_n)	Pedersen et al. 2003*
Kaolinite (66%) bentonite (33%)	unconfined compression	< 10 kPa	-	-	Lazarte and Bray 1996*
Kaolin	direct shear	220-440 kPa	10 kPa	23°	Tchalenko 1970
Kaolin	direct shear	-	46 Pa	28°	Sims 1993

Sims (1993) presented soil laboratory results of a kaolinitic clay intended for geologic scale-models. He selected the appropriate stress range to be applied in direct shear box tests, similar to the stresses generated by an about 4 cm thick clay slab. The technical problems generated in testing because of the very soft consistency of the clays, and the time it takes to determine the effective shear parameters under drained conditions (it takes at least 3 days and up to two weeks, depending on the permeability and thickness of the soil) makes this method difficult and time consuming. Moreover, traditional soil mechanics had developed strength models for two basic classes of soils; sands being frictional and brittle, and clays being cohesive and ductile, neither being appropriate for the description of the clay pastes used in analogue modelling. Modern soil mechanics demonstrated that the traditional concepts to describe soil behaviour need to be replaced by new ones taking into account the state of the material and the boundary conditions

Consequently, the present study aims to specify the physical and mechanical properties of clays at the conditions typical for tectonic experiments, in order to use them for scaled geologic models. This part is developed in the following chapter.

CHAPTER 4: MECHANICAL PROPERTIES OF SOFT CLAY USED IN ANALOGUE EXPERIMENTS

4.1. INTRODUCTION

Laboratory constituted clays are excellent analogue materials to simulate brittle and ductile deformation in a sedimentary cover, because of the following advantages:

- a- high deformability,
- b- brittle and ductile behaviour,
- c- wide range of variation in strength,
- d- delicate and persistent structural pattern.

Requirements (b) and (c) are mainly achieved through the variation of the water content of clay pastes. For this purpose, the clay paste needs to be statistically isotropic and homogeneous, i.e. laboratory constituted and not an “as is” natural deposit.

In view of dynamic scaling laws, Cloos (1928) and Hubbert (1937) emphasized that the clay pastes appropriate for tectonic analogue experiments must be of extremely low shear strength, which can only be achieved at water contents at or beyond their Atterberg liquid limit (Whitlow, 2001). The consistency of such clay pastes is simply inconvenient for soil mechanics and geotechnical laboratory testing, e.g. in direct shear or triaxial compression. So far no standard method is available to measure stresses and strains in extremely soft clays, loaded at very low effective stresses. However, modern soil mechanics provided the base to develop a suitable method taking into account the state of the material and the boundary conditions (see below). First, a short outline of those aspects of clay behaviour, relevant in tectonic analogue experiments is given. For the background, the reader is referred to textbooks on basic soil mechanics concepts (e.g. Whitlow, 2001), and on critical state soil mechanics theory (Schofield and Wroth, 1968; Atkinson and Bransby, 1978; Wood, 1990). To scale the clay experiments we need clays of extremely low shear strength and with a critical shear angle at failure similar to that of rocks in nature. In addition, we need to know the density of the clay paste at a specified water content. Physical and mechanical properties

of the clay need to be determined at the state and at boundary conditions close to those used in the analogue experiments. Therefore a new procedure to determine the basic properties of modelling clays is introduced. It is based on routine tests performed in soil mechanics laboratories, on available correlations between the determined physical properties and the shear strength parameters, and on the material state (e.g. physical and mechanical properties, degree of saturation) and boundary conditions (e.g. drainage condition, stress ratio, type of performed test).

4.2. PHYSICAL STATE CONDITIONS IN ANALOGUE MODELLING

4.2.1. Consolidation state

Soil mechanics usually classifies clays into two categories: normally consolidated clays and overconsolidated clays. The consolidation state here refers to the stress history of a natural clay since deposition, the reduction of volume or porosity during and after loading (Ladd et al., 1977; Terzaghi et al., 1996). The data are usually presented in terms of the overconsolidation ratio (OCR), calculated by

$$\text{OCR} = p'_c / p'_i \quad (3)$$

where p'_c is the yield stress, also known as preconsolidation stress, a measure of the highest stress the soil has ever experienced, and p'_i is the current mean stress.

An OCR value of 1 represents a normal consolidation state, a state in which the maximum mean stress previously experienced by a material was not larger than the current mean stress. A larger value ($\text{OCR} > 1$) describes an overconsolidated state whereby past mean stress was larger than present mean stress (i.e. loaded and then unloaded).

The constituted clay is a clay-water mixture prepared in the laboratory, and thus not subject to the typical process of consolidation. While a geoscientist would probably regard the constituted clay as being in unconsolidated state, it would be considered as normally consolidated in soil mechanics ($\text{OCR}=1$). The mixture is closer to remoulded clay, a material that has been thoroughly blended and stirred.

4.2.2. Atterberg limits and degree of saturation

In scaled clay models, a clay-water mixture is prepared to obtain a very low shear strength, and a consistency which allows easy handling and preparation of clay slabs. Most clays will display an extremely low shear strength at their liquid limit and beyond it (Atterberg's W_L). At this state the clays are fully saturated or nearly so. Originally used for soil classification purposes, the Atterberg liquid (W_L or LL) and plastic limits (W_P or PL) are the bounding water contents between which the consistency of the soil is plastic. Consistency at this point is a physical state characteristic at a given water content. The range of plastic states is given by their difference and is termed plasticity index (I_P or PI):

$$I_P = W_L - W_P \quad (4)$$

These consistency limits are determined by standard test routines in soil mechanics laboratory. Full details of the procedures and apparatus are given in various standards (e.g. British Standard 1377, American ASTM D4318, German DIN 18122). The Atterberg limits reflect the mineralogical characteristics of the clay size fraction (CF), and are directly related to the mechanical properties of clays (see below).

4.2.3. Drainage condition

When a clay material is sheared under applied stresses, an excess pore pressure is produced, the dissipation of which depends mainly on the permeability and the time available. If pore pressure dissipates, the material is drained. If the dissipation rate is too low, the modelling material is undrained, and the increase in total stress results in an equal increase in pore pressure. Clays and silty clays have a very low permeability. The analogue experiments last up to 4 hours. This time span is too short for a significant amount of water to be drained out or infiltrated during the experiment, which means that undrained conditions prevail.

4.3. SHEAR STRENGTH OF MODELLING CLAY

4.3.1. Introduction to Critical state soil mechanics

Critical state soil mechanics (Schofield and Wroth, 1968) provides a unified elastic-plastic model of soil behaviour in which stress and volume states are interrelated. It should not be confused with the "critical state" in critical taper theory (Davis et al., 1983; Dahlen et al., 1984), although both are based on the Coulomb failure criterion. The concept was initially developed for remoulded saturated clays and since then has been extended to sand (Bolton, 1986; Wood, 1990) and more recently to sediments and rocks (e.g. Jones, 1994; Zhu et al., 2002).

4.3.2. Shear strength of modelling clay

Mechanical tests show that the shear strength of clays depends primarily on the consolidation state. In the undrained condition, pore pressure increases in response to loading and becomes constant at the critical state, while the volume is kept constant throughout shearing. At failure there is a unique relationship between the critical shear stress, the normal stress, and the critical specific volume (void ratio). It occurs after a strain between 5% and 40%, depending on the plasticity index of the material, at a point on a three-dimensional failure envelope called the state boundary surface (Fig. 6A). The Critical State Line (CSL), a curved failure line on the state boundary surface represents the boundary between elastic and plastic behaviour. This line is defined by the deviatoric stress q'_{cs} , the mean normal stress p'_{cs} , and the specific volume v_{cs} for triaxial tests (Fig. 6B), defined by

$$q'_{cs} = \sigma'_1 - \sigma'_3 \quad (5)$$

$$p'_{cs} = 1/3 (\sigma'_1 + 2\sigma'_3) \quad (6)$$

$$v_{cs} = 1 + e_{cs} \quad (7)$$

where σ'_1 and σ'_3 are the maximum and minimum effective stress, and e_{cs} is the void ratio at the critical state. The void ratio e of a material is defined as the ratio of the voids volume to the volume of solids of the material:

$$e = V_v / V_s \quad (8)$$

where V_V and V_S are the volume of voids and the volume of the solid particles respectively.

For direct shear tests the axial parameters of CSL are the shear stress at failure τ_{CS} , the effective normal stress σ'_{CS} and the void ratio e_{CS} (Fig. 6B).

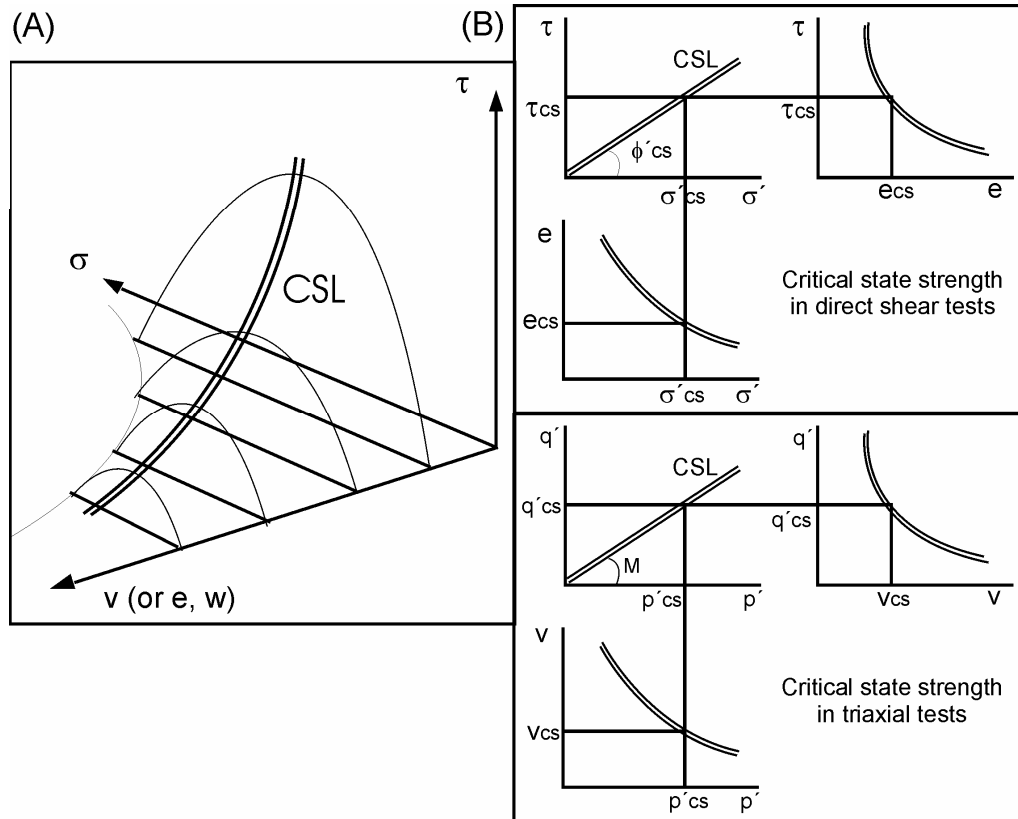


Fig. 6. A) 3D projection of the critical state line CSL (double line) on the state boundary surface (curved lines). B) The critical state line CSL in direct shear and triaxial tests (from Atkinson and Bransby, 1978). See text for explanation.

A series of tests on a normally consolidated clay will produce a critical state line passing through the origin ($\sigma' = 0$, $\tau_f = 0$), and the critical state strength is written:

$$q'_{CS} = M p'_{CS} \quad (9)$$

where M is a constant for a particular material. This is related directly to the Mohr-Coulomb failure equation, which is:

$$\tau_f = \tau_{CS} = \sigma'_{CS} \tan \phi'_{CS} = (\sigma - u) \tan \phi'_{CS} \quad (10)$$

where

τ_{CS} is the the failure shear stress at the critical state,

σ'_{CS} is the effective normal stress at the critical state,

ϕ_{cs}' is the angle of shear resistance at the critical state,

σ is the total normal stress,

u is the pore pressure

For the triaxial compression tests M and ϕ_{cs}' are related through:

$$M = (6 \sin \phi_{cs}') / (3 - \sin \phi_{cs}') \quad (11)$$

Dilatancy effects in normally consolidated clays are negligible to zero. Remoulded normally consolidated clays have no cohesion. The latter is explained in terms of an inadequate testing stress range, and any true cohesion in terms of effective stresses is either zero or very small (e.g. Bolton, 1979; Santamarina, 1997). The physical state of the material and the type of test used to determine the shear strength should match the conditions attained in the tectonic analogue experiments as close as possible.

Under undrained conditions, saturated fine grained soils will apparently display a constant limiting shear stress S_u at all values of normal stress, since the volume remains constant. The increase in total normal stress induces a similar increase in pore pressure. In this case the total stress envelope is parallel to the normal stress axis, the angle of friction (ϕ_u) is zero, and the strength envelope intercepts the shear stress axis at S_u (Fig. 7A). This value corresponds to a particular water content and specific volume. However, the scaling of models is based on the effective stress principle, in which the effective principal stress is the difference between the total principal stress and the pore water pressure (Terzaghi, 1936). As S_u depends on the effective normal stress in the soil, the effective stress parameters can be obtained provided the pore pressure at failure is known (Fig. 7B).

4.3.3. Influence of clay mineralogy and fraction on clay behaviour

Recent experimental investigations reveal that clay mineralogy affects soil behaviour (Sridharan, 2002). It emerged that the behaviour of fine grained materials at the liquid limit can be classified into two end members, kaolinitic and montmorillonitic materials, with contrasting behaviour. According to Sridharan (2002) the mechanical behaviour of kaolinitic clays is controlled by the frictional resistance at the interparticle contacts. Volume or

deformation changes occur by the shear displacements or by the sliding between the particles or both. The behaviour of montmorillonitic materials is controlled by the viscous nature of the diffuse double layer of water and its thickness.

The rheological behaviour and the shear strength of clays secondarily depend on the proportions of clay and other minerals, and on the water content. The shear strength is related to the plasticity index I_P and to the clay size fraction CF, i.e. the fraction of particles with a diameter below 2μ .

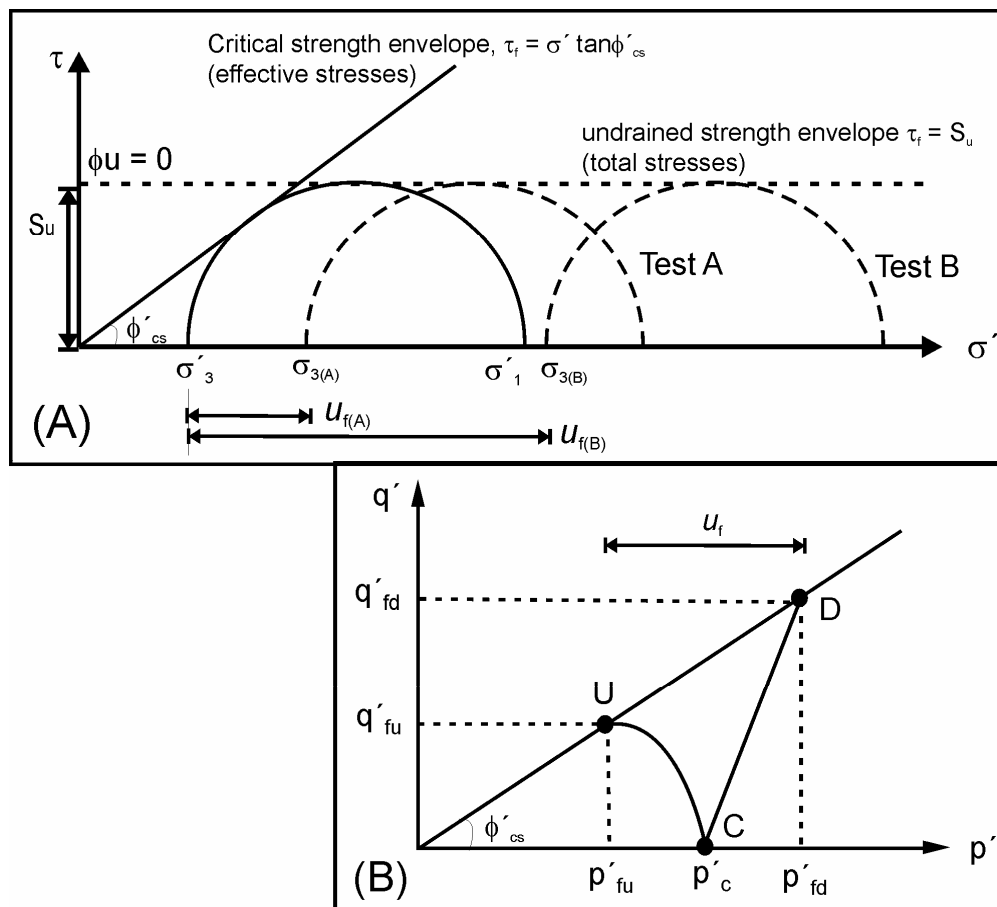


Fig. 7. A) Undrained (total) and critical (effective) strength envelopes for normally consolidated clays. B) Graph showing the location of the drained (D) and undrained (U) failure points on the CSL. q'_{fd} and p'_{fd} are the drained effective deviatoric and mean normal stresses at failure. q'_{fu} and p'_{fu} are the undrained effective deviatoric and mean normal stresses at failure (modified from Whitlow, 2001).

4.4. DETERMINATION PROCEDURE OF MODELLING CLAY PROPERTIES

The properties needed for the scaling of the models to nature are the undrained shear strength and the bulk density of the used clay; as well as the related critical shear angle at failure. These are to be determined together with the degree of saturation.

4.4.1. Determination of the degree of saturation

The degree of saturation S_r is the quantity of water present in the voids of the material, expressed by

$$S_r = V_w / V_v \quad (12)$$

V_w and V_v being the volume of water and of voids respectively.

The degree of saturation ranges from $S_r = 0$ for a perfectly dry soil, to $S_r = 1$ for a fully saturated soil. It is related to the water content of the clay material (w), also termed moisture content or humidity in soil mechanics literature. w is the ratio of the weight of water contained in the pores to the weight of the solid dry material in a soil expressed as a percentage:

$$w = M_w / M_s \quad (13)$$

where M_w and M_s are respectively the mass of water and the mass of the solid particles contained in the material. It is usually obtained in the laboratory after measuring the mass of a wet sample and the mass of the same sample when completely dry.

There is a close relationship between the degree of saturation S_r , the void ratio e , the grain specific gravity G_s , and the water content w of the clay material through:

$$S_r e = w G_s \quad (14)$$

where G_s is the grain specific gravity of the material, defined as the ratio of the mass of a given volume of the material to the mass of the same volume of distilled water at 20°C. It is determined with a specific standard test procedure (e.g. pycnometer) in soil mechanics laboratory. Thus, the degree of saturation can be calculated provided that the basic material properties above are determined.

4.4.2. Determination of the undrained shear strength

The shear strength of a material should be determined in similar conditions to those found in the tectonic analogue experiments. The shear strength of a clay paste at a certain water content and specific volume under undrained conditions is S_u in terms of total stresses (or τ_f ; see eq. (10) and Fig. 7A), and is equivalent to the effective shear strength since water carries no shear stresses (Bolton, 1979). The undrained shear strength is best measured with a

laboratory or a hand operated shear vane (Pilcon/Geonor™, used in this study), which is commonly used in the geotechnical engineering practice. It is easy to handle and offers a direct reading dial that is engraved on the head of the vane. The dial reading values carried out on remoulded clays correspond to critical state ones (e.g. New Zealand Geotechnical Society, 2001). Serota and Jangle (1972) found that the determined values compared well to those obtained in undrained triaxial compression results.

4.4.3. Determination of the critical angle of friction

The critical angle of friction ϕ'_{cs} (see Fig. 7) is generally determined in triaxial compression tests. It is subject to technical problems caused by the extremely soft consistency of the modelling clay, however. An empirical correlation between the plasticity index (I_P in eq. (4)) and the critical angle of friction (ϕ'_{cs}) obtained in triaxial compression tests on normally consolidated clays (e.g. Ladd et al., 1977; Terzaghi et al., 1996) shows that the lower the plasticity index the higher is the critical angle of friction.

Based on the considerations above, silty clays and clays of the kaolinitic group with a low clay fraction ($CF < 50\%$) are most suitable for the purpose of tectonic analogue modelling. They have a low to medium plasticity index ($I_P < 20\%$, and $W_L < 40\%$) and their critical shear angle ϕ'_{cs} ranges between 29° and 38° .

4.5. MATERIAL PROPERTIES OF THE CLAY SLABS

4.5.1. Mineralogical composition and Grain size distribution

The material used to model the sedimentary cover in our strike-slip experiments is a silt-rich clay commercialised for ceramic purposes under the name "Kaolin-O". It is supplied by Erbslöh/Geisenheim Vertb., Germany, whose laboratories determined the mineralogical and chemical compositions (Table 3). The clay minerals are kaolinite and illite. Quartz in the silt-fraction makes up about 30 % of the material. The physical and mechanical properties required for scaling have been determined at the soil mechanics laboratory of the Ruhr-University Bochum, Germany. The errors on the measurements are estimated to be less

than ± 2 on the last digit quoted in the tables; they are considered as insignificant for the present purpose. Kaolin-O, a well graded silty clay, shows a wide distribution of particle sizes (from 1.5 μm to 55 μm), the clay size fraction CF being 45% (Fig. 8).

Table 3. Mineralogical and chemical composition of Kaolin-O, determined by the supplier Erbslöh/Geisenheim Verb., Germany.

Chemical analysis	Si O ₂	Al ₂ O ₃	TiO ₂	Fe ₂ O ₃	CaO	MgO	K ₂ O	Na ₂ O	Loss
Percent.	60.50	25.90	1.00	1.08	0.22	0.30	4.70	0.29	5.85
Mineral analysis	Kaolinite		Illite		Quartz				
Percent.	25		45		30				

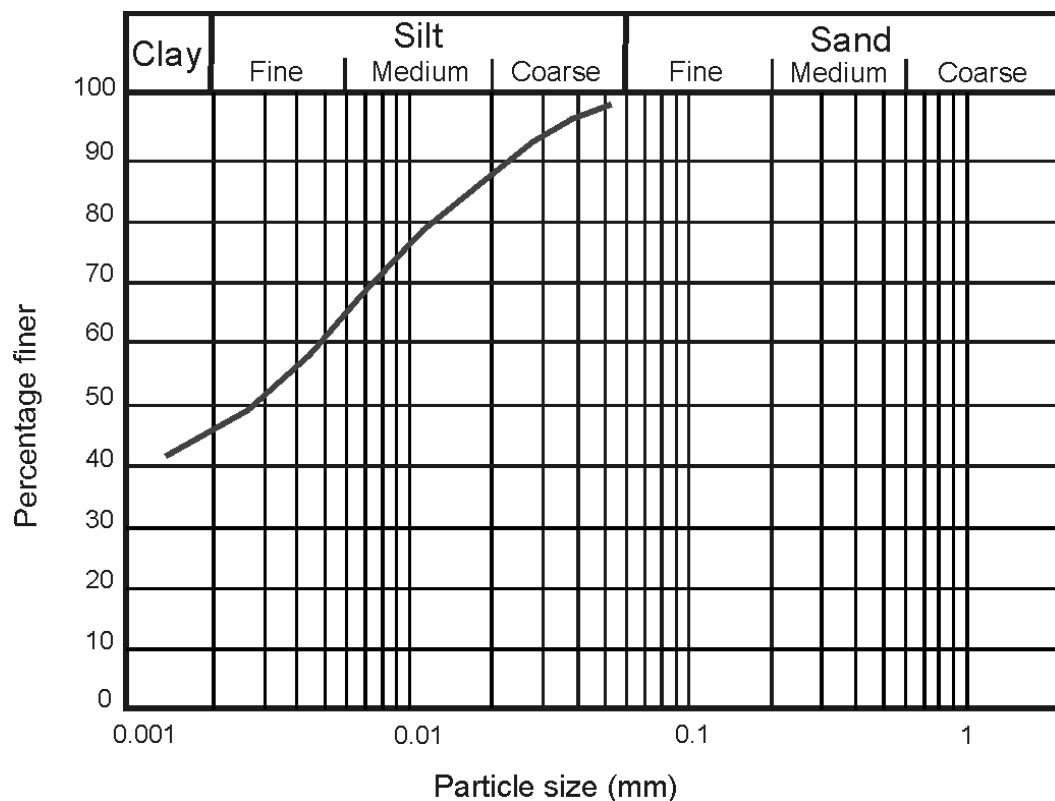


Fig. 8. Particle size distribution curve for Kaolin-O, determined at the soil mechanics laboratory of the Ruhr-University Bochum, Germany according to DIN 18123. The material is a well graded silty clay. It has a wide distribution of particle sizes, from 1.5 μm to 55 μm . The clay size fraction CF of particles below 2 μm is about 45%.

4.5.2. Index properties

The Atterberg liquid and plastic limits of Kaolin-O are determined as 33 % and 23 %, respectively. The corresponding plasticity range I_p is 10% and relatively low. The material is of low plasticity according to the British Soil Classification System of fine-grained soils (Fig. 9).

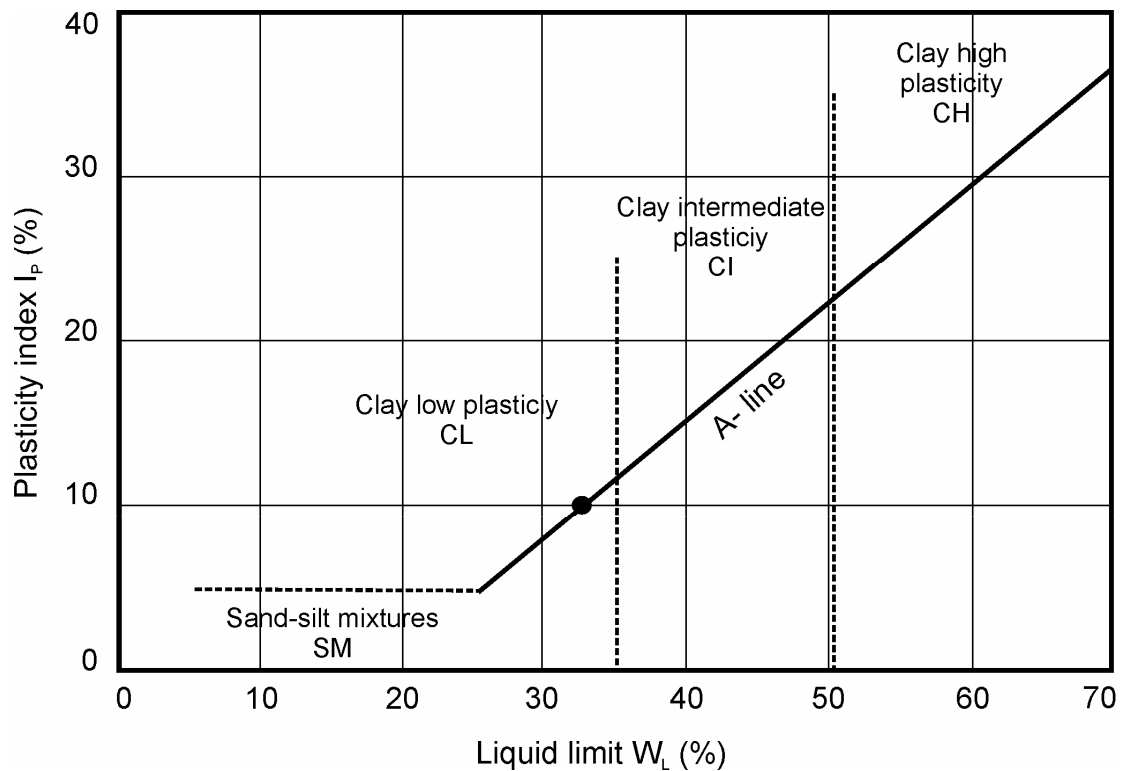


Fig. 9. Kaolin-O within the plasticity chart for classification of fine-grained soils. The consistency limits were determined at the soil mechanics laboratory of the Ruhr-University Bochum, Germany according to DIN 18122. The A-line separates the clay and silty soils. Kaolin-O (black point) being on the A-line and having a W_L below 35%, is classified as a silty clay soil of low plasticity.

4.5.3. Undrained shear strength, densities, void ratio, degree of saturation

The shear strength of the clay pastes was varied by variation of the water content (w , %). For each particular water content w , the corresponding bulk density ρ_b and dry density ρ_d were habitually determined according to specific laboratory testing methods.

The bulk density (ρ_b) is the density of the total sample including pore fluid, and the corresponding dry density (ρ_d) is the ratio of the mass of merely the solid particles to the total volume of the sample:

$$\rho_h = \frac{\text{total mass}}{\text{total volume}} = \frac{\text{mass of solids} + \text{mass of water}}{\text{total volume}} \quad (15)$$

$$\rho_d = \frac{\text{mass of solids}}{\text{total volume}} \quad (16)$$

The bulk density, void ratio, degree of saturation, and the shear strength determined for the three materials used in our experiments, controlled by the water content ($w = 38\%$, $w = 42\%$ and $w = 48\%$), are presented in Table 4. Figure 10 shows the relationship between the water content and both densities. The curves are useful in that they allow the direct extraction of both bulk and dry densities for any particular water content. In a similar manner, the undrained shear strength (S_u) was measured for the clay pastes at various water contents. The shear vane was inserted several times into the material and rotated until the material failed. The plot of the obtained shear strengths in figure 11 for a range of water contents shows a hyperbolic relationship.

Table 4. Bulk density (ρ_b), undrained shear strength (S_u), void ratio (e), and degree of saturation (S_r) corresponding to the water content of the clay pastes (w) used in this study. Note: water content is also termed moisture content or humidity in soil mechanics literature. It is the ratio of the weight of water contained in the pores to the weight of the solid dry material in a given mass of soil expressed as a percentage.

Water content w (%)	ρ_b (g/cm³)	S_u (kPa)	e	S_r (%)
38	1.79	2	1.1	95
42	1.75	1.5	1.2	96
48	1.70	0.5	1.3	99

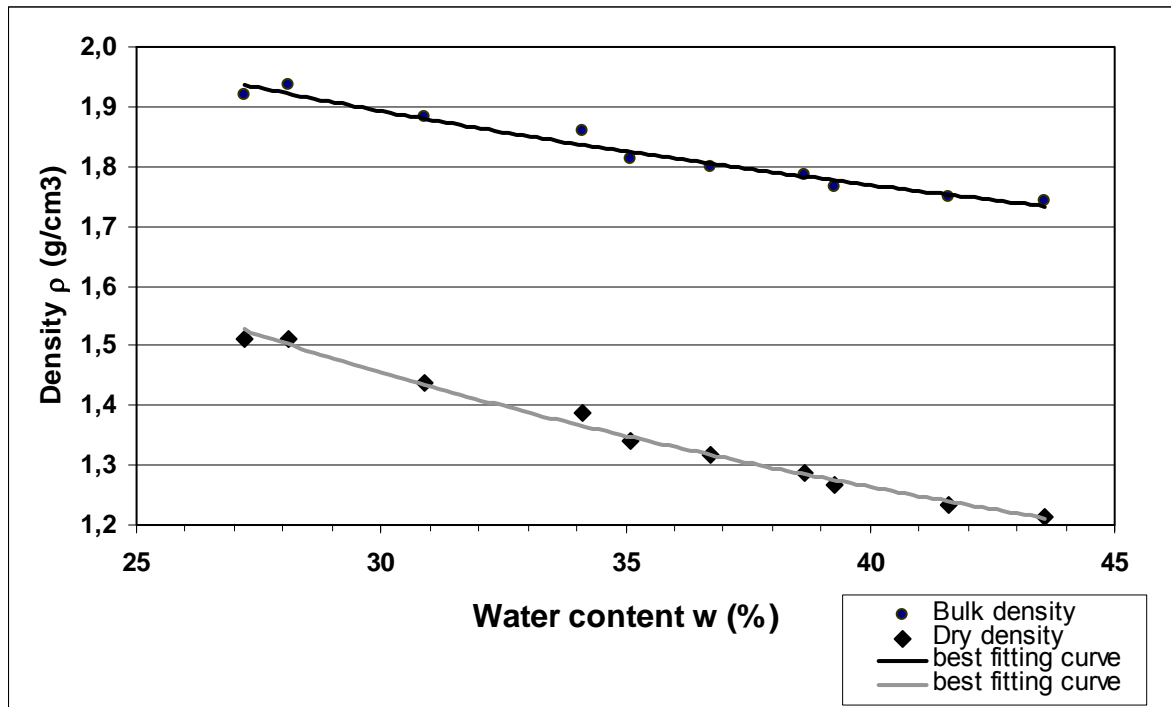


Fig. 10. Dry (ρ_d) and bulk (ρ_b) densities of Kaolin-0 pastes at different water contents w , determined at the soil mechanics laboratory of the Ruhr-University Bochum, Germany according to DIN 18125.

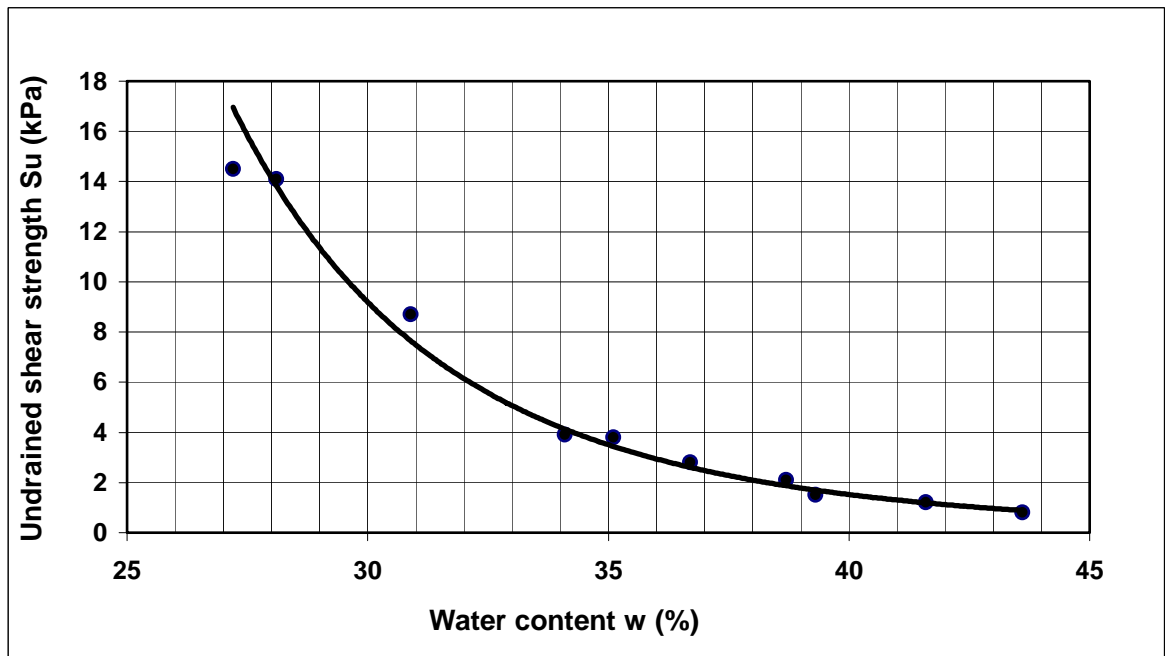


Fig. 11. Undrained shear strength S_u of Kaolin-0 pastes at different water contents w , obtained in hand held shear vane tests. The values were determined at the soil mechanics laboratory of the Ruhr-University Bochum, Germany according to the recommendations of the manufacturer and of the New Zealand Geotechnical Society 2001.

4.5.4. Critical angle of shearing friction

Following critical state soil mechanics (Schofield and Wroth, 1968), the Kaolin-O is classified as a normally consolidated clay; it has no cohesion intercept and fails according to equation (10) at

$$\tau_f' = \sigma' \tan \phi_{cs}'.$$

To derive the angle of internal friction ϕ_{cs}' from the plasticity index of the material we used the empirical correlation curve of Terzaghi et al. (1996), which was obtained from triaxial compression tests on normally consolidated clays. The plasticity index of 10% corresponds to $\phi_{cs}' = 32^\circ$ (Fig. 12).

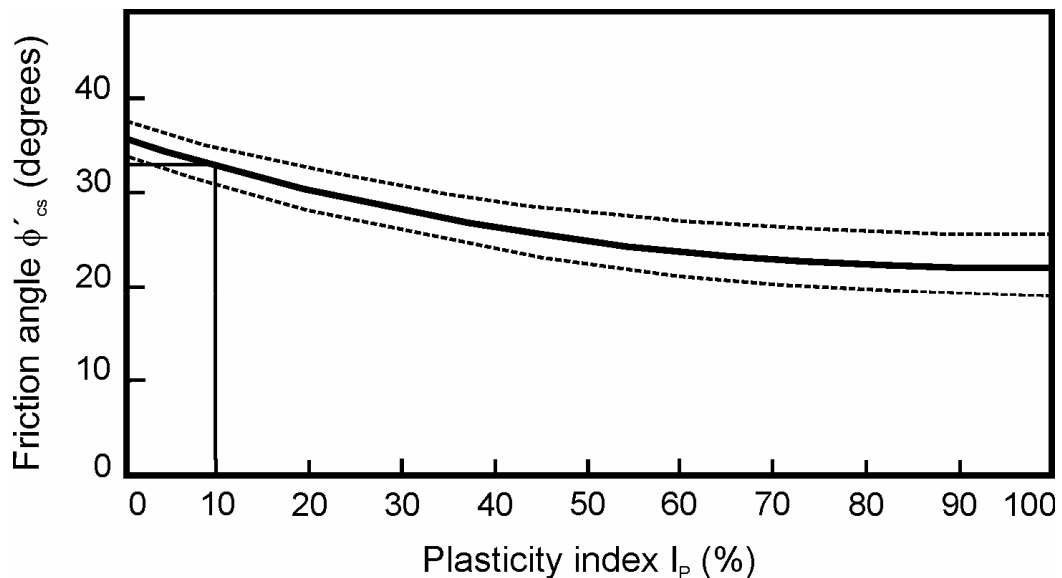


Fig. 12. Empirical correlation between critical friction angle (ϕ_{cs}') and plasticity index (I_p) from triaxial compression tests on normally consolidated clays. The average curve (thick line) is within the standard deviation field (dashed lines) for mainly soft clays. Modified from Ladd et al. (1977) and Terzaghi et al. (1996).

4.6. SCALING OF KAOLIN-O PROPERTIES

Frictional sliding of mainly clastic sedimentary rocks at shallow depths ($z < 10$ km) may be described by a Mohr-Coulomb criterion, as discussed by Weijermars et al. (1993), where cohesion is taken as zero as in our model (see chapter 3.2). In this case, the model to nature ratio of shear strength follows equation (2):

$$\tau^* = \sigma^* \tan \phi^* = \rho^* g^* \lambda^* \tan \phi^*$$

where σ^* , ρ^* , g^* , λ^* and ϕ^* are the model to nature ratios of normal stress, density, gravity, length and friction angle. Provided that the angle of internal friction of the modelling material corresponds to that of sedimentary rocks, this will send us back to the scaling law introduced by Hubbert (1937). Table 5 summarises the scaling properties of the used clays and of sedimentary rocks. The experiments being performed in the same gravity field as in nature, 1 cm in the model corresponds to a length between 50 and 500 m in nature. A 4 cm thick clay slab is then equivalent to a 200-2000 m thick sedimentary cover.

Table 5. Properties of the modelling material and of sedimentary rocks with the scaling ratios.

	Sedimentary rocks	Model	Ratio
Bulk density (g/cm³)	1.7 to 2.7	1.75	0.64 - 1
Shear strength (Pa)	[10 - 100] x 10 ⁶	1.5 x 10 ³	2 x 10 ⁻⁴ to 10 ⁻⁵
Friction angle (°)	25 - 40	32	1

CHAPTER 5: EXPERIMENTAL SET-UP

5.1. THE DEFORMATION TABLE

The Riedel shear experiments were performed on a deformation table designed at the tectonic laboratory at the Ruhr-University Bochum (Brix et al., 1985). The motor-driven deformation table consists of two rigid plates, each 1 m long and 0.5 m wide. One of the plates is fixed to the frame of the apparatus, while the other is moved horizontally at a constant rate of 0.4 mm/min. The discontinuity between the plates simulates a dextral strike-slip fault in the basement, the pre-defined principal displacement zone (PDZ, Fig. 13A). The long dimension of the clay slab can be extended up to 4 m with available accessories mounted on top of the deformation table. The amount of horizontal displacement is read from a fixed ruler, with a pointer connected to the moving plate. Glued sandpaper on the plates assures good adhesion of the clay paste to the surface of the plates, and secures transmission of the basal movement into the clay slab.

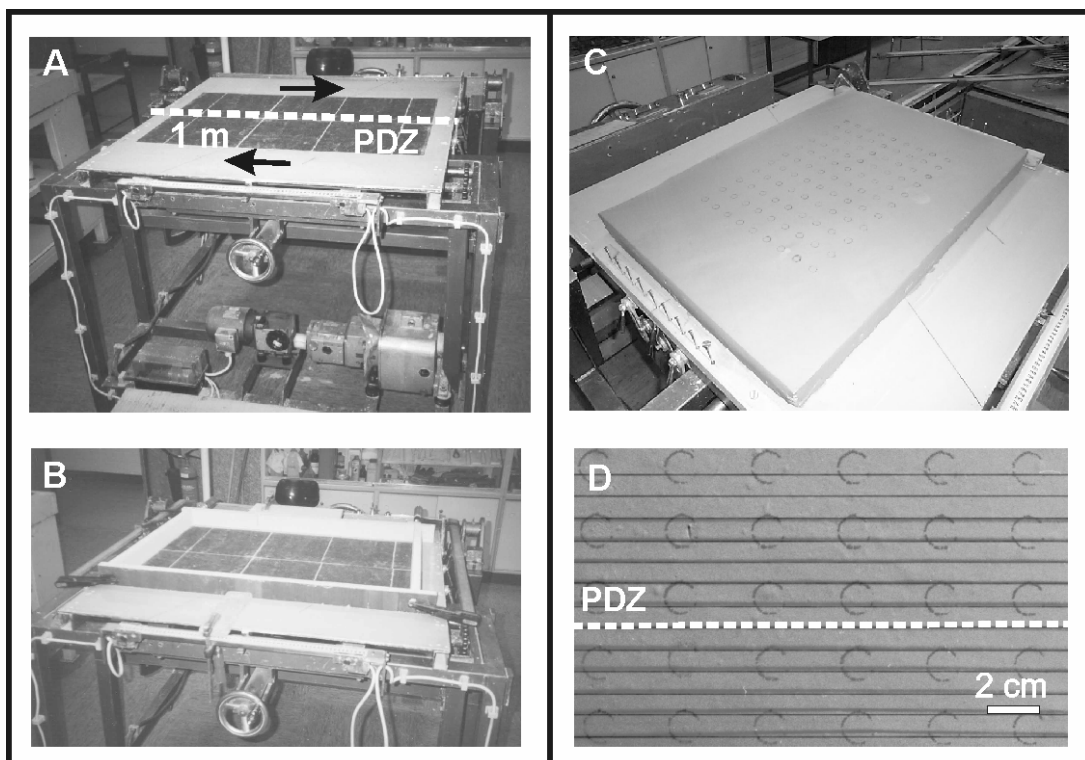


Fig. 13. Experimental set-up. A) The deformation table. PDZ: principal displacement zone, a discontinuity between two rigid boards. B) Installation of wooden frame for filling with clay and smoothing of surface. C) Removal of wooden frame, extension of strings above surface. D) Plane view of slab surface before deformation.

5.2. THE CLAY SLAB

A wooden frame was used to fill the modelling material to the desired thickness (4 cm in the standard experiment), and to smooth the upper surface of the slab (Fig. 13, C). Passive dark circular markers made of siliciumcarbide powder (SiC) were then drawn on the upper surface to visualise the deformation process and to allow displacement measurements (Fig. 13D).

Special attention was given to the smoothing procedure. Repetitive smoothing of the surface with the same direction of motion induces an anisotropy. Kalthoff (1970) and Schrader (1970) assumed that the long axes of the clay particles, attained a preferred orientation perpendicularly to the smoothing direction in the upper few millimetres of the slab surface. Hoepfener and Schwarz (1980) and Erkan (1982) later found that the created anisotropy controls the type of shear fracture formed in the modelling material (Fig. 14).

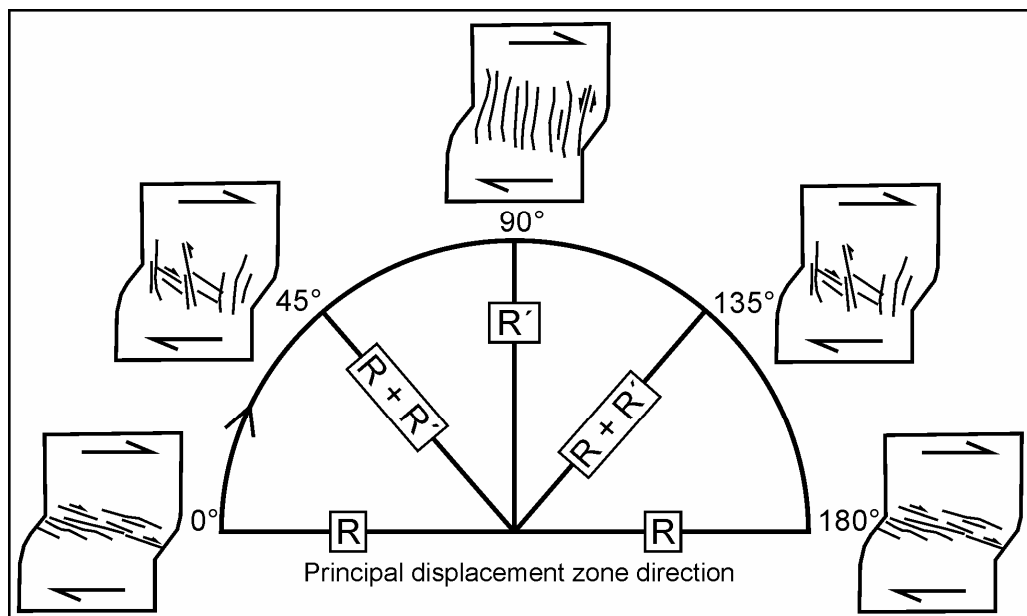


Fig. 14. Control of clay smoothing direction on the type of Riedel shear formed in the slab. The anisotropy of direction, shown by the arrow on the half-circle, is induced by the repetitive smoothing of the clay surface at a given angle to the principal displacement zone. Riedel shears (R) form when the smoothing direction is parallel to the principal displacement zone (angle close to 0° and 180°). The conjugate Riedel shears (R') form when the smoothing direction is perpendicular to the principal displacement zone (angle close to 90°). Both R and R' form when the smoothing direction is close to 45° and 135°. Synthesised from Erkan (1982).

It turned out to be possible to produce either one or two Riedel type of shear fractures (R, or R', or R and R'), simply by choosing the smoothing direction. Based on this experience, the

clay slabs used in the present study were smoothed in a direction between 125° and 135° to the principal displacement zone PDZ, which resulted in the formation of both the Riedel and conjugate Riedel shear fractures in the experiments (Fig. 14). Finally one or more strings were extended a few centimetres above the surface of the clay slabs, and parallel to the shear direction. Also two to four needles of known height were placed randomly near the edges of the slab. They were added for the purpose of monitoring the vertical displacements generated along the shear zone. Their purpose is to cast shadow lines, a method that is dealt with in section 5.4.

5.3. RECORDING METHOD

Photos taken at regular intervals document the progressive deformation and formed the basis for further analysis. In some experiments a digital video recorder was used. The cameras and the camcorder were mounted on a rail, which is fixed on the laboratory's ceiling just above the deformation table. The view is perpendicular to the upper surface of the slab. A first image was always taken before performing the experiments to show the initial state, and the second image was commonly taken as soon as the first fractures appeared on the upper surface of the slabs.

5.4. MEASUREMENT OF HEIGHTS

5.4.1. Concept of shadow line casting

Shadow line casting allows the extraction of height values from normal 2D photos. The concept is based on the use of the shadow traces of strings that are extended a few centimetres above the surface of the slab (Fig: 15). A source of light, here a slide projector, is directed towards the slab surface at an oblique angle. The lighted strings generate fine and sharp shadow traces on this surface, which shapes reflect the topographic profiles along the slab. When the surface is flat, the shadow lines are straight. As soon as the surface is deformed, the shadow lines undulate. This method is simple of use and needs no expensive

and complex apparatus. It is a non-destructive procedure that allows the direct measurement of the vertical displacement along profiles, and was applied to each recorded deformation stage used to measure the other geometrical elements of the Riedel shear zone.

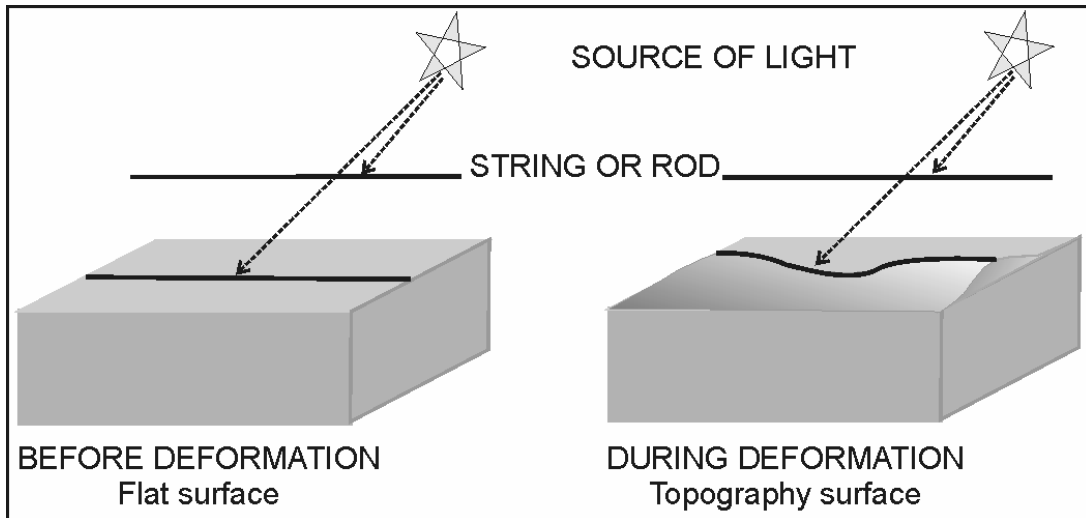


Fig. 15. The concept of shadow line casting method, and geometry of the shadow line formed on the surface of the slab before and during deformation. See text for explanation.

5.4.2. Determination of heights

The height is determined along the profiles by use of a trigonometry formula (Fig. 16A and B). The approach developed in the present study is similar to that used by Walmann (1998).

The parameters dealt with are as follow:

- P is any point on the string, its shadow point on the surface of the slab is M and its height is h.
- α is the angle the incident light makes with the horizontal
- β is the angle between incident light direction and the string direction
- dr is the real distance separating the points P and M
- D is the distance between the string and the shadow point M, measured on the photograph orthogonal to the string (Fig. 16A).

Before that deformation starts ($t = 0$), the surface of the slab is flat, and all the points M will be at the same initial height H. At a time $t = t_n$ after the onset of deformation, the height of a point M becomes h:

$$h = dr \tan \alpha \quad (17)$$

and

$$dr = D / \sin \beta \quad (18)$$

consequently

$$h = \frac{D \cdot \tan \alpha}{\sin \beta}$$

(19)

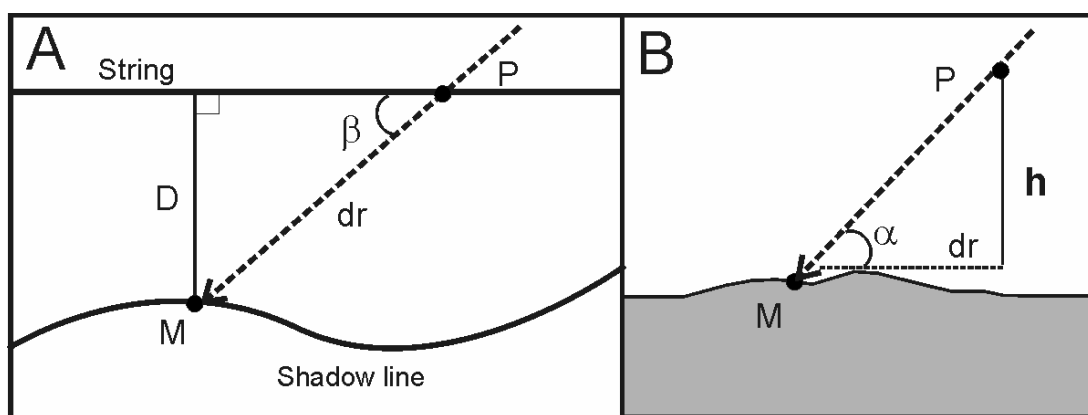


Fig. 16. Determination of the height h separating point P on the string from its shadow point M on the surface of the slab. A) Surface view of the clay slab surface shown on the photograph. B) Perspective view. See text for details.

The vertical displacement V of point M at a time t would be the difference of its heights H before deformation and h at a certain value of basal shear displacement. The constant $\tan \alpha / \sin \beta$ can be determined for each set of photos by two methods. The first simply consists on the direct measurement of D on the photo taken before deformation. In this case, the initial height H of the string above the surface is determined during the experimental set-up and noted in the protocol. The second way is more time consuming and is used only when the first method cannot be applied i.e. the measurement of H during the experimental set-up was forgotten. Here 2 to 4 needles of known height are put on the slab's surface, $\tan \alpha$ and $\sin \beta$ are calculated for each needle, and their average is used.

Additionally, the heights of the push-up ridges and the depths of the pull-apart structures were measured at the end of each performed experiment.

5.5. PHOTO ANALYSIS AND DATA EVALUATION

The scanned photographs and digital images were enhanced. Selected images of each deformational stage were then analysed using an image analysis software (Core Image Analysis software system, C.I.A.[™]), which allows the tracing of the shear fractures and the measurement of properties such as length, distance, area, and angles with very high precision. The examination of the vertical slip distribution within the strike-slip zone of each model was limited to a single topographic profile in the central area, where height changes are greatest. The locations of maximum vertical slip are generally located in-line, but deviations occur. The topographic lines were obtained with the shadow line casting method described in section 5.4. The measurement error on the lengths and distances are based on the scale precision of the software, which is equal to 0.1 mm. The values of these properties are thus given with a measurement error of ± 0.05 mm. All the data gathered with CIA were exported to Excel files for further calculation, evaluation and display.

The progressive development of the Riedel shear fractures depends on the amount of horizontal basal displacement D (Fig. 17). In the present study the dextral basal displacement is normalised with respect to the thickness Z of the clay slab (NBD = normalized basal displacement), the width of the formed strike-slip zone in the model being dependent on the thickness of the slab. This normalisation allows the objective comparison of the different models.

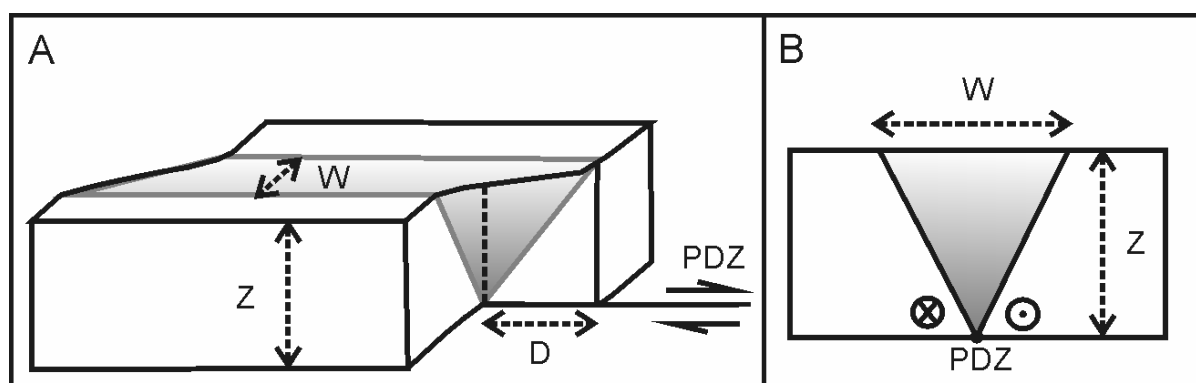


Fig. 17. The geometrical features of the strike-slip deformation zone (in gray) formed in scaled clay experiments. A) Block diagram. B) View in profile. W : width; Z : thickness; D : basal displacement amount; PDZ: principal displacement zone.

5.6. OVERVIEW OF PERFORMED EXPERIMENTS

A total of 10 experiments have been performed for this study, which varied in purpose, dimension and material strength (water content) (Appendix A). Five principal experiments have been selected for detailed analysis in the present thesis; they represent the whole range of results detailed in the following chapter.

First a standard model with a clay slab of constant thickness (4 cm) and shear strength (1.5 kPa) was conducted. Then the parameters were varied in two series of experiments. In series (A) the shear strength of the clay slabs was varied, while the thickness was similar to the standard model. In series (B) the thickness of the clay slabs was varied while their shear strength remained unchanged. The experiments were performed to a maximum displacement of 83 mm, at a displacement rate of 0.44 ± 0.045 mm/min.

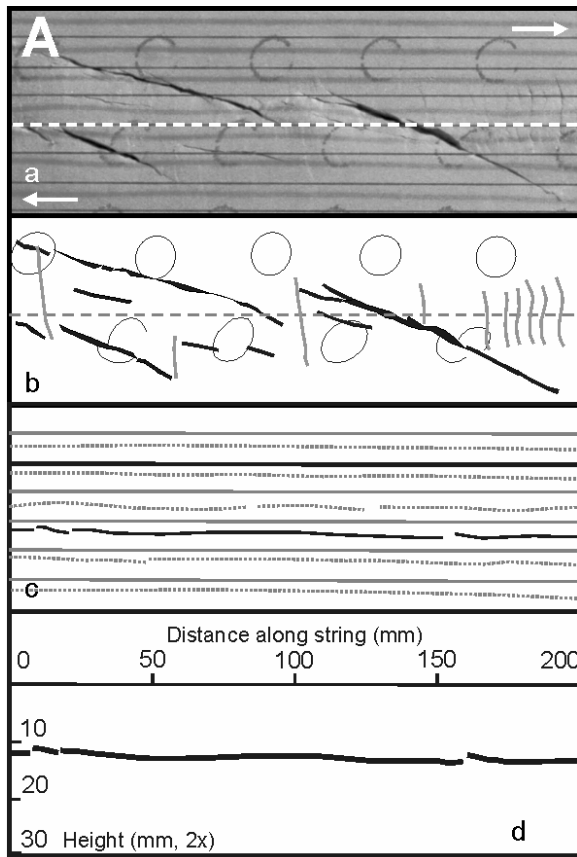
CHAPTER 6: ANALYSIS AND RESULTS

6.1. STANDARD EXPERIMENT

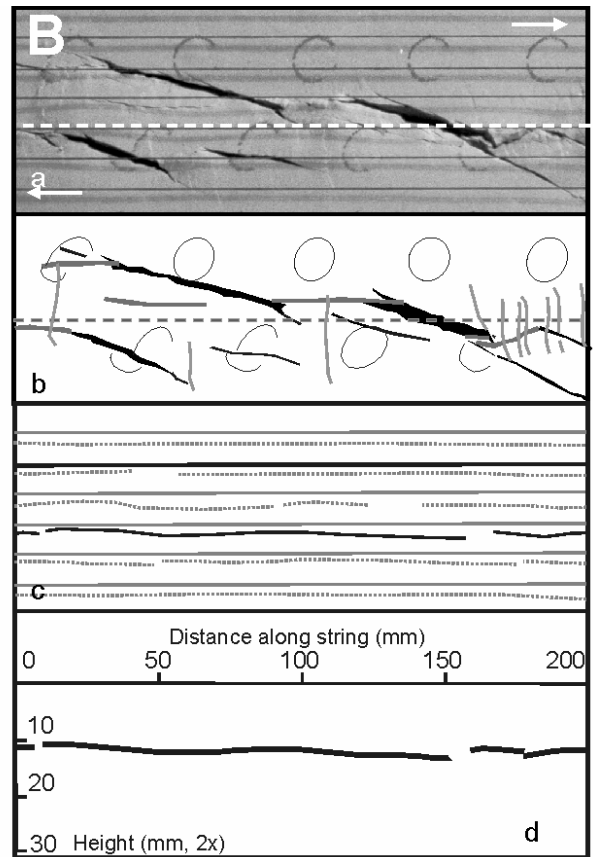
6.1.1. Development of pull-apart structures

The standard experiment produced a series of typical pull-apart structures in the model. Their progressive development can be subdivided into three stages, depending on the normalized basal displacement amount (NBD, section 5.5). The initial stage comprises the formation of Riedel shear fractures, as observed in other studies (e.g. Sylvester, 1988). The first visible fractures appeared on the surface of the model after a NBD of 0.34 (i.e. after 1.36 cm of displacement). These first order fractures are of very small size (less than 1 mm), distributed along a deformation zone with a total width of about 5 cm at the surface and V-shaped in profile. Upon further displacement, these fractures coalesced to form an echelon left-stepping synthetic and antithetic shear fractures, in the following referred to as Riedel and conjugate Riedel shears. They became fully developed at a NBD of about 0.6. The lengths of the Riedel shears range between 2 and 8.8 cm, and their orientations vary between 8° and 23° to the principal basal displacement zone (Fig. 18A). Although horizontal shear is the primary motion, these fractures often show a minor dip slip component, as revealed by the shifting of casted shadow lines near the Riedel shear traces. Some of these Riedel shears display an extensional component, which here is a displacement normal to the shear direction. In the example shown in Figure 18A, the Riedel shear fractures open by up to 14% of the amount of basal displacement, following a clockwise rotation by a few degrees. The presence of shear displacement as well as the small angle to the basal displacement zone distinguish them from the tension fractures, which are usually oriented at about 45° to the principal displacement zone and do not show any shear displacement. In the experiments by Cloos (1928) and Riedel (1929) tension fractures were observed to form only when water was sprayed on the surface of clay models.

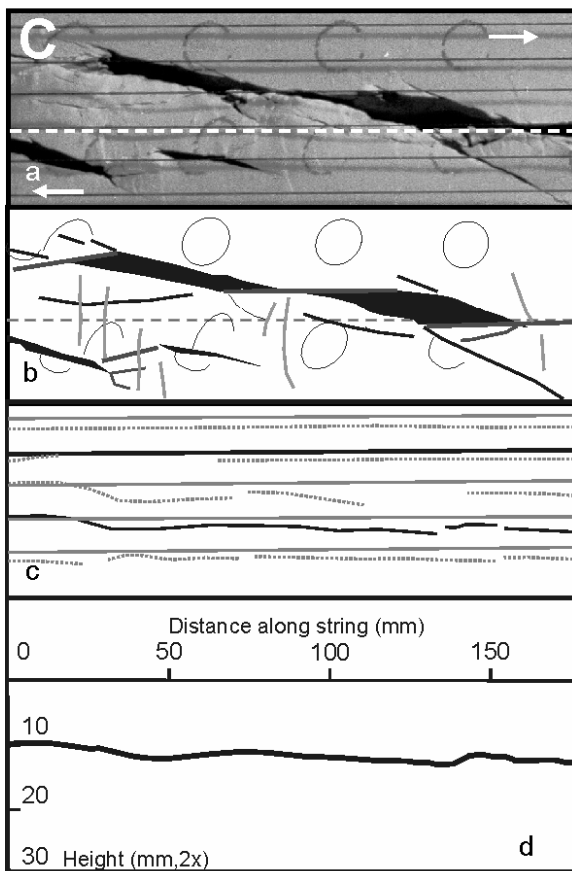
The conjugate Riedel shears concentrate at the overstepping areas between the Riedel shears, with initial angles of orientation of 70° - 75° to the shear direction. They show shear



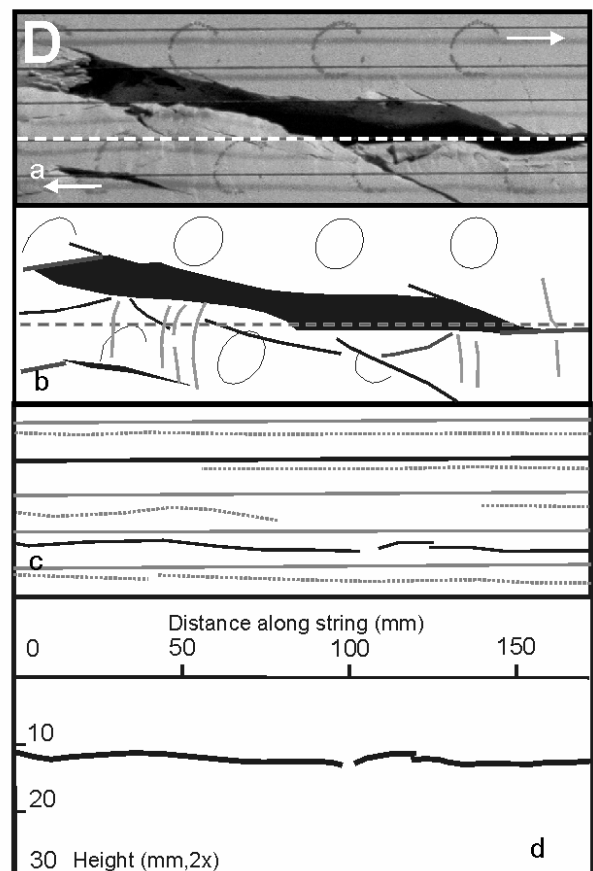
NBD = 0.6



NBD = 0.82



NBD = 1.35



NBD = 1.9

Fig. 18. Progressive development of pull-apart structures and secondary push-up ridges in standard experiment NA4 at normalised basal displacement (NBD). A) Initiation and development of Riedel shears. B) Initiation and development of the Y- and P-shears, incipient pull-apart structures. C) Fully formed pull-apart structures and push-up ridges at the Riedel shears. D) Coalescence of neighbouring pull-apart structures. (a) Raw image. Arrows show sense of shear and dashed line marks the location of the PDZ below the slab. (b) Drawing of the shear fractures and circular markers. (c) Drawing of the extended strings above the slab (grey lines) and their corresponding shadow lines casted on the surface of the slab (dotted lines). The interrupted thin black line in the middle of the drawing is the shadow line of the string highlighted in black, for which the topographic profile in the following sub-figure is constructed. (d) Topographic profile along the central part of the strike-slip zone, where the maximum vertical displacements occur, drawn along the shadow line presented in (c). The method of determination of heights is detailed in chapter 5.4. See also text for more details.

displacement and progressive rotation. They are observed to rotate 18° to 20° clockwise, while new ones developed at the initial angles. Rotation results in the characteristic 's' shape. The conjugate Riedel shears serve to transfer the horizontal displacement from one Riedel shear to the adjacent one. They are not analysed further, since they are not directly related to the formation of the pull-apart structures.

At a NBD of about 0.82 (i.e. $D = 3.28$ cm), Y- and sometimes P-shears initiate at some places along the strike-slip zone. These are synthetic shear fractures that are roughly parallel to the principal displacement zone (Fig. 18B). The Y- shears are regarded as the surficial segments paralleling the principal displacement zone. They preferentially form at the tips of the Riedel shears, rarely cutting through them, and accommodate the continuing strike-slip deformation while pulling the sides of the now passive Riedel shears further apart. Where the formation of the Y-shears was delayed, push-up structures developed instead at the restraining overstepping areas. Vertical displacement is expressed through the presence of a reverse component at the conjugate Riedel shears, and of small scale fold, reverse and thrust features.

Once the boundary Y- and P-shears were fully developed, the rhombic shape characterising the pull-apart basins is easily recognised (Fig. 18C). The angle of intersection between the two sets is below 30° . With further displacement two or more neighbouring structures can coalesce to form a long, narrow and deep complex or composite pull-apart basin (Fig. 18D).

6.1.2. Development of push-up ridges

The left-stepping arrangement of the Riedel shear fractures and the presence of the free surface (no vertical load and no upper confinement) promote the formation of push-up ridges (or pop-up structures) at the overstepping areas. The vertical displacements at these contractional structures are visible on the photographs with the casting shadow lines method described in section 5.4, and are presented on the subfigures c and d of Figure 18. Before deformation, the initial surface of the clay slab is flat and 13.2 mm below the strings. Their corresponding shadow lines are straight and parallel to PDZ direction (Fig. 13D and Fig. 15). In order to illustrate the development of the push-up ridges, successive topographic profiles have been constructed from the shadow line of the same string, which is marked by the black line marked in Figure 18c. The shadow line is located close to the middle of the strike-slip zone, where horizontal and vertical displacements are greatest near the PDZ (dashed line in Fig. 18a, b).

At the first stage of deformation, when no shear fracture is seen yet, discrete bulges develop on the surface of the deformation zone. This is shown by the slight undulation of the shadow lines, which continues to develop after the initiation of the first order shear fractures (NBD of 0.34). After the full development of the Riedel and conjugate Riedel shear fractures at a NBD of 0.6, the topographic profile is traced with a vertical scale exaggerated twice (Fig. 18Ad). The obtained sinusoidal trace is of irregular wave lengths, between 60 and 100 mm. Its amplitudes vary between 0.17 mm in the centre of the analysed image and 0.82 mm at its left extremity. The vertical displacement continues to increase as long as the Riedel shear fractures are active, provided that newly formed Y-shear fractures do not link the neighbouring incipient pull-apart structures. The following Figures 18B and 18C illustrate well the contrasting development of the vertical displacement within two areas of the deformation zone. In the centre of image a), a Y- shear fracture develops and links the two incipient pull-apart structures, whereas in the left-hand side area the Y- shear fractures are not fully developed and do not connect the pull-apart structures. The shadow lines and the topographic profiles at these two areas show that the vertical amplitude stagnates at about

0.3 mm as soon as the incipient pull-apart structures are linked by the Y-shear fractures. Instead, a push-up ridge develops on the left-hand side, where the vertical displacement increased to 3.5 mm above the initial surface after a NBD of 1.35.

The vertical displacement continued to increase at the push-up ridge till the end of the experiment, when the Y-shear fracture managed to cut through the structure completely. Consequently a total of 5.6 mm vertical displacement took place at this ridge after a NBD of about 2, when the basal displacement was nearly twice the thickness of the slab (Fig. 19). The magnitude of vertical displacement corresponds to 14% of the thickness of the slab and 7.4% of the basal displacement; the equivalent basement-induced shearing of a 4 km thick sedimentary cover would induce a vertical displacement by 500 m at the push-up ridges.

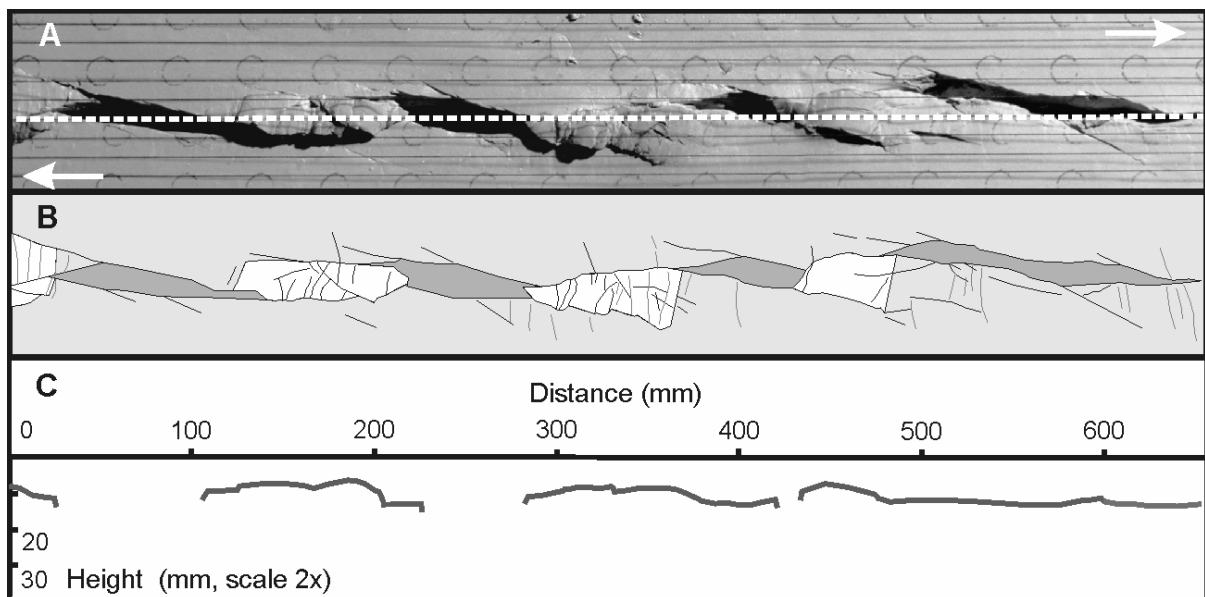


Fig. 19. Structural features of a part of the standard experiment NA4 after a NBD of 2 (basal displacement is twice the thickness of the slab). A) The raw image shows the strike-slip zone formed of alternating pull-apart structures with push-up ridges. The dashed line indicates the location of the PDZ at depth, and the arrows the dextral motion of the plates. B) Drawing of the image emphasizing the structural features. Push-up ridges and pull-apart structures are white and dark grey respectively. C) Topographic profile along the dashed line in (A), obtained with the shadow line casting method. The vertical scale has been twice exaggerated. Discontinuities along the profile correspond to the gaps of the pull-apart structures.

6.1.3. Structural features of the Strike-slip zone at a NBD of 2

The strike-slip zone in the standard experiment NA4 is formed mainly of an alternation of 11 pull-apart structures with 9 push-up ridges (Fig. 19). Three pull-apart structures are the result

of the coalescence of neighbouring smaller ones as detailed in section 6.1.1. Consequently, the length to width ratio (l:w) varies within the deformation zone from 5.7:1 for the simple single pull-apart structures to 20:1 for the composite ones. Their depth, measured at the end of the experiment, does not exceed 3.6 mm. The presence of flattened areas at the bottom of these structures indicates ongoing decollement at the base of the slab. The push-up ridges vary also in size and shape. Some consist of a smooth antiform (fourth structure from left of Fig. 19), others are complex contractional ridges formed of small scale fold, reverse and thrust features (second and third ridges from left of Fig. 19). The shapes were found to depend on the nature of the bounding shear fractures. The Riedel, Y- and P-shear fractures bound elongated triangular to rhomboidal structures. The vertical displacement at the different structures ranges between 2 and 6.8 mm, and does not exceed 17% of the thickness of the slab and 9% of the total basal displacement.

The uplift of the push-up ridges is primarily driven by the horizontal motion at the Riedel shear fractures and later at the initiated Y-shear fractures. However, a direct relation between the vertical and the horizontal components of motion was difficult to establish. At the ridges, the horizontal motion is first accommodated by the development of an antiform, and then by contractional structures such as small scale folds, reverse and thrust faults.

6.2. INFLUENCE OF SHEAR STRENGTH AND THICKNESS OF THE CLAY SLAB

The development of pull-apart structures at the Riedel shear fractures and of push-up ridges at the oversteps, as described in section 6.1.1 and 6.1.2 respectively, was observed in all experiments. The variation of the thickness and the shear strength of the clay slab was found to affect the width of the deformation zone and the number of shear fractures, pull-apart structures, and push-up ridges within the deformation zones, counted for a slab length of 50 cm. These results are displayed visually in Figure 20 (A, B), and in Table 6.

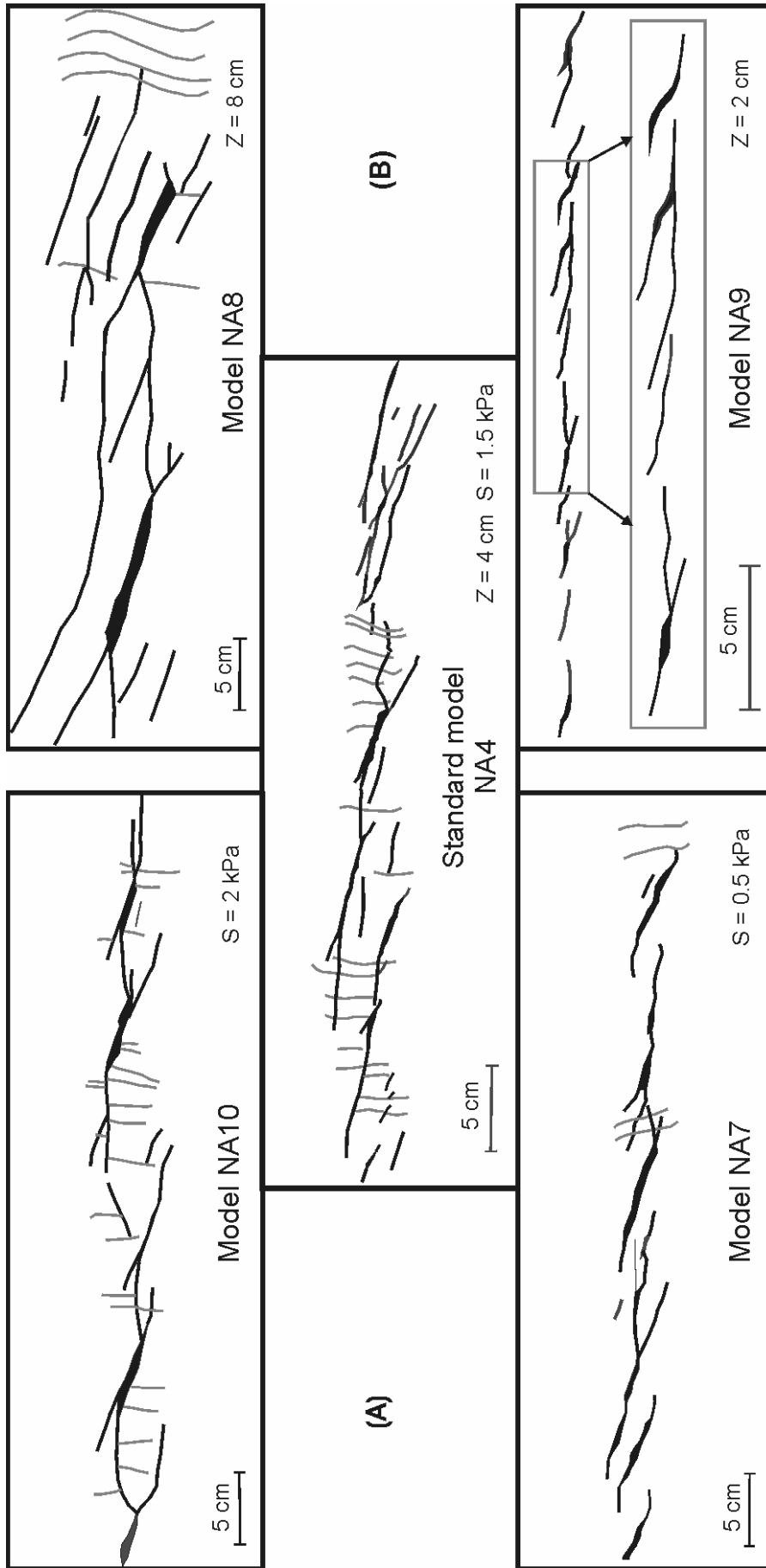


Fig. 20. Plane view of strike-slip deformation zones in various models by comparison to the standard model. Series (A) Models of similar thickness (4 cm) and varying shear strengths. Series (B) Models of similar shear strength (1.5 kPa) and varying thickness value. The structures are shown for a normalised basal shear displacement to thickness ratio of about 0.82. Z and S are respectively the thickness and the shear strength of the clay slab.

6.2.1. Influence of the shear strength (series A)

In series A clay slabs with water contents between 38% and 48% were used. This range corresponds to undrained shear strengths between 0.5 and 2 kPa. Even for relatively small differences in water content compared to the standard model (NA4 in Fig. 20A), significant variations in deformation zone geometry were observed. First, the width of the shear zone increases with increasing shear strength for a constant thickness (Fig. 21; Table 6). The width of the strike-slip zone is 4.1 cm in the low strength model (NA7) and 5.7 cm in the high strength model (NA10). Second, the experiment with low shear strength (NA7) shows only few conjugate Riedel shears. These structures are much more frequent in the experiment with higher strength (NA10). Moreover, the number of the Riedel shears and of the related pull-apart structures increases with decreasing shear strength, and their spacing decreases accordingly (Fig. 20A, Table 6). However, no obvious relationship was found between the material's strength and the number of the push-up ridges.

Also, the first shear fractures appear at the surface of the slab at a higher NBD when the shear strength of the clay is reduced. The first shear fractures appeared at a NBD of 0.38, 0.34 and 0.32 in models NA7, NA4, and NA10 respectively. The effect of shear strength is noticeable on Figure 20A. At a NBD of about 0.82, the Y-shears are at an initial stage of development in model NA7, whereas they are already well developed at the same NBD in model NA10. Finally, the amount of vertical motion (uplift) at the push-up ridges increases markedly with increasing shear strength of the clay slabs (Table 6, Fig. 22). Although the ridges behave in a similar manner during the initial stages of deformation, the amount of uplift differs after a NBD of about 0.5. The influence of the shear strength on the vertical displacement is evident on Figure 22. At a NBD of 1.6, the maximum vertical displacement reaches 12 mm in model NA10, which corresponds to 18.8% of the total basal displacement

and 30% of the thickness of the slab. Conversely at a NBD of 2, this amount does not exceed 9% of the total basal displacement and 17% of the thickness of the slab in model NA4.

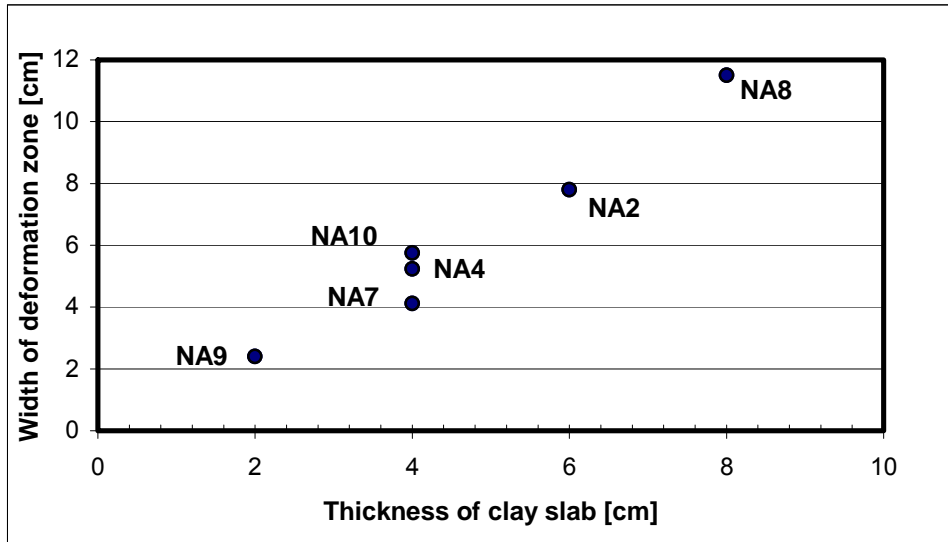


Fig. 21. The dependency of the width of the strike-slip zones on the thickness and the shear strength of the clay scaled models.

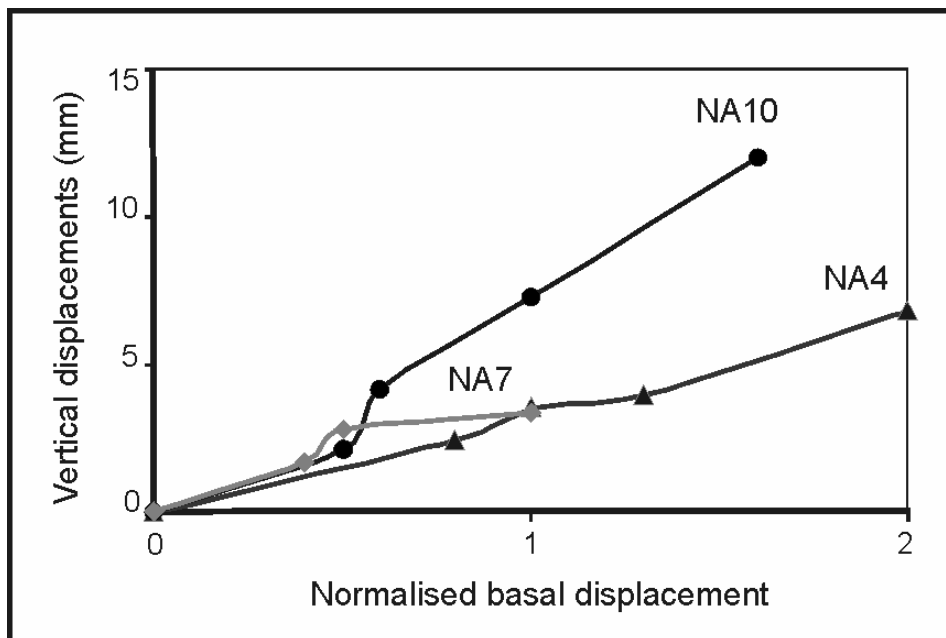


Fig. 22. Evolution of vertical displacement (uplift) at the push-up ridges with respect to the normalised basal shear displacement NBD for models NA7 (0.5 kPa), NA4 (1.5 kPa) and NA10 (2 kPa) with different shear strengths.

Table 6. Influence of the shear strength (S_u) and thickness (Z) of the clay slabs on the geometrical characteristics of the deformation zones formed in the models. Measurement error of width (W), average distance, and vertical uplift (U_{max}) is ± 0.05 mm. Measurement error of depth of pull-apart structures is 0.5 mm.

	NA4	NA7	NA8	NA9	NA10
Dimension (cm)	36 X 90	35 X 90	35 X 90	20 X 90	35 X 90
Thickness Z (cm)	4	4	8	2	4
Water content w (%)	42	48	42	42	38
Undrained shear strength S_u (kPa)	1.5	0.5	1.5	1.5	2
Displacement rate (mm/min)	0.41	0.44	0.43	0.42	0.40
Width of shear zone W (cm)	5.2	4.1	11.5	2.2	5.7
Number pull-apart structures	4	7	2	8	5
Average distance between pull-apart structures (cm)	9.7	3.9	13.2	4.4	9.1
Length to width ratio of the pull-apart structures	6:1 to 11:1	5:1 to 7.4:1	3.4:1 and 5.6:1	2.2:1 to 4.6:1	2.8:1 to 5.4:1
Depth of pull-apart structures (cm)	3.6	3	3 and 4.3	0.5 - 2	1 – 3.8
Number of push-up ridges	3	4	2	4	5
Vertical displacement U_{max} at the ridges (mm)	6.8	3	3.4	5.6	12
U_{max} in percent of thickness Z	17%	7.5%	4.3%	28%	30%
NBD for which U_{max} was measured	2	1	1	1.8	1.6

6.2.2. Influence of the thickness of the clay slab (series B)

The Riedel experiments of series B are characterised by a similar shear strength (1.5 kPa), and a variable thickness of the clay slab between 2 and 8 cm (Fig.20B). The thickness of the clay slab turns out to control the width of the deformation zone, as shown in Table 6 and

Figure 21. The width of the strike-slip deformation zone is proportional to the thickness of the slab. Also, the number and the spatial distribution of the shear fractures formed within the deformation zone are strongly controlled by the thickness of the clay slab. For example, the conjugate Riedel shears are completely absent in the model with a clay slab thickness of 2 cm (NA9 in Fig. 20B). A minimum thickness of 4 cm is required for their development. Also, the number of Riedel shears evolving into pull-apart structures per unit length is inversely proportional to the thickness of the clay slab (Table 6).

Figure 20B shows how these Riedel shears are distributed in space. The shear fractures developed in an echelon pattern in all models, with a tendency for domains to overlap with increasing thickness of the clay slabs. They form a simple echelon arrangement in model NA9 (2 cm thick), a mixed form of an echelon arrangement with domains of double- to triple-parallel traces in model NA4 (4 cm thick), and a more complex arrangement in model NA8 (8 cm thick). In this model 3 to 4 Riedel shears form domains with parallel traces. In this case, one of them is observed to become dominant and to develop into a pull-apart structure. Additionally, the greater is the thickness of the clay slab, the larger is the amount of basal shear displacement required for the shears to appear at the surface. For a NBD of 0.82 as in Figure 20B, the basal displacement D was 16 mm, 33 mm and 64 mm in models NA4, NA9 and NA8 respectively.

The maximum vertical displacement at the push-up ridges seems to be independent of the thickness, and to be increasing with increasing basal displacement (Fig. 23). The amounts of displacement measured at several NBD values are within the same range for all models as seen on the graph of figure 23. Yet when these amounts are presented in percent of the thickness of the clay slab Z (Table 6), they show that the maximum vertical displacements may reach 28% of the thickness value at higher NBD (NA9). It should be noticed also, that the vertical displacement might have increased further in model NA8, the experiment being stopped at a NBD of 1. Shearing this thick clay slab to higher NBD values would have taken more time, the clay material would have been affected by dehydration and change of properties.

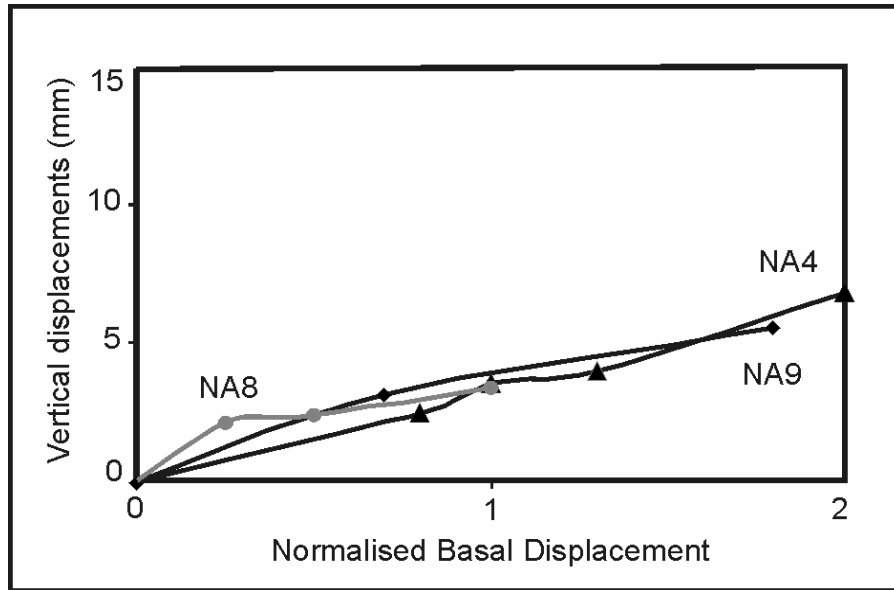


Fig. 23. Evolution of the maximum vertical displacements at the push-up ridges with respect to the normalised basal shear displacement NBD for models NA9 ($Z = 2$ cm), NA4 ($Z = 4$ cm) and NA8 ($Z = 8$ cm) with different thicknesses.

CHAPTER 7: COMPARISON WITH OTHER ANALOGUE MODELLING STUDIES

7.1. INTRODUCTION

In this chapter the results of the present study are compared with previous Riedel type experimental studies. The specific properties of the Riedel type experiments are (1) the presence of a free upper surface (no vertical load is applied, and no general confinement), (2) the maximum principal stress is horizontal and not vertical as in the case of soil mechanics tests, and (3) the shear propagation and rotation is transferred from the basement to the upper surface. The latter property is referred to as basement induced wrenching by Mandl (1988). Distributed (simple) shear models and layered (upper crust/lower crust) models are not considered here.

7.2. COMPARISON WITH PREVIOUS SAND MODELS

The results related to the simultaneous evolution of pull-apart basins and push-up ridges (section 6.1) are similar to those obtained by Soula (1984) in single layer models of various types of sand and talc powder. He simulated the evolution of inter-mountain basins, which open during strike-slip deformation with a Riedel type experimental set-up. In addition to the Riedel and conjugate shear fractures, tension fractures were formed. The opening of pull-apart structures at the Riedel shear fractures was contemporaneous to the formation of push-up ridges at the oversteps separating them; the contraction taking place at the push-up ridges compensates the ongoing extension at the pull-apart structures (see his Fig. 7 p. 94). Among other interesting results, Soula found a relationship between the distance separating the pull-apart structures and the grain size of the used granular materials. Finally, he appraised the role of analogue tectonic modelling as a method to analyse complex structures.

Our results describing the influence of the shear strength and the thickness of the modelling material on the structural features of the deformation zone cannot be compared to those obtained by Soula (1984). According to him the used sand and talc had a rather high

cohesion, while Deramond et al. (1983) report the opposite. The physical and mechanical properties of the used materials are not described further by these authors.

Sandbox experiments dedicated to the influence of material properties on the development of strike-slip structures have been recently presented by Schöpfer and Steyrer (2001). This study relies on a detailed specification of the physical and mechanical properties of the used materials, which allows their comparison with other sandbox studies. However, pull-apart structures did not form in these sandbox models. Though similar in terms of cohesion and internal friction, sand and clay behave quite differently during deformation, which makes their comparison difficult. The differences are mainly related to the grain size distribution and grain shape, and to the behaviour of water in the pore space. Dry sand under stress deforms mainly by intergranular slip and rotation, which lead to dilatancy and frictional flow (e.g. Reynolds, 1885; Bagnold, 1966), whereas hydro-physico-chemical effects at the interparticle contacts are important for clays (e.g. Ladd et al., 1977; Bolton, 1979; Sridharan, 2001). The clay particles are of platy shape, small size, and have electric charges in presence of water. Wet clay under stress deforms by sliding along the long platy surfaces of the particles, strongly affected by pore pressure under undrained conditions.

7.3. COMPARISON WITH PREVIOUS CLAY MODELS

In contrast to sandbox experiments, the properties of the clays used for physical modelling are rarely specified, with the exception of Tchalenko (1970 and references to earlier work), and of Lazarte and Bray (1996). Because clays show a wide range of behaviour at different states and conditions, it is very difficult to pinpoint which property or combination of properties might result in the opening of Riedel shear fractures. It is not clear, for instance, whether the plasticity index of the clay material is important, and what is the influence of the mineral composition and the strength.

The development of pull-apart structures presented in this study has not been described in the Riedel experiments of Tchalenko (1970) and Lazarte and Bray (1996). The plasticity index I_p of Kaolin-O used in our study is very low (10), whereas it was very high for the

kaolinite-bentonite mixtures used by Lazarte and Bray (1996) (104 and 118, see Table 7). As described in a section above, the plasticity index reflects the clay size fraction of the material and the nature of the minerals, and has a direct effect on the mechanical behaviour. The clay fraction of the kaolinitic clay used by Tchalenko (1970) was more than 95%. This might explain the absence of the opening of the Riedel shears at the later stages of deformation. Also, the deformation rate might be of importance for the geometry of the failure structures. For the purpose of earthquake simulation experiments, Lazarte and Bray (1996) used very high basal displacement rates (0.17 to 1.19 mm/s), compared with the displacement rates of 0.45 mm/min used in the present study. They obtained smoothly curved surfaces in plane view and in profile. The marked V-shape was not observed. They noted that boundary conditions such as the model geometry and the presence or absence of boundary constraints (lateral confinement) and the material ductility (here referred to as plasticity) had a significant influence on the model response. Tchalenko (1970) concluded that continued research on the mechanisms of shear zone evolution should take into account other parameters.

Table 7. Comparison of material properties between different clays. Sources: Tchalenko (1970), Morgenstern and Tchalenko (1967) and Lazarte and Bray (1996). P_L and W_L : Atterberg's plastic and liquid limits; PI: plasticity index or range; CF: clay fraction with size below 2 μm .

Property	Tchalenko (1970)	Clays of Lazarte and Bray (1996)		Present study
Name and composition	kaolin	Mix A kaolinite/bentonite	Mix B kaolinite/bentonite	Kaolin-O kaolin/silt
P_L and W_L	24 - 60	21 - 125	22 - 140	23 - 33
PI	36	104	118	10
Water content	45 to 56%	103 to 113%	112 to 118%	38 to 48%
consolidation	unknown	normal		normal
Shear strength	unknown	Slightly above 2 kPa		0.5 to 2 kPa
CF	95%	unknown		41%
Friction angle	23°	unknown		32°

CHAPTER 8: NATURAL EXAMPLES

8.1. RIEDEL TYPE PULL APART BASINS

Natural pull-apart basins that may have formed by the Riedel mechanism described in the present study are observed at different length scales on Gozo Island (Malta), which belongs to the Plio-Quaternary Strait of Sicily Complex rift zone (Fig. 24). It is located on the eastern Pelagian Platform of the Central Mediterranean, midway between Sicily and Tunisia. This WNW-ESE trending complex rift is about 380 km long and 100 km wide, and marks the boundary between continental lithosphere of the African and the Eurasian plates. Its structure has been explored in geophysical studies, boreholes, and structural analyses carried out on the Pelagian islands and at Cap Bon in Tunisia. Details, interpretations and reviews of these different studies are given by Reuther (1980, 1990), Cello (1987), and Boccaletti et al. (1990).

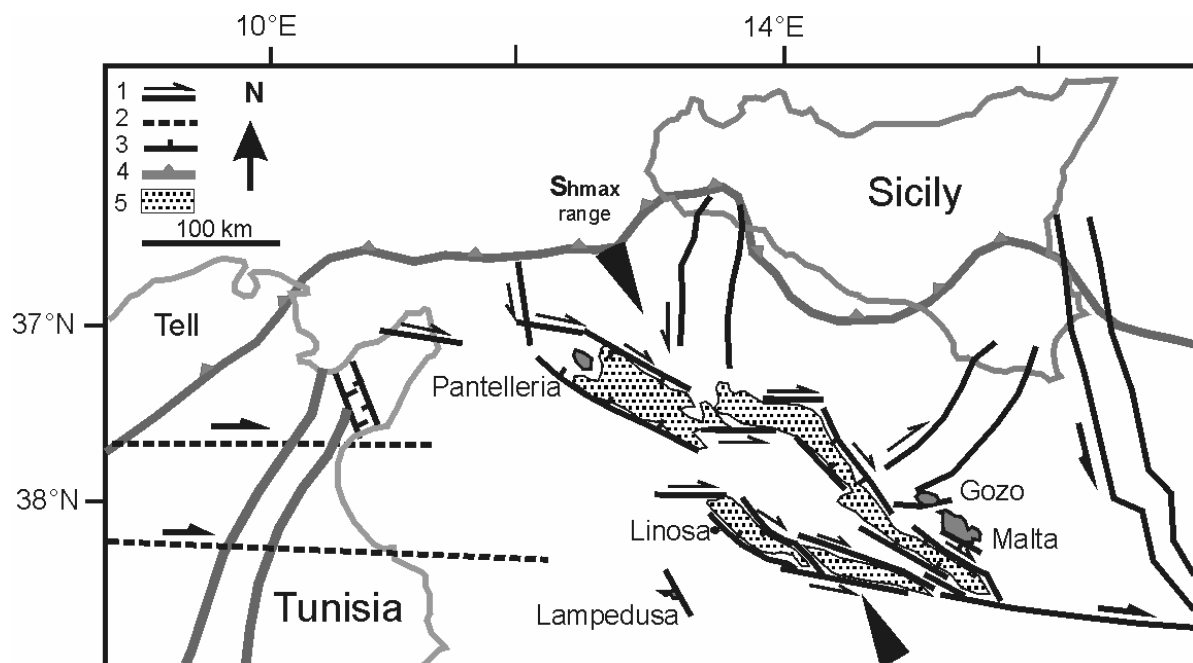


Fig. 24. The Strait of Sicily Complex rift zone. Modified after Boccaletti et al. (1990) and Reuther (1990). 1. strike-slip fault. 2. deep basement fault. 3. normal fault. 4. thrusts and nappes front. 5. Plio-Quaternary basins.

8.1.1. Structure of the strait of Sicily Complex rift zone

The continental crust in the strait of Sicily is about 20 km thick, and the sedimentary cover primarily consists of Meso-Cenozoic platform carbonate series about 5 km thick. The

Pantelleria, Malta, and Linosa basins are the major structural depressions associated with the complex rift zone (Fig. 24). They are 70 to 140 km long, and 15 to 30 km wide. The sedimentary filling of these basins consists of mainly Plio-Pleistocene turbidites, with an average thickness of 1 to 2 km, locally exceeding 3 km.

Most of the NW-SE to E-W trending bounding faults show oblique displacement with a significant dextral shear component. The post-Miocene remote stress field inferred from structural data, fault plane solutions and in-situ stress measurements is characterised by a NW-SE to NNW-SSE trending maximum horizontal stress. E-W to WNW-ESE trending transfer faults, which had developed during the Jurassic, were reactivated in the early Miocene as a result of dextral strike-slip motion between the African and the Eurasian plates (Morgan et al., 1998). The fault systems of the major depressions in the sedimentary cover began to develop in the late Miocene to early Pliocene. Deformation continues to the present day, related to ongoing extension and dextral displacement (Jongsma et al., 1985).

8.1.2. The pull-apart basins and structures on Gozo Island

One of these E-W trending dextral strike-slip fault zones is located south of Gozo Island, where various stages of pull-apart basin development are observed on several length scales (Reuther, 1980, 1990). A similar structural pattern was recently described by Kim et al. (2003) in the area north of Gozo Island, where pull-apart structures are developed along mesoscopic strike-slip zones. According to these studies, first-generation synthetic shears and faults (Riedel and conjugate Riedel shears) are formed, which are succeeded by extension fractures (Fig. 25A). Reuther (1990) also described the reverse sequence. The faults occur on several length scales, with lengths ranging from centimetres to several hundreds of metres. Second-generation synthetic faults that are sub-parallel to the major fault zones (Y- and P-shears) link and pull the sides of the first-generation shears and extension fractures apart. It has been observed that the shape of the pull-apart structures formed from the Riedel shears was relatively long, narrow, and trapezoid, whereas the pull-apart structures formed from the extension fractures were wide trapezoids with higher

intersection angle (Fig. 25A). Reuther (1980) observed that horizontal clockwise rotation up to 20° is associated with the pull-apart structures of larger size, as well as formation of new Riedel shears and extension fractures. Plio-Quaternary pull-apart basins of km-scale, formed by the mechanism described here, may be found offshore the Pelagian platform.

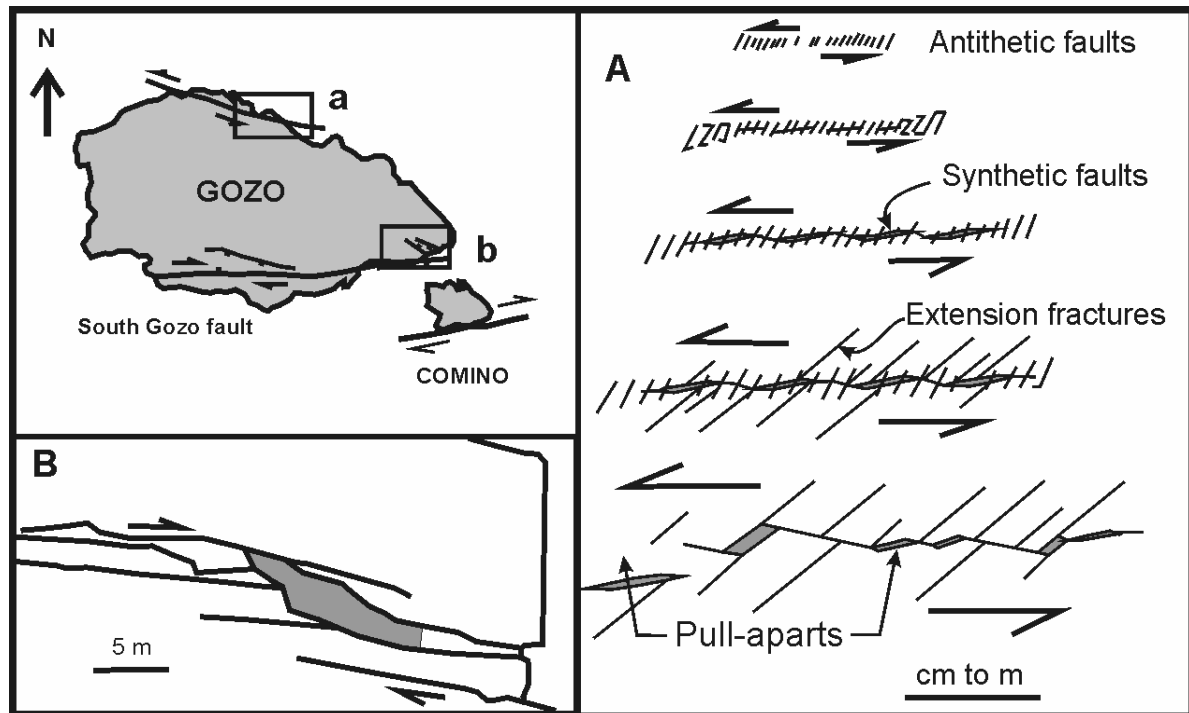


Fig. 25. Centimetre to several hundreds of metres long pull-aparts formed by Riedel shear mechanism on Gozo, Malta. A) after Kim et al., (2003); B) after Reuther (1990).

8.2. SIMULTANEOUS FORMATION OF PULL-APART BASINS AND PUSH-UP RIDGES

The performed Riedel experiments resulted secondarily in the formation of push-up ridges at the same time as the pull-apart structures. This co-development may have occurred in the strike-slip zone of the Marmara Sea basin, which is among the most interesting cases in nature. The Marmara Sea is located on the northern strand of the dextral North Anatolian Fault Zone (NAFZ) in northern Turkey. The NAFZ is a nearly E-W oriented strike-slip boundary fault between the Aegean-Anatolian and the Eurasian plates, which parallels roughly the southern Black Sea shores (Fig. 26A). Since the catastrophic earthquakes of August 17 1999, the high seismicity of Marmara Sea region led to intensive geological, geophysical, geodetic and marine exploration. The details used in this study are obtained

from the latest literature (e.g. Aksu et al., 2000; Imren et al., 2001; Le Pichon et al., 2001, Armijo et al., 2002), and the recent tectonic synthesis of the NAFZ by Şengör et al. (2005).

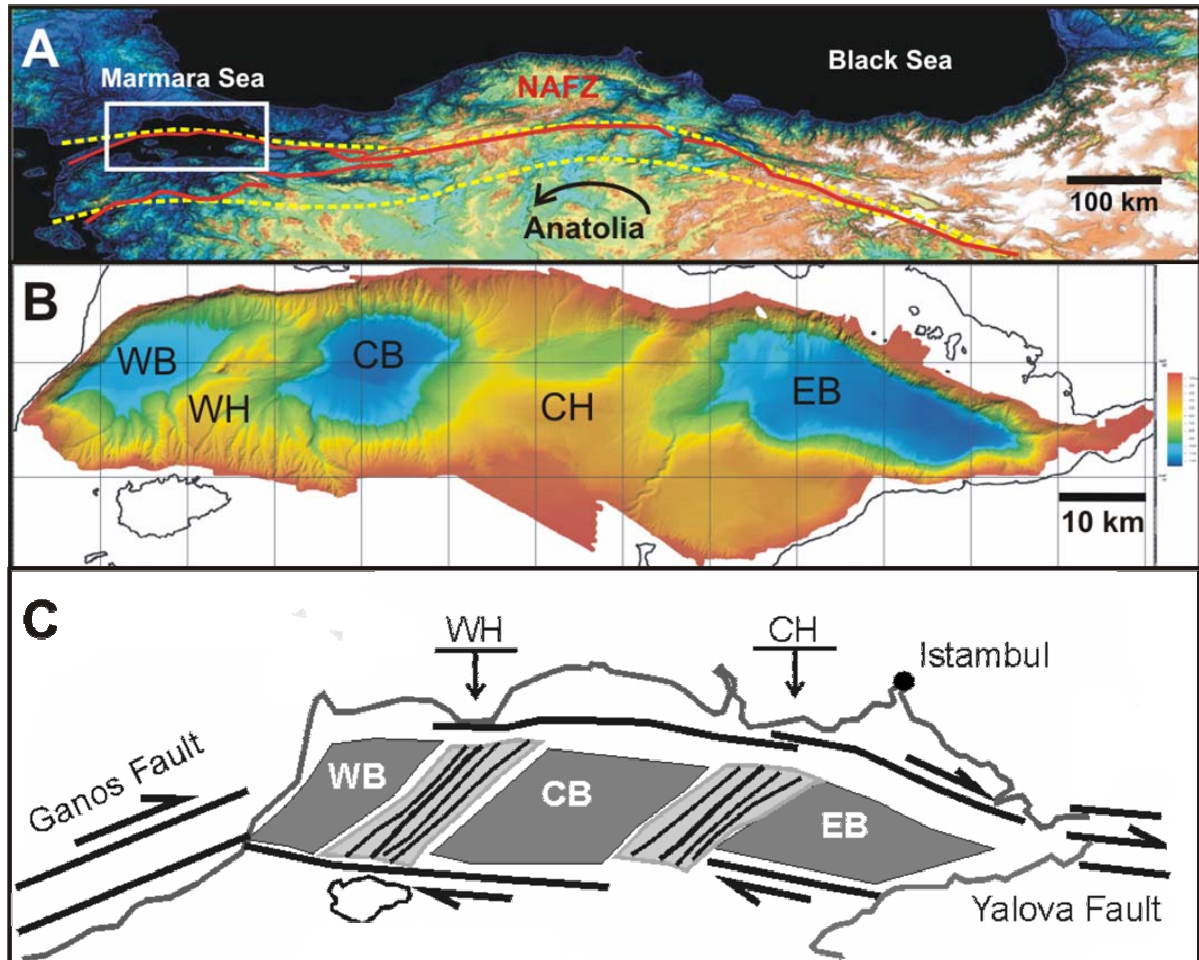


Fig. 26. The Marmara Sea basin. A) Digital elevation model of northern Turkey showing the North Anatolian Fault Zone (NAFZ) in red, and its place within the North Anatolian Shear Zone (NASZ) in yellow discontinuous lines. The white box delimits the Marmara Sea and the northern strand of the NAFZ crossing it. The black arrow indicates the direction of motion and the rotation of the Anatolian block (Image from US Geological Survey, tectonic data after Şengör et al., 2005). B) Colour shaded bathymetric map realised by Ifremer, Ecole Normale Supérieure, on board Le Suroit. The map shows the deformation zone, where three deep basins (in blue) are separated by two highs. C) Tectonic sketch of the complex Marmara Sea basin, NW Turkey. Modified after Aksu et al. (2000) and Imren et al. (2001). The North Anatolian Transform Fault Zone (NATFZ) consists of the two Ganos and Yalova Faults west and east of the sea respectively. The complex basin is a deformation zone formed of several basins (dark grey) and push-up ridges (light grey). The principal structures are: (WB) Western Basin, called Tekirdağ; (WH) Western High; (CB) Central Basin; (CH) Central High; (EB) Eastern Basin, called Çınarcık.

8.2.1. Geology of the North Anatolian Fault Zone (NAFZ)

The NAFZ is an approximately 1500 km long dextral strike-slip fault zone extending from the Karliova triple junction in the east to the North Aegean Sea in the west. It formed along a tectonic boundary separating subduction complexes and accreted crust to the south from

older continental basement to the north. Its cumulative offset has been estimated to 85 ± 5 km. However, considerable strike-slip motion occurred in a much broader shear zone of similar trend, the so called North Anatolian Shear Zone (NASZ) before the deformation became localised and led to the formation of the NAFZ (Şengör et al., 2005; Fig. 26A). The NASZ is a westerly widening dextral shear zone of late Palaeozoic to early Tertiary age, whereas the NAFZ initiated 13 to 11 Ma ago in the east and propagated westward. The accretionary complexes in the Marmara Sea region are bordered to the east by the Istanbul Zone. Together they form the basement for the hydrocarbon bearing Mid-Eocene to Oligocene sedimentary cover of the Thrace Neogene Basin. The northern strand of the NAFZ reached the Marmara Sea only about 200 ka ago. It consists of two subaerial segments east and west of the sea, the Yalova and Ganos faults respectively, which still need to be connected through a fully developed submarine segment. Especially the area west of Istanbul region constitutes a structural and seismic gap.

8.2.2. Structure of the Marmara Sea basin

Beneath the Sea of Marmara there is an arc-shaped E-W trending deformation zone about 150 km long and 35 km wide, delimited by steep boundary faults that dip toward its axis. The western and eastern margins are linked to the Ganos and Yalova fault segments of the northern strand of NAFZ respectively. The deformation zone consists of principally three bathymetric basins deeper than 1200 m, which are separated by two push-up ridges that rise about 600 m above the adjacent basins (Fig. 26B). These alternating contractional and extensional structures form an echelon rhombohedral to elongate blocks with aspect ratios of about 2.3:1. The Plio-Quaternary basins are from west to east Western Basin WB (or Tekirdağ), Central Basin CB, and Eastern Basin EB (or Çınarcık), whereas the separating ridges are termed Western High WH and Central High CB. The basins are filled with Upper Miocene to Recent unconsolidated sediments over 2 km in thickness, mainly mud to clay and sandy to silty turbidite layers. The basins are bound by three sets of faults: (1) WNW-ESE trending dextral strike-slip faults, (2) NE-SW to ENE-WSW trending oblique strike-slip faults,

and (3) E-W trending dextral strike-slip faults (Fig. 26C). The ridges are formed of NE trending thrust faults and folds which bend clockwise toward the boundary faults, compatible with dextral shear displacement (Aksu et al., 2000). In the Central High, the folds are organised into a broad antiform bounded by two major thrust faults. Gravity-driven extension faults occur along its upper surface (Yaltirak, 2002; Fig. 27).

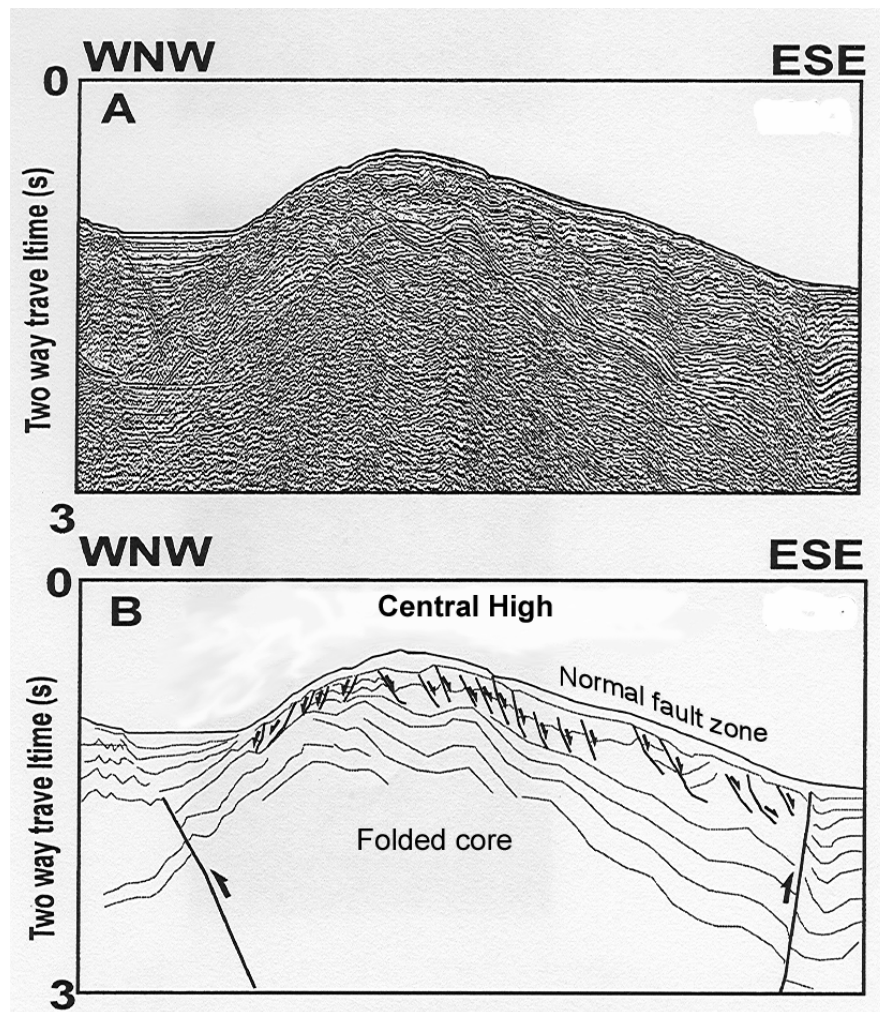


Fig. 27. A) Time-migrated seismic reflection profile along Seismic Line M13 showing the Central High. B) Structural interpretation according to Yaltirak (2002). The push-up ridge is an antiform bounded by two major thrust faults. The core is folded, and shallow normal faults develop on a detachment surface (simplified from Yaltirak, 2002).

CHAPTER 9: INTERPRETATION AND DISCUSSION

9.1. RIEDEL TYPE PULL APART BASINS

9.1.1. The Strait of Sicily Complex rift zone

The natural examples described above show that both extension fractures or normal faults and shear fractures or strike-slip faults can bound pull-apart structures formed along a strike-slip zone. Kim and Sanderson (2004) found that the strike-slip faults on Gozo Island shared many geometric features at different scales, the self-similarity of the deformation zone structure being supported by a fractal analysis. The strike-slip zones in the Plio-Quaternary Strait of Sicily Complex rift zone are interpreted to be due to the reactivation of deep seated E-W to WNW-ESE trending faults, and to fault propagation into the overlying sedimentary rocks. Assuming that the processes are similar to the Riedel type mechanism, the results of our experiments may help to understand their formation and evolution.

The first brittle structures that form in the clay models are the en echelon Riedel and conjugate Riedel shears. In the natural examples, this corresponds to the synthetic and antithetic strike-slip faults. No extension fractures were generated in our experiments, while earlier studies (e.g. Riedel, 1929; Wilcox et al., 1973; Smith and Durney, 1992) showed that such structures can appear at an early stage of deformation. The extension fractures and normal faults described by Reuther (1990) and Kim et al. (2003) also formed at an early stage. The Y- and P- shears formed at a later stage in our models correspond to the E-W trending synthetic faults in the natural examples. In this case the strike-slip motion is transferred to the E-W trending segments of the fault zone, pulling apart the previously formed synthetic and antithetic strike-slip and normal faults apart and creating the basins. This explains the major strike-slip component observed along the faults bounding the basins, as well as the small angle of about 22° (Fig. 25B) between the long axis of the basin and the E-W principal fault. For a bounding normal fault an angle close to 40° would be expected.

At a much larger scale, two models have been proposed for the evolution of the Plio-Quaternary Strait of Sicily Complex rift zone, both corresponding to the experimentally

observed Riedel type mechanism. The differences between the two models are mainly due to differing assumptions on the orientation of the maximum horizontal stress: Reuther (1980, 1990) assumes σ_H to be oriented in a NW-SE direction, Cello (1987) and Boccaletti et al. (1990) assume a NNW-SSE direction. Both models neglect the strike-slip component observed along the bounding basins and their axial orientation.

The pull-apart structures produced in our present Riedel type experiments offer an alternative explanation, which is intermediate between the two proposed models. All the structural trends developed during the Pliocene to Quaternary tectonic activity within the Strait of Sicily Pelagian platform can be found in our model for σ_H oriented at about 45° to several E-W to WNW-ESE dextral principal displacement zones at depth. In this case the basin bounding faults, which show both normal and dextral displacement, are suggested to represent Riedel type strike-slip faults. In our dextral shear experiments, the Riedel shears initiated at angles between 8° and 23° to the principal displacement zone, but were affected by a clockwise rotation of up to 4° . The bounding oblique faults of the major basins of the Strait of Sicily Complex rift zone are mainly oriented at angles between 10° and 40° to the inferred principal E-W trending strike-slip faults at depth. This suggests that rotation of these structures may be more important than in the model. Reuther (1980) reports rotations by up to 20° in the pull-apart basins along the South Gozo fault.

9.1.2. Models of pull-apart basin formation

Nilsen and Sylvester (1999) recognised six main types of strike-slip basins based on geometry and kinematic setting, of which only the simple pull-apart type has been experimentally modelled so far. Also, many of the natural pull-apart basins may have a complex history. The different experimental setups used to model these basins are not contradictory (e.g. Hempton and Neher, 1986; McClay and Dooley, 1995; this study). They demonstrate several feasible mechanisms, one of which may be dominant at a certain stage or certain scale during the evolution of the basins. For natural pull-apart basins, the underlying Riedel mechanism can be identified from geological and geophysical field

evidence. The main criteria are (1) presence of both a normal and a strike-slip component along the bounding faults of the incipient basins, (2) the relatively low angle between the oblique bounding faults and the principal strike-slip segments (below 30°), and (3) the high aspect ratio of the basins: with a long axis, a small width, and great depth.

The proposed evolution is close to the model of composite pull-apart basins proposed by Aydin and Nur (1982, their Model 1, Fig. 6 on p.99), where the length of the basin is equal to the offset at the bounding strike-slip faults, and the width of the basin is the sum of the widths of the initial pull-apart elements (Fig. 28A). In the experiments, the length of the pull-apart structures, usually used to estimate the strike-slip offsets in nature, does not reflect the total horizontal displacement along the basal deformation zone. The reason is that the initial Riedel shear fractures which bound the developing pull-apart structures accommodated a significant amount of the basal displacement prior to the formation of the basins (Fig. 28B).

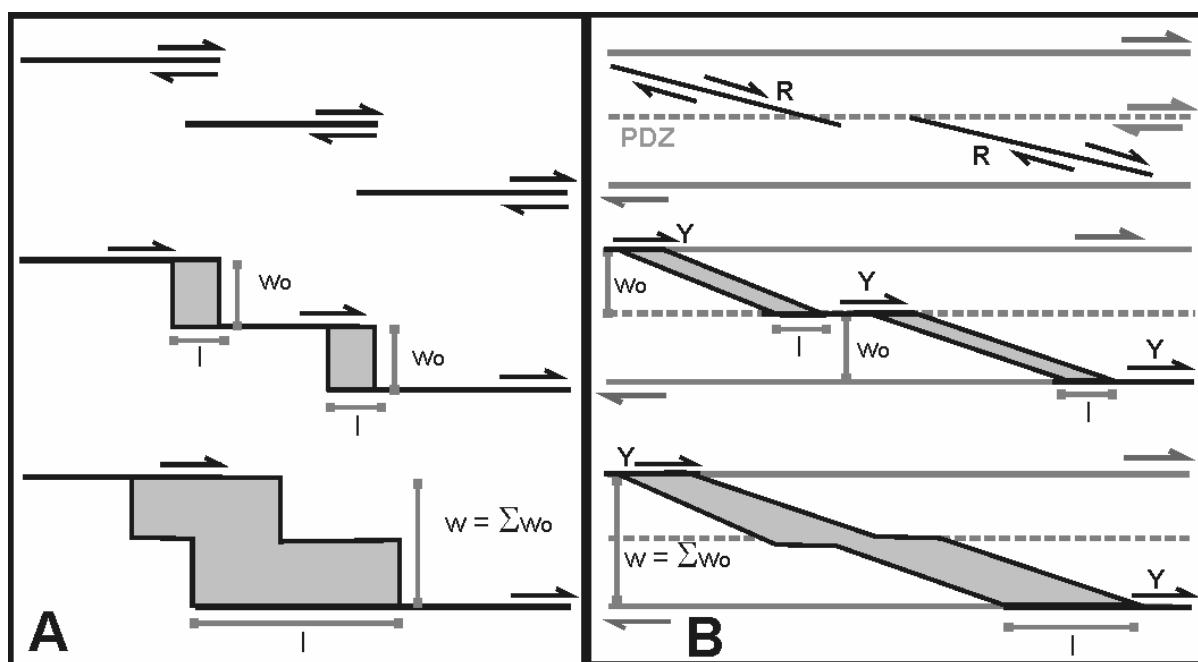


Fig. 28. Evolution of widths and lengths of pull-apart basins according to A) Aydin and Nur (1982), and B) the results of our clay analogue models. w_0 : initial width of pull-apart basin; w : width of coalesced pull-apart basin; l : length of basin equal to fault offset; PDZ: principal displacement zone; R: Riedel shears/faults; Y: shears/faults parallel to PDZ.

9.2. COEVAL FORMATION OF PULL-APART AND PUSH-UP STRUCTURES

9.2.1. The complex Marmara Sea basin

The complex structural architecture of the Marmara sea basin inspired several tectonic models. Yaltirak (2002) classified them into three groups: (1) the pull-apart and combined models; (2) the en echelon fault segments models; (3) the single buried master fault models (Fig. 29). For more information about these models, which total a number of 10, and their differences, the readers are referred to Yaltirak (2002). The conflicting tectonic interpretations are based on the different existing models explaining the formation of strike-slip basins.

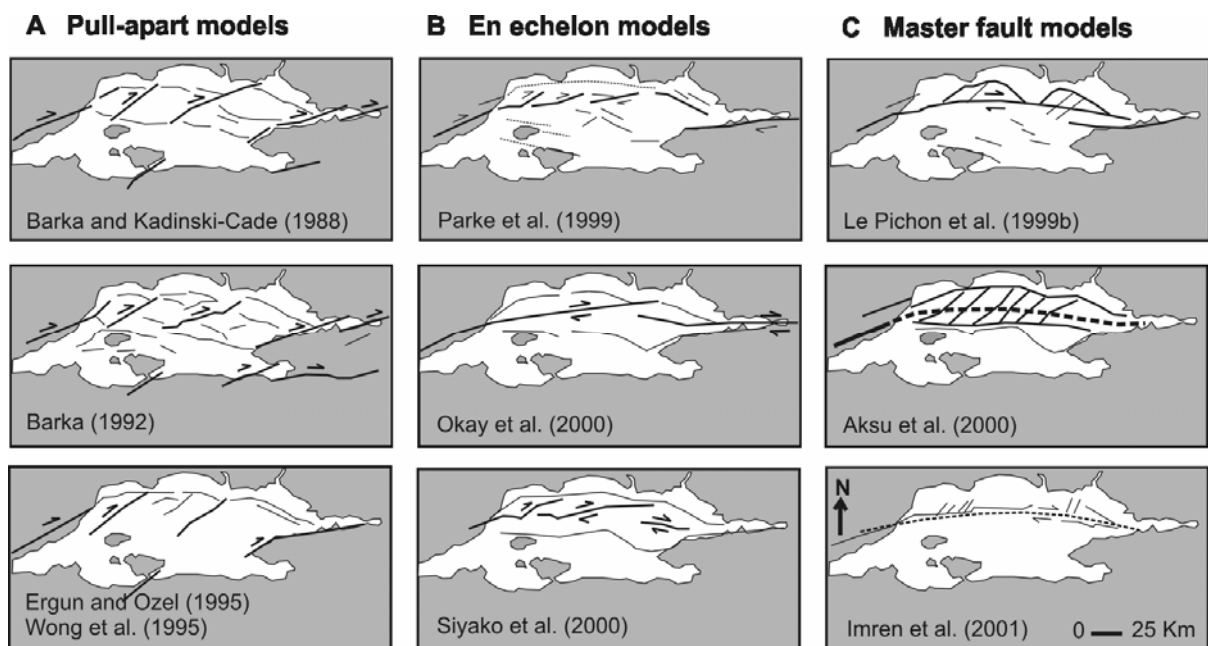


Fig. 29. The proposed tectonic models of the Marmara Sea after Yaltirak (2002, references therein). Bold lines represent the main active faults that form the Marmara Sea basin; thin lines show secondary faults. Dashed lines in (C) are the buried master fault in the basement.

In summary, these models are consistent interpretations when based on a certain number of data sets, but they do not allow a coherent geological synthesis (Şengör et al., 2005). They are commonly based on the assumption that the NAFZ created all the structures. It was found however, that the NAFZ alone cannot have caused the formation of the basins and ridges within the Marmara Sea, since most of them are older than the NAFZ. Recently, the tectonic interpretation has shifted towards a modified single buried master fault model, based

on the combination of geologic, recent geophysical, geodetic and seismotectonic studies (Yaltirak, 2002; Şengör et al., 2005). Thus, the northern strand of the NAFZ in the Marmara Sea region is recognised as the main through-going dextral strike-slip fault equivalent to the Y-type faults formed by the Riedel shear mechanism. A single sub E- W basement fault of the NASZ, buried at about 5 km depth below the Marmara Sea, created the progressive strike-slip deformation zone in the overlaying sedimentary layers (Aksu et al., 2000; Yaltirak, 2002; Şengör et al., 2005).

The geometrical architecture of this deformation zone and its kinematics (as described in section 8.2) match very well those of the deformation zones generated in the present scaled Riedel type experiments. This holds particularly for the standard model NA4 (sections 6.1.2 and 6.1.3). In this case the dextral motion along the buried basement fault generated in the Miocene to Pliocene normal, Riedel and conjugate Riedel faults in the sedimentary cover along the actual deformation zone. These are the en echelon WNW-ESE to NW-SE trending dextral strike-slip and oblique fault segments, as well as the now rotated NNE-SSW trending antithetic faults. The latter concentrate with the NE-SW folds, mainly in the overstepping areas separating the Riedel faults as shown by the analogue experiments. Progressive strain localised in the P- and Y- type segments actually constituting the NAFZ, which developed in the Pliocene to Recent. Most of these faults merge at depth with the basement fault, as described by Aksu et al. (2000).

In the NAFZ and the deformation zone of Marmara Sea, the P-type faults predominate rather than the boundary Y-shears in the analogue models. This difference results either from the influence of the older tectonic fabric of the intra-Pontide suture (Şengör et al., 2005), or from the geometrical influence of the wide arc the trace of NAFZ follows (Fig. 26A). Şengör (1995) studied the initiation and evolution of faults and related pull-apart structures within strike-slip zones along the NAFZ. He not only found similarities with the Riedel shear experiments of Tchalenko (1970), but described field cases where pull-apart basins initiated along tension gashes, Riedel faults and conjugate Riedel faults (Fig. 30). If one accepts the self-similarity of the Riedel shear mechanism at different scales (e.g. Tchalenko, 1970; Kim and

Sanderson, 2004; Şengör, 1995; Şengör et al., 2005), the Marmara Sea complex basin may have formed with this process.

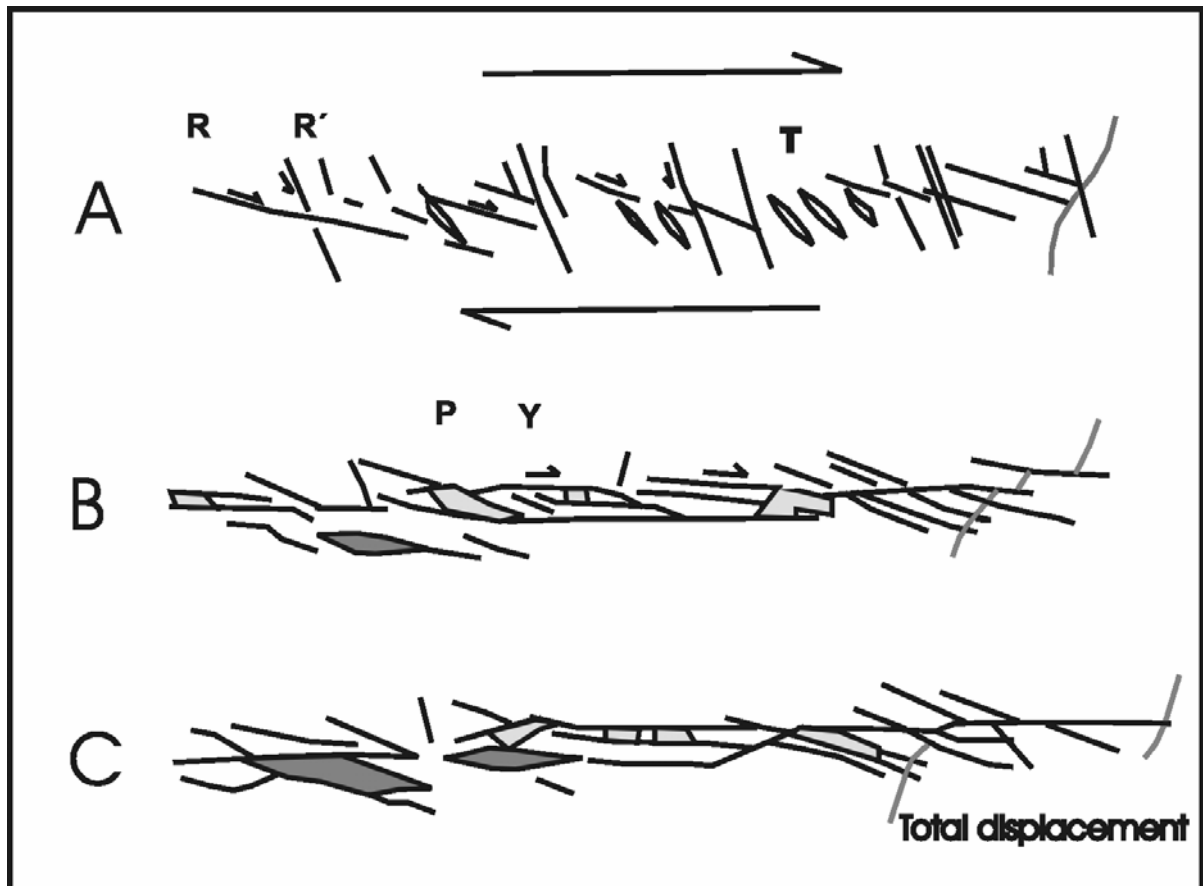


Fig. 30. Development of faults and related pull-apart basins in a strike-slip zone formed by the Riedel shear mechanism. A) Initiation of the Riedel and conjugate Riedel shears (R and R'), and of the tension fractures (T). B) Initiation of the Y- and P- shears. C) Strike-slip zone at a mature stage of development. Dark filling: pull-apart basin formed on a Riedel fault. Light fillings: pull-apart basins formed on conjugate Riedel faults and tension gashes. (simplified from Sengör, 1995).

9.2.2. Models of complex strike-slip basin formation

The coexistence and simultaneous development of pull-apart and push-up (also pop-up or pressure) structures as exemplified by the deformation zone in the Marmara Sea has been observed and described along strike-slip zones at various length scales (e.g. Aydin and Nur, 1982; Soula, 1984; Biddle and Christie Blick, 1985; Bergerat and Angelier, 2003; Fu et al., 2004). Also Schwarz (1990) and Hagglaue-Ruppel (1991) studied in detail the structural and geometrical architecture of natural and physically modelled push-up structures developed by the Riedel shear mechanism.

The generic analogue models performed in this study show that both extensional and contractional structures may originate from the same Riedel shear mechanism. The left-stepping arrangement of the Riedel shear fractures generates contraction at the overstepping areas, where the conjugate Riedel shears predominate (Fig. 31A). Both shear fractures rotate clockwise, although by different angles. The Riedel shear fractures accommodate the horizontal displacement, whereas the conjugate Riedel fractures mainly rotate. Small scale antiforms and reverse faults initiate at the push-up structures (Fig. 31B). Pull-apart structures develop at the Riedel shear fractures as explained in section 9.1, whereas small scale thrust faults form at the push-up structures. Their full development is possible only when the linkage of the Y- and P- shears is delayed (Fig. 31C). At further basal shear displacement the shear activity in the cover is transferred progressively from the Riedel shears to P- and Y- shear fractures. If Y-shear fractures develop and link immediately after the formation of the Riedel shear fractures, the full development of push-up structures at the oversteps is inhibited (Fig. 18 and Fig. 28B).

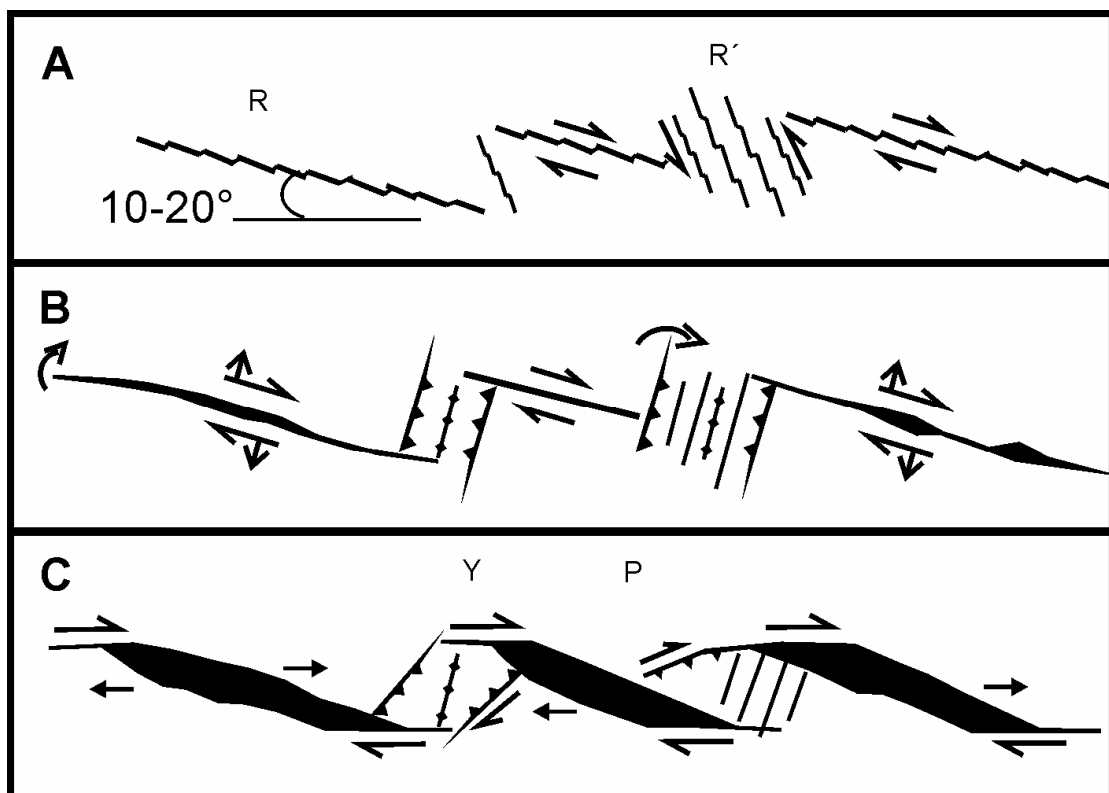


Fig. 31. Coeval evolution of pull-apart basins and push-up ridges generated by the Riedel mechanism. A) Formation of the Riedel and conjugate Riedel shear fractures. B) Clockwise rotation of the fractures, shear and dilatation of the Riedel shears. Small scale folding and reverse faulting at the push-up ridges. C) Development of

P- and Y-shear fractures. Formation of pull-apart structures at the Riedel shears. Further contraction at the push-up ridges till full linkage of the Y-shears within the strike-slip zone.

9.3. INFLUENCE OF THE MATERIAL PROPERTIES

In all three mechanisms introduced in the first chapter, the displacement magnitude along the PDZ in the basement is important, since formation of pull-apart basins commences only after the development of the Y- and P-segments. In contrast, models based on the en echelon basement strike-slip fault type mechanism show that step-over geometry in the basement is a primary factor controlling the location and geometry of the pull-apart structures.

During the processes that lead from original sediment deposition to the formation of consolidated rocks, material properties of the sediments and sedimentary rocks undergo significant changes. Our scaled analogue experiments have shown that material properties distinctly influence the development and geometry of pull-apart basins forming above a single and linear basement strike-slip fault. The physical properties of the clay material indicate that hydro-mechanical effects are coupled in the deformation of sediments and sedimentary rocks below water table. This infers that in nature the processes of pull-apart basin formation may differ if they take place in sedimentary rocks of different stages of consolidation. Although traditionally deformational structures are thought to form after consolidation and lithification of the sediments into sedimentary rocks, the presented example of the complex basin in the Marmara Sea affected also saturated and poorly lithified or unconsolidated sediments. Similarly, Maltman (1994, 1998) has shown a wide variety of structures that formed early in the burial history of sediments as a result of tectonic stresses associated with plate convergence. Therefore it is crucial for the understanding of pull-apart basin formation in nature to know the exact timing and history of basin evolution in relation to depositional and diagenetic processes. Such an approach requires a combination of geophysical structural imaging, geological field work, and laboratory experimental modelling.

CHAPTER 10: CONCLUSIONS

The Riedel mechanism of pull-apart and associated push-up formation is investigated in scaled analogue experiments with clay slabs of variable thickness and shear strength representing the sedimentary cover. The experiments produced a series of typical pull-apart structures. At the initial stages of the development of the deformation zone within the clay slab, the synthetic shear fractures (Riedel shears) display dilatational behaviour. With increasing basal displacement these dilated shears rotate and open further. The shear displacements and the low angle of orientation to the direction of principal basal displacement distinguish them from the tension fractures. Synthetic segments (Y-shears), which are parallel to the basal principal displacement fault, develop in a later stage and accommodate the continuing strike-slip deformation. They bound the troughs at the two tips of the initial Riedel shears and pull the sides further apart. Many rhomb shaped structures which characterise the pull-apart basins are then recognised. This development mechanism of pull-apart basins may explain why some en echelon segments of strike-slip faults display an extensional component in addition to the main shear displacement (transtension).

The shear strength of the clay slab (controlled by the water content) and the thickness control the width of the deformation zone, the number and spacing of the Riedel shears, the presence or absence of the conjugate Riedel shears and the amount of basal shear displacement required for the shear fractures to appear at the surface. The dependencies can be summarised as follows:

- (1) The width of the strike-slip deformation zone increases with increasing shear strength and with increasing thickness of the clay slab.
- (2) The number of the conjugate Riedel shears increases with increasing shear strength. A minimum thickness of 4 cm (corresponding to 0.2 to 2 km in nature) is required for their development.

(3) The number of the Riedel shears increases with decreasing shear strength, and their spacing decreases accordingly. Also, the number of Riedel shears per unit length is inversely proportional to the thickness of the clay slab.

(4) The shear fractures developed in an en echelon pattern in all models, with a tendency for more complex arrangement with increasing thickness of the clay slab.

(5) The amount of basal shear displacement required for the first shears to appear at the surface increases with decreasing shear strength and increasing thickness of the clay slab.

In order to scale such models, clays of extremely low shear strength and with a critical shear angle at failure similar to that of sedimentary rocks are needed. In addition, we need to know the density of the clay at a particular water content. It is important that the physical and mechanical properties of the clays are determined at the state and boundary conditions corresponding to those attained in the tectonic analogue experiments. Clays that fulfill the above criteria are nearly saturated silty clays and clays of the kaolinitic group, deformed under undrained conditions at very low effective stresses. Such clays are characterized by a low clay fraction ($CF < 50\%$), a low to medium plasticity index ($PI < 20\%$, and $W_L < 40\%$), and an angle of internal friction ϕ'_{cs} between 29° and 38° .

In the experiments, the length of the pull-apart structures, usually used to estimate the strike-slip offsets in nature, does not reflect the total horizontal displacement in the basement. The initial Riedel shear fractures bounding the developing pull-apart structures accommodated a significant amount of the basal displacement prior to formation of the basins. The left-stepping arrangement of the Riedel shear fractures promotes the formation of push-up ridges at the overstepping areas separating them. The progressive clockwise rotation of the conjugate Riedel shears within these structures shows the partial transfer of horizontal motion from one Riedel shear to the adjacent one. A part of the horizontal motion is accommodated by the development of contractional features (folds, reverse and thrust faults) and the increase of vertical displacements at the push-up ridges, as long as the Riedel shear fractures are active. The amplitude of the vertical motions stagnates when Y-shear fractures are fully formed, which accommodate thereafter the continuing basal shear deformation. A

higher shear strength of the modelling material enhances the vertical displacement. Also, a thicker clay slab requires larger amounts of basal displacement to cause a significant vertical displacement at the ridges.

The experimental results compare well with the natural pull-apart basins in the Strait of Sicily rift zone. The coexistence and simultaneous development of pull-apart basins and push-up ridges is shown to be possible with the Riedel shear mechanism, as exemplified by the complex strike-slip basin of the Marmara Sea. Also, the performed experiments suggest that the mechanisms of basin formation may be scale-independent.

REFERENCES

- Aksu A, Calon TJ, Hiscott RN, Yasar D (2000) Anatomy of the North Anatolian Fault Zone in the Marmara Sea, Western Turkey: extensional basins above a continental transform. *GSA Today* 10, 6:3-7
- An L-J, Sammis CG (1996) Development of strike-slip faults: shear experiments in granular materials and clay using a new technique. *J Struct Geol* 18:1061-1077
- Armijo R, Meyer B, Navarro S, King G, Barka A (2002) Asymmetric slip partitioning in the Sea of Marmara pull-apart: a clue to propagation processes of the North Anatolian Fault? *Terra Nova* 14, 2:80–86
- Atkinson JH, Bransby PL (1978) *The mechanics of soils: an introduction to critical state soil mechanics*. McGraw-Hill, London, pp 1-375
- Attewell PB, Farmer IW (1976) *Principles of engineering geology*. John Wiley & Sons, New York, USA
- Audemard F, Pantosti D, Machette M, Costa M, Okumara K, Cowan H, Diederix H, Ferrer C and participants of SAWOP 1998 (1999) Trench investigation along the Merida section of the Bocono fault (Central Venezuelan Andes), Venezuela. *Tectonophysics* 308:1-21
- Aydin A, Nur A (1982) Evolution of pull-apart basins and their scale independence. *Tectonics* 1:91-105
- Bagnold RA (1966) The shearing and dilation of dry sand and the 'singing' mechanism. *Proc R Soc Lond A* 295:219-232
- Barlett WL, Friedman M, Logan JM (1981) Experimental folding and faulting of rocks under confining pressure *Tectonophysics* 79:255-277
- Belousov VV (1961) Experimental geology. *Scientific American* 204:97-106
- Belousov VV and Gzovsky MV (1965) Experimental tectonics. In: Ahrens LH, Press F, Runcorn SK Urey HC (eds.). *Physics and chemistry of the Earth*. Pergamon Press, Oxford, pp 409-499
- Beltran C (compiler) (1993) *Mapa Neotectonico de Venezuela*. Funvisis 1:2,000,000 scale
- Bergerat F and Angelier J (2003) Mechanical behaviour of the Arnes and Hestfjall faults of the June 2000 earthquakes in southern Iceland: inferences from surface traces and tectonic model. *J Struct Geol* 25:1507-1523
- Biddle KT, Christie-Blick N (1985) Strike-slip deformation, basin formation, and sedimentation. *Soc Econ Paleont Min Spec Publ*:37
- Bjørlykke K (1997) Lithological control on fluid flow in sedimentary basins. In: Jamtveit B, Yardley B (eds.). *Fluid flow and transport in rocks. Mechanics and effects*. Chapman and Hall, Oxford, pp 15-34

- Boccaletti M, Cello G, Tortorici L (1990) Strike-slip deformation as a fundamental process during the Neogene-Quaternary evolution of the Tunisian-Pelagian area. *Annales Tectonicæ Special issue 4*:104-119
- Bolton M (1986) The strength and dilatancy of sands. *Geotechnique* 36:65-78
- Bolton M (1979) A guide to soil mechanics. Macmillan Press, London, pp.1-439
- Brix M, Schwarz H-U, Vollbrecht A (1985) Tektonische Experimente als Beitrag zu Strukturanalysen im Ruhrkarbon. *Glückauf-Forschungshefte*, 46 (H.4):192-199
- Carmichael RS (1990) Practical handbook of physical properties of rocks and minerals. CRC Press, USA
- Cello G (1987) Structure and deformation processes in the Strait of Sicily "rift zone". *Tectonophysics* 141:237-247
- Cloos H (1928) Experimente zur inneren Tektonik. *Centralbl Mineral Pal* 5:609-621
- Cloos E (1955) Experimental analysis of fracture patterns. *Geol Soc Am Bull* 66:241-256
- Dahlen FA, Suppe J, Davis D (1984) Mechanics of fold-and-thrust belts and accretionary wedges: cohesive Coulomb theory. *J Geophys Res* 89:10087-10101
- Davis D, Suppe J, Dahlen FA (1983) Mechanics of fold-and-thrust belts and accretionary wedges. *J Geophys Res* 88:1153-1172
- Deramond J, Sirieys P, Soula JC (1983) Mécanismes de déformation de l'écorce terrestre: structures et anisotropie induites. 5th Congress Intern Soc Rock Mech Melbourne F:89-93
- Dewey JF (1978) Origin of long transform-short ridge systems. *Geol Soc America* 10:388
- Dooley T, McClay K, (1997) Analogue modelling of pull-apart basins: American Association of Petroleum Geologists Bulletin 81:1804–1826
- El-Gharbawy SL (1998) The pullout capacity of suction caisson foundations for tension leg platforms. Ph.D. dissertation, The University of Texas at Austin, USA
- Erkan M (1982) Experimentelle Untersuchungen der Weiterentwicklung vorgegebener Seitenverschiebungen der Schrägabschiebungen in einem ungestörten Gebirge. Dipl –Arb. Ruhr-University of Bochum, Germany
- Fu B, Awata Y, Du J, Ninomiya Y, He W (2005) Complex geometry and segmentation of the surface rupture associated with the 14 November 2001 great Kunlun earthquake, northern Tibet, China. *Tectonophysics* 407:43-63
- Gamond J-F (1983) Displacement features associated with fault zones: a comparison between observed examples and experimental models. *J Struct Geol* 5:33-45
- Gamond J-F (1987) Bridge structures as a sense of displacement criteria in brittle fault zones. *J Struct Geol* 9:609-620
- Gapais D, Fiquet G, Cobbold PR (1991) Slip system domains, 3. New insights in fault kinematics from plane-strain sandbox experiments. *Tectonophysics* 188:143-157

- Gölke M, Cloetingh S, Fuchs (1994) Finite-element modelling of pull-apart basin formation. *Tectonophysics* 240:45-58
- Hagglauer-Ruppel B (1991) Kinematik und Begleitstrukturen von Scherzonen: Experimente und Beispiele Mitteleuropas (mit besonderer Berücksichtigung des Osning-Lineamentes). Unpublished Ph.D. thesis, Ruhr-University of Bochum, Germany
- Hempton M, Neher K (1986) Experimental fracture, strain and subsidence patterns over an echelon strike-slip faults: implications for the structural evolution of pull-apart basins. *J Struct Geol* 8:597-605
- Hoeppener R, Kalthoff E, Schrader P (1969) Zur physikalischen Tektonik. Bruchbildung bei verschiedenen affinen Deformationen im Experiment. *Geol Rdsch* 59:179-193
- Hoeppener R, Schwarz H –U (1980) Experimentelle Untersuchungen über Schiefergefüge und Gefüge in geschieferten Gesteinsverbänden. *N Jb Geol Paläont Abh* 160, 3:363-379
- Hubbert MK (1937) Theory of scale models as applied to study of geological structures. *Geol Soc Am Bull* 48:1459-1520
- Hubbert MK (1951) Mechanical basis for certain familiar geologic structures. *Geol Soc Am Bull* 62:355-372
- İmren C, Le Pichon X, Rangin C, Demirbağ E, Ecevitoglu B, Görür N (2001) The North Anatolian Fault within the Sea of Marmara : a new evaluation based on multichannel seismic and multibeam data, revision stage. *Earth Planet Sci Lett*, 186:143-158
- Jongsma D, van Hinte JE, Woodside JM (1985) Geologic structure and neotectonics of the North African Continental Margin south of Sicily. *Marine and Petroleum Geol* 2:156–179
- Jones M (1994) Mechanical principles of sediment deformation. In: Maltman A (ed.). *The geological deformation of sediments*. Chapman and Hall, London, pp 37-71
- Japan Nuclear Cycle Development Institute (2000) The geological environment of Japan. In *Geological Isolation Research Project, Overview Report H12, English version*.
- Kalthoff E (1970) Bruchbildung in Modellsubstanzen bei Deformationen mit axialer und rhombischer Symmetrie. Unpublished Ph.D. thesis, Ruhr-University of Bochum, Germany
- Katzman R, ten Brink US, Lin J (1995) 3-D modelling of pull-apart basins: Implications for the tectonics of the Dead Sea Basin. *J Geophys Res* 100:6295-6312
- Kim Y-S, Peacock DCP, Sanderson D (2003) Mesoscale strike-slip faults and damage zones at Marsalforn, Gozo Island, Malta. *J Struct Geol* 25:793-812
- Kim Y-S, Sanderson D (2004) Similarities between strike-slip faults at different scales and a simple age determining method for active faults. *Island-Arc* 13:128-143

- Krantz RW (1991) Measurements of friction coefficients and cohesion for faulting and fault reactivation in laboratory models using sand and sand mixtures. *Tectonophysics* 188:203-207
- Ladd CC, Foott R, Ishihara K, Schlosser F, Poulos HG (1977) Stress-deformation and strength characteristics. *Proc 9th Int Conf on soil mechanics and foundation engineering Tokyo* 2:421-482
- Lazarte CA, Bray JD (1996) A study of strike-slip faulting using small-scale models. *Geotech Testing J* 19:118-129
- Le Calvez JH, Vendeville BC (2002) Experimental designs to model along-strike fault interaction. In: Schellart WP, Passchier C (eds.). *Analogue modelling of large-scale tectonic processes*. *J Virtual Explorer* 7:7-23
- Le Pichon X, Şengör AMC, Demirbağ E, Rangin C, İmren C, Armijo A, Görür N, Çağatay N, Mercier de Lepinay B, Meyer B, Saatçılar R, Tok B (2001) The active Main Marmara Fault. *Earth Planet Sci Lett*, 192:595-616
- Logan JM, Dengo CA, Higgs NG, Wang ZZ (1992) Fabrics of experimental fault zones: their development and relationship to mechanical behaviour. In: Evans B, Wong T-F (eds.). *Fault mechanics and transport properties of rocks*. Academic Press, London, pp 33-67
- Lohrmann J, Kukowski N, Adam J, Oncken O (2003) The impact of analogue material properties on the geometry, kinematics, and dynamics of convergent sand wedges. *J Struct Geol* 25:1691-1711
- Maksimovic M (1996) A family of non-linear failure envelopes for non-cemented soils and rock discontinuities. *Electron Journ Geotechn Eng* vol. 1
- Maltman AJ editor (1994) *The geological deformation of sediments*, Chapman and Hall, London
- Maltman AJ (1998) Deformation structures from the toes of active accretionary prisms. *J Geol Soc* 155:639-650
- Mandl G (1988) *Mechanics of tectonic faulting*. Elsevier, Amsterdam, pp 135-152
- Mann P, Hempton MR, Bradley DC, Burke K (1983) Development of pull-apart basins. *J Geol* 91:529-554
- Marone C (1998) Laboratory-derived friction laws and their application to seismic faulting. *An Rev Earth Planet Sci* 26:643-696
- McClay K, Dooley T (1995) Analogue models of pull-apart basins. *Geology* 23:711-714
- Morgan MA, Grocott J, Moody RTJ (1998) The structural evolution of the Zaghouan-Ressas Structural Belt, northern Tunisia. In: Macgregor DS, Moody RTJ, Clark-Lowes DD (eds.). *Petroleum geology of North Africa: Geol Soc London, Spec Publ* 132:405-422

- Morgenstern NR, Tchalenko JS (1967) Microscopic structures in kaolin subjected to direct shear. *Geotechnique* 17:309-328
- New Zealand Geotechnical Society Inc. (2001) Guideline for hand held shear vane test. 10p
- Nilsen TH, Sylvester AG (1999) Strike-slip basins. Part 1. *The Leading Edge* 18:1146-1152
- Oertel G (1965) The mechanics of faulting in clay experiments. *Tectonophysics* 2:343-393
- Pedersen CR, Olson RE and Rauch AF (2003) Shear and interface strength of clay at very low effective stress. *Geotechnical Testing Journal* 26:71-78
- Pinto da Cunha A ed. (1993) Scale effects in rock masses. Proc 2nd International Workshop Lisbon Portugal June 1993. Balkema, Rotterdam.
- Rahe B, Ferill DA, Morri, AP (1998) Physical analogue modelling of pull-apart basin evolution. *Tectonophysics* 285:21-40
- Reches Z (1988) Evolution of fault patterns in clay experiments. *Tectonophysics* 145:141-156
- Reuther C-D (1980) Das Pantelleria Rift. Kinematik miozäner bis rezenter Krustendehnungsprozesse bei Konvergenter Intraplattentektonik im zentralen Mittelmeer. Habilitation manuscript, Fridericiana University of Karlsruhe, Germany, pp 1-139
- Reuther C-D (1990) Strike-slip generated rifting and recent tectonic stresses on the African foreland (Central Mediterranean region). *Annales Tectonicæ Spec issue* 4:120-130
- Reynolds O (1885) On the dilatancy of media composed of rigid particles in contact, with experimental illustrations. *Phil Mag* 20:469-481
- Riedel W (1929) Zur mechanik geologischer Brucherscheinungen. *Zentralblatt Mineral Geol Paläont B*:354-368
- Rodgers DA (1980) Analysis of pull-apart basin development produced by en-echelon strike-slip faults. *Int Assoc Sedimentol Spec Publ* 4:27-41
- Rummel F (1982) Fracture and flow of rocks and minerals. In: Angenheister G (ed.). *Physical properties of rocks/Physikalische Eigenschaften der Gesteine*. Springer Verlag, Heidelberg, Berlin, Subvol B:141-238
- Santamarina JC (1997) "Cohesive soils": a dangerous oxymoron. *Electronic Journal of Geotechnical Engineering, iGEM Magazine*
- Schellart WP (2000) Shear test results for cohesion and friction coefficients for different granular materials; scaling implications for their usage in analogue modelling. *Tectonophysics* 324:1-16
- Schofield AN, Wroth CP (1968) *Critical state soil mechanics*. McGraw-Hill, London
- Schopper JR (1982) Porosity and permeability of rocks. In: Angenheister G (ed.). *Physical properties of rocks/Physikalische Eigenschaften der Gesteine*. Springer Verlag, Heidelberg, Berlin, Subvol A:184-304

- Schöpfer MPJ, Steyrer HP (2001) Experimental modelling of strike-slip faults and the self-similar behaviour. In: Koyi HA, Mancktelow NS (eds.). *Tectonic Modeling. A volume in honor of Hans Ramberg*. Geol Soc Am Memoir 193:21-27
- Schrader P (1970) Bruchbildung in Modellschubstoffen durch Deformation mit monokliner Symmetrie. Unpublished Ph.D. thesis, Ruhr-University of Bochum, Germany
- Schreurs G (2003) Fault development and interaction in distributed strike-slip shear zones: an experimental approach. In: Storti F, Holdsworth RE, Salvini F (eds.). *Intraplate strike-slip deformation belts*. Geol Soc London Spec Publ 210:35-52
- Schubert C (1982) Neotectonics of the Bocono fault western Venezuela. *Tectonophysics* 85:205-220
- Schwarz H-U (1990) Modellversuche zur Deutung der Struktur Husum-Schneeren. Unpublished report for Preussag Erdöl und Erdgas GmbH. Bochum, 120 pages
- Segall P, Pollard D (1980) Mechanics of discontinuous faults. *J Geophys Res* 85:4337-4350
- Şengör AMC, Tüysüz O, İmren C, Sakiñç M, Eyidoğan H, Görür N, Le Pichon X, Rangin C (2005) The North Anatolian Fault: a new look. *Annu Rev Earth Planet Sci.* 33:37-112
- Şengör AMC (1995) Sedimentation and tectonics of fossil rifts. In: Busby CJ, Ingersoll RV (eds). *Tectonics of sedimentary basins*. Blackwell, Oxford. pp: 53-117
- Serota S, Jangle A (1972) A direct-reading pocket shear vane. *Civil Eng ASCE* 42:73-76
- Smith JV, Durney DW (1992) Experimental formation of structural assemblages in oblique divergence. *Tectonophysics* 216:235-253
- Sims D (1993) The rheology of clay: a modeling material for geologic structures. *EOS, Transactions of the American Geophys. Union, Abstracts*, 74:569
- Soula J-C (1984) Genese de bassins sédimentaires en régime de cisaillement transcurrent: modèles expérimentaux et exemples géologiques. *Bull Soc Belge de Géologie* 93 (1-2):83-104
- Sridharan A (2002) Engineering behaviour of clays: influence of mineralogy. In: Di Maio C, Hueckel T, Loret B (eds.). *Chemo-mechanical coupling in clays: from nano-scale to engineering applications*. Swets and Zeitlinger, Lisse, pp 3-28
- Summers HS (1932) Experimental tectonic geology. *Aust & New Zealand Assoc Adv Sci Report* 21:49-74
- Sylvester AG (1988) Strike-slip faults. *Geol Soc Am Bull* 100:1666-1703
- Tchalenko J S (1970) Similarities between shear zones of different magnitudes. *Geol Soc Am Bull* 81:1625-1640
- ten Brink US, Rybakov M, Al Zoubi A, Hassouneh M, Frieslander U, Batanyeh AT, Goldschmidt V, Daoud N, Rotstein Y, Hall JK (1999) Anatomy of the Dead Sea transform: Does it reflect continuous changes in plate motion? *Geology* 27(10):887-890

- Terzaghi K (1936) The shearing resistance of saturated soils and the angle between the planes of shear. Proc 1st Inter Conf Soil Mech Found Eng, Harvard, 1:54–56
- Terzaghi K, Peck RB, Mesri G (1996) Soil mechanics in engineering practice. John Wiley, New York, pp 1-208
- Walmann T (1998) Dynamics and scaling properties of fractures in clay-like materials. Ph.D. thesis, University of Oslo, Norway.
- Weijermars R, Jackson MPA, Vendeville BC (1993) Rheological and tectonic modelling of salt provinces. *Tectonophysics* 217:143-174
- Whitlow R (2001) Basic soil mechanics. Pearson Education Ltd, London, pp 1-571
- Wilcox RE, Harding TP, Seely DR (1973) Basic wrench tectonics. *Am Assoc Petr Geol Bull* 57:74-96
- Wohlenberg J (1982) Densities of rocks. In: Angenheister G (ed.). *Physical properties of rocks/Physikalische Eigenschaften der Gesteine*. Springer Verlag, Heidelberg, Berlin, Subvol A:113-119
- Wood MD (1990) Soil behaviour and critical soil mechanics. Cambridge University Press, Cambridge
- Woodcock NH (1986) The role of strike-slip fault systems at plate boundaries. *Phil Trans R Soc London A317*:13-29
- Yaltirak C (2002) Tectonic evolution of the Marmara Sea and its surroundings. *Marine Geology* 190:493-529
- Zhu W, Laurent GJ, Montesi, Wong TF (2002) Effects of stress on the anisotropic development of permeability during mechanical compaction of porous sandstones. In: De Meer S, Drury MR, De Bresser JHP, Pennock GM (eds.). *Deformation mechanisms, rheology and tectonics: current status and future perspectives*. *Geol Soc London Spec Publ* 200:119-136

APPENDIX A: OVERVIEW ON PERFORMED EXPERIMENTS

	V29	NA1	NA2	NA4	NA5	NA6	NA7	NA8	NA9	NA10
DIMENSION (cm)	60 X 90	60 X 90	60 X 90	36 X 300	36 X 400	35 X 90	35 X 90	35 X 90	20 X 90	35 X 90
THICKNESS (cm)	18	6	6	4	4	2	4	8	2	4
WATER CONTENT (%)	40	42	42	42	42	47	48	42	42	38
TOTAL BASAL DISPLACEMENT (mm)	82	74	74	83	74	32	40	82	36	60
DISPLACEMENT RATE (mm/min)	0.42	0.46	0.49	0.41	0.40	0.48	0.44	0.43	0.42	0.40
WIDTH OF DEFORMATION ZONE (cm)	35.8	7.6	7.8	5.2	5.5	2.7	4.1	11.5	2.2	5.7

APPENDIX B: LABORATORY WORK

1. PREPARATION OF CLAY- WATER MIXTURES

The method describes the procedure used in this study to prepare the clay material, which is a mixture of a commercial kaolinitic powder and normal water. A mixing machine like the ones used in the bakeries is required (photo).

Procedure:

- 1- Put a quantity of dry clay into the container of the mixing machine.
- 2- Add a large quantity of water, enough to obtain a mud like consistency, or a thick slurry.
- 3- Let the machine mix the paste for at least 20 minutes. After this time the paste must be homogeneous and smooth. It is then ready for use. Water content and shear strength can be determined.
- 4- Let the upper surface of the container open to allow evaporation of water if a clay material of lesser water content is needed. Mix the material regularly. When the sought water content is reached, cover the machine container with a airtight plastic sheet, or store the material in well closed plastic containers.



2. DETERMINATION OF THE WATER CONTENT

The mechanical properties of fine-grained materials are related to their Atterberg limits and index property. These in turn are based on the variation of the water content of the material. It is very important to know that water content in soil mechanics is expressed as a percent of the oven-dry mass of the sample. A gravimetric method is used in which a soil sample is dried at 105°C to a constant weight. The dry weight of the soil is used as the divisor in the calculation because it expresses the absolute quantity of material present.

Equipment needed:

- A drying Oven which maintains constant temperatures between 105 and 115°C.
- Wide mouth ceramic jars or containers of medium to small size, without lid. One container for each water determination.
- A sensitive preferably digital balance (accurate to 0.1 g for samples weighing over 200g).
- Miscellaneous such as tongs, gloves, spatulas, knives.

Procedure:

- 1- Weigh the empty sample container and record the weight (tare weight).
- 2- After placing the sample in the container weigh the jar and record the weight.

3- Place immediately the sample container in the oven and let dry at $110 \pm 5^\circ\text{C}$ for at least 12 hours (better overnight).

4- Remove the sample container from the oven, cover it with a lid and let it cool at room temperature.

5- Remove the lid, weigh and record the value.



Calculation:

$$\text{Water content (\%)} = (M_w - M_d) / M_d \times 100$$

M_w = Mass of wet material sample (wet weight - tare weight) (grams)

M_d = Mass of dry material sample (dry weight - tare weight) (grams)

3. TEST METHOD FOR HAND HELD SHEAR VANE TEST

The text is extracted from the guideline of the New Zealand geotechnical society (2001). The guideline includes a recommended test method for using a hand shear vane, and recommendations for the use of the vane in particular applications.

Traditionally Pilcon has been the brand of hand held shear vane used in NZ. Pilcon state that the dial reading is the undrained shear strength, based on correlation with quick undrained compression tests on samples of London Clay. The Pilcon manufacturer uses this empirical calibration to calibrate each vane spring, and each vane dial is individually engraved to match its spring. There have been two common approaches to reporting the Vane Shear Strength, either:

- use of the dial reading as the undrained strength (Pilcon's recommendation), or
- use of the BS1377 calculation.

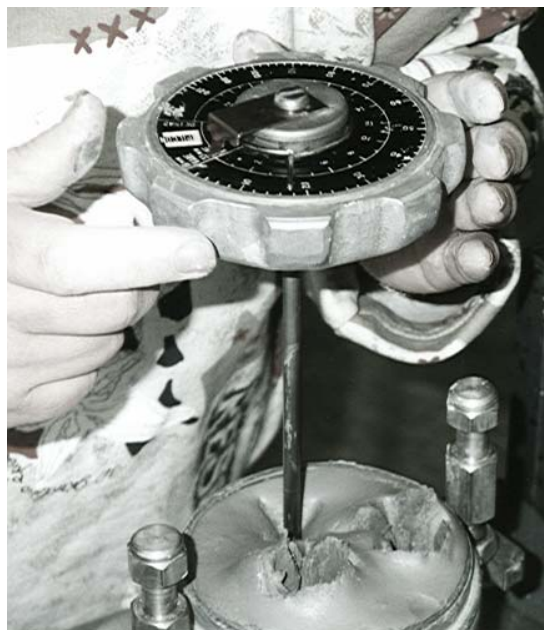
Apparatus

- Vane head (torsion head), complete with pointer, stop pin, circumferential graduated scale, calibrated torsion spring and serial number.

- Vane blades: The standard size 19 mm diameter by 29 mm high vane blade including shaft with thread for connecting directly to vane head or to extension rods. Alternative blade sizes are available for softer materials.
- Extension rods: Rods shall be of sufficient stiffness for the intended application.
- Calibration chart or factor for the particular vane kit giving the Vane Shear Strength for the dial readings. The chart or factor bears the serial numbers of both the vane head and vane blade, and is only applicable to the particular vane head and blade.

Procedure

- 1- Check that the vane head and vane blade are both clean and dry, and that the pointer is free to move and does not stick at any position on the head.
- 2- Hold the shear vane perpendicular to the material surface and push the vane blade into the soil to a depth at least twice the length of the vane blade, usually 70 to 80 mm. The depth of vane embedment should not exceed the length of the vane blade shaft. Avoid any excessive sideways movement when pushing the vane into the material.
- 3- Check that the vane pointer is at the correct starting position on the vane head.
- 4- Hold the vane head in one hand (or both hands) clear of the pointer and rotate the vane head slowly at a uniform rate.
- 5- When the material shears, the force on the torsion device is released and the pointer registers the maximum deflection to which the spring was subjected. Record the maximum deflection, from the scale on the vane head appropriate to the blade size.
- 6- Make several measurements and use the average value.



ACKNOWLEDGEMENTS

This study would not have been possible without the unfailing support and encouragement of Prof. Bernhard Stöckhert and Dr. Nina Kukowski, who directed me enthusiastically in this research, smoothed the way and kept the pressure off me. They are also thanked for their patience. I wish to thank DAAD (Deutscher Akademischer AustauschDienst) for awarding me a research scholarship at the Ruhr-University of Bochum, and Prof. Hans-Ulrich Schwarz for the unvaluable introduction to the tectonic laboratory of the GMG Department at the Ruhr-University, with special design for clay work. I would like to acknowledge my debt to Dr. Diethard König from the soil mechanics, who introduced me to his fascinating discipline, opened the soil mechanics laboratory to my inquiries and supplied me with information that resulted into chapter Four. My sincere thanks go to Dr. Jo Lohrmann, Dr. Alberto Adriasola, Dr. Jens Steffahn, Dr. Stuart Thomson and Dr. René Schäfer for their help and discussions. I am also grateful to my colleagues and friends at the institute for their help, especially during the performance of the experiments, their encouragement and conviviality. They are Maria del Carmen, Claudia Trepmann, Annette Lämmerhirt, Rolf Neuser, Oliver Schreiner, Jens Nüchter, Miriam Fischer, Dorote Dorner, and Klaus Röller among many others.

Curriculum vitae

Personal background

Born on 24.02.1968 in Algiers, Algeria

Algerian and German nationalities

Married, single child

Education

1988 – 1994 “Université des Sciences et de la Technologie Houari Boumedienne (USTHB), Institut des Sciences de la Terre” Algiers; Algeria.

“Ingénieur d’état” diploma in Geology, passed with a very good distinction.

The subject was related to the polyphased tectonism and diapirism in a region of the tellian Atlas, which was of interest for petroleum exploration.

1955 – 1999 University of Nairobi, Department of Geology, Nairobi, Kenya.

M.Sc. degree in structural geology, sponsored by ANSTI, a UNESCO agency network for education in Africa. The thesis “ Structural analysis of neotectonic joints at Lake Magadi area, and their relationship with regional faults using remote sensing imagery interpretation” enlightened the deformational structures found in southern Kenya Rift and resulted in a publication.

2000 – 2005 Ruhr-University of Bochum, Institute of Geology, Mineralogy and Geophysics, Germany.

Ph.D. studies sponsored by DAAD.

Work experience

1993 – 1994 SONATRACH – Exploration (Société Nationale de transport des Hydrocarbures), Algiers, Algeria.

I was trained as structural geologist for the company. I had to carry out geological mapping and structural analysis.

Feb. – Apr. UNESCO – Nairobi Office, Division of Earth Sciences.

1999 Internship as assistant of Prof Dr. Thomas Schlüter, programme specialist in Earth Sciences. During this time I was specifically engaged in editorial work of the proceedings of an international workshop at the Pan African conference on sustainable coastal management, held in Maputo, Mozambique, in July 1998.